

**Development of Methodologies for the Noninvasive
Estimation of Blood Perfusion**

by

Paul S. Robinson, B.S.

Thesis submitted to the Faculty of the
Virginia Polytechnic Institute and State University
in partial fulfillment of the requirements for the degree of

Master of Science

in

Mechanical Engineering

Dr. Thomas E. Diller, Co-advisor
Dr. Elaine P. Scott, Co-advisor
Dr. Hugo Veit

February 1998

Blacksburg, Virginia

© Copyright by Paul S. Robinson, 1998

Development of Methodologies for the Noninvasive Estimation of Blood Perfusion

Paul S. Robinson, B.S.

Virginia Polytechnic Institute and State University, 1998

Supervisor: Dr. Thomas E. Diller/Dr. Elaine P. Scott

ABSTRACT

This work focuses on the development of a system to noninvasively estimate blood perfusion using thermal methods. This is accomplished by the combination of a bioprobe, biothermal model, and parameter estimation techniques. The probe consists of a heat flux sensor and surface thermocouple placed in contact with tissue while the opposite side is cooled by jets of room temperature air. The biothermal model predicts the temperature and heat flux within tissue and probe based upon the input of blood perfusion and the thermal contact resistance between probe and tissue. Parameter estimation techniques are developed that use the model to simultaneously estimate blood perfusion and contact resistance based on experimental heat flux and/or temperature. A gradient based system minimizes a sum of squares error function based on either or both heat flux and temperature. This system is tested on human forearms and in controlled flow rate experiments using tissue phantoms. Blood perfusion estimates from the controlled experiments are positively correlated with experimental flow rate. Experimental measurements and statistical analysis show distinct variations in the heat flux signal and rises in perfusion estimates with increasing flow rate. This research validates the use of thermal and parameter estimation methods to develop a practical, noninvasive probe to clinically measure blood perfusion.

Acknowledgments

I would like to thank the Vatel Corporation and Virginia's Center for Innovative Technology (CIT) (Grant No. BIO-97-005) who provided funding for this research.

Thanks also to Dr. Tom Diller for 'selling' this project to me and helping my decision to come back to Virginia Tech in pursuit of this degree. Thanks to Dr. Diller and Dr. Elaine Scott for serving as my advisors and not letting me get too caught up in all my graphs; also to Dr. Hugo Veit for serving on my committee, providing a non-engineering opinion, and helping me procure lab equipment.

Among my friends and colleagues that deserve mention are my Heat Transfer Lab mates (Alex Hanuska, Christie Staton, Greg Walker, Jim Dolan) for helping me stay grounded and sane; the 'other committee' (Mark Cooper, David-Batt Ellis, and Aaron Snyder) for keeping in touch and occasionally forcing my mind out of nerdism; and Tom Leitch for his unselfishness with needed resources. Greg and Jim helped immeasurably with setting up and maintaining the computer resources necessary for my research, as well as tirelessly answering annoying questions.

Finally, to my family (my parents: George and Carol Robinson, my sisters and brothers-in-law: Cindy and Tom Peterson, Jen and Ritch Grafton), thank you for your endless support and encouragement.

PAUL S. ROBINSON

Virginia Polytechnic Institute and State University

February 1998

Contents

Abstract	ii
Acknowledgments	iii
List of Tables	viii
List of Figures	x
Nomenclature	xiii
Chapter 1 Introduction	1
1.1 Objectives	3
Chapter 2 Literature Review	5
2.1 Biothermal Heat Transfer Models	5
2.2 Blood Perfusion Measurement Efforts	6
2.3 Parameter Estimation	8
Chapter 3 The Bioprobe	10
3.1 Heat Flux Sensors	10
3.1.1 Thermopile Core	10
3.1.2 Manufacturing Processes	11
3.2 Bioprobe Designs	12
3.2.1 Early Designs, Bioprobe A	12
3.2.2 Current Design, Bioprobe B	14
3.3 Bioprobe Properties	19
3.3.1 Physical and Thermal	19

3.3.2	Calibration	20
3.4	Anatomy of Bioprobe Heat Flux and Temperature Signals	22
Chapter 4 Biothermal Model and Parameter Estimation		24
4.1	Biothermal Model	24
4.1.1	Theoretical Model	24
4.1.2	Mathematical Equations and Assumptions	27
4.1.3	Solution Technique	29
4.2	Parameter Estimation	31
4.2.1	Sensitivity Coefficients	31
4.2.2	Estimation Procedure	32
4.2.3	Error Estimation and Confidence Intervals	36
Chapter 5 Experiments		39
5.1	Setups	39
5.1.1	Data Acquisition	39
5.1.2	Convection Coefficient Experiments	43
5.2	Experimental Procedures	45
5.2.1	Arm Experimental Procedure	45
5.2.2	Phantom Experimental Procedure	46
5.3	Kapton Experiments (Probe A1)	53
5.4	Kapton-Aluminum Experiments (Probe A2)	53
5.5	Bioprobe Experiments (Probe B)	55
5.5.1	Arm Experiments	56
5.5.2	Phantom Experiments	57
Chapter 6 Evaluations and Results		66
6.1	Biothermal Model Evaluation	66
6.1.1	Environmental and System Parameters	67
6.1.2	Probe Parameters	72
6.1.3	Probe Surface Temperature Evaluation	80
6.2	Evaluation of Parameter Estimation Program	82

6.3	Sensitivity Analysis: Bioprobe A	84
6.4	Results with Previous Data	86
6.5	Results of A1 and A2 Experiments	88
6.5.1	Runs and A1 Trials	88
6.5.2	A2 Trials and Alums	88
6.6	Results of Aluminum Phantom Experiments	90
6.6.1	Convective Heat Flux Experiments on Aluminum Phantom	91
6.6.2	Aluminum-Arm Comparisons	102
6.7	Results of Arm Tests with Bioprobe B	102
Chapter 7 Sponge Phantom Experimental Results and Evaluation		104
7.1	Results	104
7.1.1	Qualitative Evaluation of Sponge Phantom Thermal Response	104
7.1.2	Parameter Estimation Results	107
7.2	Further Evaluation of the Parameter Estimation Procedure	111
7.3	Statistical Evaluation of Experiments	117
7.4	Experimental Noise Evaluation	119
Chapter 8 Summary and Conclusions		121
8.1	Summary	121
8.2	Conclusions	122
Chapter 9 Recommendations		126
Bibliography		129
Appendix A Biothermal Heat Transfer Model		135
A.1	Biothermal Model Subroutine	135
A.2	Main Program for Calling Biothermal Model Alone	143
Appendix B Model Related Application Programs		144
B.1	Objective Function Calculation	144
B.2	Main Program for Calculating Sensitivity Coefficients	145
B.3	Main Program for Estimating Inherent Error	147

B.4 Main Program for Calculating Heat Flux and Temperature Slopes	148
Appendix C Parameter Estimation Code	151
C.1 Main Program	151
C.2 Sample Input File	157
Appendix D Sponge Experiments Parameter Estimation Results	158
Vita	160

List of Tables

3.1	Bioprobe Physical and Thermal Properties	20
3.2	Bioprobe Calibration Coefficients	21
5.1	K Thermocouple Linearization Data	41
5.2	Comparison of Data Acquisition Settings	43
5.3	Convection Coefficients for Each Probe Type	44
5.4	Skin and Blood Properties	47
5.5	Conditions of First Kapton Experiments	54
5.6	Settling Conditions for Early Experiments (1)	54
5.7	Settling Conditions for Early Experiments (2)	54
5.8	Conditions of A2 Experiments	55
5.9	Conditions of Bioprobe B Skin Experiments	57
5.10	Properties of Duocel Porous Aluminum Samples	60
5.11	Conditions of First Porous Aluminum Experiments	61
5.12	Conditions of Aluminum-Arm Comparison Experiments	62
5.13	Properties of Sponge Samples	64
5.14	Conditions for Sponge Tests	65
6.1	Property Values for Thermocouple Capacitance Model	81
6.2	Results of Estimation Procedure on Simulated Data, Heat Flux and Temperature	83
6.3	Results of Estimation Procedure on Simulated Data, Varying Error	84
6.4	Estimation Results; Previous Data	86
6.5	Estimation Procedure Results; Alum Experiments	90
6.6	Results of Varied Estimation Procedures on 19925 Data	95

6.7	Calculation Times for Determining Heat Flux and Temperature Slope with Respect to Contact Resistance and Blood Perfusion	96
7.1	Results of Parameter Estimation for Four Sponge Experiments	107
7.2	Results of Estimation with Changes to ‘Known’ Model Parameters	114
7.3	Overall Perfusion Averages at Each Flow Rate, Sponge Phantom Experiments	118
8.1	Summary of Parameter Estimation Methods	124
D.1	Results of Parameter Estimation for All the Sponge Experiments	159

List of Figures

3.1	Foil Style Thermopile Representation	12
3.2	Bioprobe A, Top View of Sensor and Air Jet Housing	14
3.3	Circular Thermopile Pattern of Bioprobe B	15
3.4	Representative Cross Section of Episensor (Probe B)	16
3.5	Iterations of Foil Thermocouple Placement on Episensor	17
3.6	Bioprobe B, Air Jet Housing Schematic	18
3.7	Bioprobe B, View of Sensor Surface and Side of Air Jet Housing	18
3.8	Diagram of R-Matic Heat Flux Sensor Calibration	22
3.9	Typical Heat Flux (Top) and Temperature (Bottom) Data from Bioprobe Showing Different Response Areas	23
4.1	Sketch of Bioprobe on Tissue, Side View	26
4.2	Bioprobe Finite Difference Model	26
4.3	Pennes Biothermal Control Volume	28
4.4	Flow Chart of Sequential Estimation Process	36
5.1	Diagram of Previous HP Data Acquisition Set Up	42
5.2	Diagram of New, PC-Based Data Acquisition Set Up	43
5.3	Picture of Arm Experiment: Probe Placement	46
5.4	Desired Flow Pattern Within Phantom Media (Two Dimensional View)	48
5.5	Diagram of Phantom Experimental Set Up	50
5.6	Picture of Phantom Experimental Set Up, Water Bath	51
5.7	Picture of Phantom Experimental Set Up, Sample Box	51
5.8	Picture of Phantom Experimental Set Up, Equipment	52

6.1	Comparison of Conductive Heat Flux Calculated within the Probe and Across the Probe-Tissue Interface	68
6.2	Effect of Convection Coefficient on Model Output	69
6.3	Effect of Contact Resistance on Model Output	70
6.4	Effect of Blood Perfusion on Model Output	71
6.5	Effect of Changes in Core and Air Stream Temperatures on Conductive, Convective Heat Flux and Probe Surface Temperature	72
6.6	Model Output Due to Changes in Probe Specific Heat or Density	73
6.7	Resistance Network for Lumped Capacitance Probe Model	74
6.8	Comparison of Biothermal Model and Lumped Capacitance Model for the Probe During Transient Times	75
6.9	Effect of Probe Conductivity on Model Output	75
6.10	Effect of Probe Radius on Heat Flux Sensitivity to Blood Perfusion	77
6.11	Heat Flux Distribution Across Probe Surface for Different Probe Radii	78
6.12	Temperature Distribution Across Probe Surface for Different Probe Radii	79
6.13	Bias Between Experimental and Model Probe Surface Temperature	80
6.14	Resistance Network for Lumped Thermocouple Model	82
6.15	Non-dimensional Sensitivity Coefficients of Heat Flux and Temperature to Blood Perfusion for the Type A Probes	85
6.16	Non-dimensional Sensitivity Coefficients of Heat Flux and Temperature to Contact Resistance for the Type A Probes	85
6.17	Experimental Data and Model Output for Previous Tests	87
6.18	Heat Flux Residuals from Previous Test 1	87
6.19	Comparison of Run1 Data and Previous Test Heat Flux	89
6.20	Comparison of Experimental and Model Heat Flux Outputs; Alum Tests	91
6.21	Heat Flux and Temperature Output for First Aluminum Phantom Tests	92
6.22	Dimensionless Sensitivity Coefficients of Convective Heat Flux and Surface Temperature to Contact Resistance and Perfusion for Bioprobe B on Aluminum Media	93
6.23	Heat Flux Data from Aluminum Media Tests at Different Flow Rates Showing No Correlation with Flow Rate	94

6.24 Heat Flux Data from Aluminum Media Tests at the Same Flow Rate Showing Non-Repeatability	94
6.25 Model Heat Flux Output for Varying Perfusion Values at Constant Contact Resistance, Phantom	98
6.26 Conductive Heat Flux Slopes over Time Plotted Against Blood Perfusion	99
6.27 Model Heat Flux Output for Varying Blood Perfusion Values at Constant Contact Resistance, Skin	100
6.28 Conductive Heat Flux Slopes over Time Plotted Against Blood Perfusion	101
6.29 Comparison of Aluminum Phantom and Arm Heat Fluxes	103
6.30 Results of Arm Experiments with Bioprobe B, Episkin Tests	103
7.1 Comparison of Heat Flux from Sponge and Arm Experiments Using Bioprobe B	105
7.2 Representative Heat Flux Data from Four Sponge Tests at Different Flow Rates	106
7.3 Sensitivity Coefficients of Heat Flux and Temperature to Contact Resistance and Perfusion for Sponge Experiments	106
7.4 Heat Flux from Experiment and Model Based on Parameter Estimates for Four Sponge Experiments	108
7.5 Contact Resistance Estimates vs. Experimental Flow Rate for Sponge Phantom Tests	109
7.6 Perfusion Estimates vs. Experimental Flow Rate for Sponge Phantom Tests	110
7.7 Estimated Perfusion Compared to Experimental ‘Perfusion’ Calculated Using the Entire Sponge Volume	111
7.8 Heat Flux Sensitivities with Respect to ‘Known’ Model Parameters	113
7.9 Model Output Based on Changes to Tissue Thermal Conductivity and Diffusivity	115
7.10 Model Output Based on Changes to Fluid Specific Heat and Probe Thickness	116
7.11 Overall Perfusion Averages at Each Flow Rate, Sponge Phantom Experiments	118
7.12 Frequency Spectra Magnitudes for Heat Flux Signals Taken at Four Different Flow Rates	120

Nomenclature

a, c	constants
\mathbf{b}, \mathbf{b}	estimated parameters (vector)
c_p	specific heat (J/kg K)
e	heat flux residual (W/m ²)
E	voltage (V)
h	conduction heat transfer coefficient (W/m ² K)
k	thermal conductivity (W/m K)
L	length variable (m)
m	slope
N	number of time steps (data points)
n	number of parameters or nodes
p	number of estimated parameters
q'', \mathbf{q}''	heat flux (W/m ²) (vector)
R_c	thermal contact resistance (m ² K/W)
RMS	root-mean-squared error
s	standard deviation of a sample
S	objective function (sum of squares)
S_q	sensor sensitivity (mV/W/cm ²)
t	time (s)
T, \mathbf{T}	temperature (°C) (vector)
T_{core}	subject core body temperature (°C)
T_{H_2O}	water bath temperature (°C)
T_∞	environment or air stream temperature (°C)

V_f	volume fraction (%)
w_b	perfusion, blood or water (ml/ml/s)
x	average of a sample
X	sensitivity coefficient
\mathbf{X}	sensitivity matrix
α	thermal diffusivity (m ² /sec)
$\beta, \boldsymbol{\beta}$	unknown parameters to be estimated (vector)
δ	probe thickness (cm)
Δ_L	distance between nodes (m)
λ	time constant
ρ	density (kg/m ³)
σ^2	variance
σ_{known}^2	model output uncertainty
σ_{tot}^2	total of model and experimental uncertainties

Subscripts

a	artery
b	blood
c	calculated, model
$conv$	convection
$cond$	conduction
eff	effective
i	initial condition
int	internal
k	K thermocouple
m	measured, experiment
n	node or parameter index
o	nominal value
p	probe
q	heat flux
Rc	contact resistance
t	tissue

T	temperature
v	vein
w	perfusion

Superscripts

-	time averaged
+	dimensionless
T	transpose
k	iteration number

Chapter 1

Introduction

Blood perfusion is defined as the blood volume flow exchange per volume of tissue. Blood flow, expressed as volume exchange per time, in arteries and veins is directional (vector) and usually referenced in terms of these larger vessels. Blood perfusion represents the local flow through the capillary network and extracellular space of perfuse tissue. This flow is so convoluted as to be considered non-directional (scalar) at the macroscopic level. Blood flow and blood perfusion are related, but perfusion abnormalities may exist even in the presence of normal blood flow. In some cases, blood may flow through the larger vessels but not actually be getting to the capillary level and reaching all parts of the tissue as in myocardial infarction for example. Blood perfusion is a separate and equally important quantity to measure in the assessment of tissue physiology.

Blood perfusion is crucial for normal tissue physiology. For one, blood perfusion is a chief component in the temperature regulatory system of the body. Core temperature blood warms or cools peripheral tissues, such as skin and muscles, as it flows through and around them to help the body maintain an isothermal environment. Also, blood brings nutrients to and removes waste from tissue. Without this, tissue cells would soon become degenerate and die. Alterations in perfusion are often caused by a vascular reaction to abnormal and oftentimes unwanted physiologic or pathologic conditions. Therefore, perfusion changes are linked with a variety of pathologic or disease processes.

The ability to measure blood perfusion, then, is a valuable medical diagnostic. For example, tumors alter the local perfusion. Measuring these disruptions could aid in finding and evaluating the extent of tumors and other skin lesions. Blood perfusion measurements

can also determine the success or failure of skin grafts and any related healing. Other conditions such as heart disease, diabetes, vibration white finger, and abnormal conditions of the pulmonary and circulatory systems result in abnormal perfusion rates. Further, direct evaluation of the micro-circulation of myocardial, renal, intestinal, and other tissues during surgery can relate to tissue viability and patient prognosis and be significant in choosing correct surgical procedures. Monitoring of blood perfusion in recently repaired ischaemic tissue can predetermine and help prevent the common problem of reperfusion injury. Many clinical applications would be improved or made possible by a reliable method to measure blood perfusion.

Most current methods of measuring blood perfusion are invasive. One method is monitoring the clearance of a chemical marker such as a radio-isotope. Another method is the insertion of a thermistor bead into the perfusion area and measurement of its cooling response (Valvano et al., 1984; Bowman, 1985; Valvano and Nho, 1991). These invasive methods can cause patient discomfort, infection, and possibly alter the perfusion being measured. One noninvasive method makes use of laser light delivered to the tissue and measurement of the Doppler shift of the returned light (Shepherd and Å. Öberg, 1990). The Doppler shift is brought about by the light intercepting moving red blood cells. This method is expensive and does not produce absolute measurements, but rather relative measurements of perfusion (Hoke et al., 1994). It is also highly dependent on optical properties that can greatly vary.

This research focuses on development of a noninvasive method to measure blood perfusion absolutely, accurately, and inexpensively. The basic concept employed is measurement of the thermal response of tissue with a bioprobe. The bioprobe is comprised of two sensors, one to measure heat flux and one to measure temperature. The probe is placed in contact with the exterior of the tissue under study while the opposite side of the sensors are cooled by low-pressure jets of room temperature air to set up a thermal gradient. The probe then measures the heat flux flowing from the tissue and temperature of the probe surface in contact with the tissue.

A biothermal model based on the Pennes bioheat equation is used to theoretically describe the physical tissue and probe system. A finite difference method solves for heat flux and temperature at various locations in the tissue and probe based on the input of environmental conditions and two important parameters, blood perfusion and contact re-

sistance. Blood perfusion is the parameter of prime interest in this research. Because the contact between probe and tissue is imperfect the thermal contact resistance is also an important factor that can vary among applications. A core model was developed previously by Michener (1991) and modified by Gonzales (1995). Further modification is necessary to more accurately describe the physics of the system and to account for changes in probe design.

Parameter estimation techniques exist that can incorporate experimental data and a related model to ‘back out’ input parameters. Applying these techniques to the bioprobe measurements and biothermal model allow for the estimation of blood perfusion and contact resistance. One of the more popular methods that has been successfully used in thermal studies is Gauss Minimization with the Box-Kanemasu modification. This research saw the development of such methods as well as the experimental protocols to best implement them.

Because this research is on the frontier of blood perfusion measurement and medical utilization of heat flux sensors, experimental protocols have not been previously developed. Experimental procedures need to be described that both yield consistent, repeatable results and fit with the theory. Also, a tissue phantom system is required to test the bioprobe concept in a controlled environment. These phantoms provide a multi-directional perfusion pattern and act like biological tissue in terms of internal flow and thermal characteristics. This leads to validation of a new concept; measuring surface heat flux to determine internal flow through a porous media, specifically blood perfusion through tissue.

1.1 Objectives

The objectives of this study covered three areas of research, theoretical modeling of the bioprobe system, parameter estimation applications, and experimentation. The specific objectives from these areas are outlined as follows:

- 1.) Further develop a biothermal model for the probe and tissue system.
- 2.) Develop parameter estimation techniques that use experimental measurements in conjunction with the biothermal model to estimate blood perfusion and contact resistance.

- 3.) Develop experimental protocols for both live tissue and non-biologic tissue perfusion testing.
- 4.) Evaluate model and system dependencies on certain variables such as environmental conditions and tissue and probe properties.
- 5.) Validate the bioprobe concept.

This document explains how the above objectives were completed. First, a description of the bioprobe and its related technology is given. Also included is a description of the iterative bioprobe designs used at different points in this research. Next comes an explanation of the biothermal model, the solution technique, and the method of parameter estimation developed to simultaneously estimate blood perfusion and contact resistance. The experimental apparatus, procedures, and developed protocols are then described in detail. An evaluation of the biothermal model as developed here, the results of the various experiments, results from application of the parameter estimation scheme, and all relevant conclusions are all presented over the next few chapters. Finally, this document shows the validity of the bioprobe and parameter estimation in measuring perfusion and provides some recommendations for further progression of this work.

Chapter 2

Literature Review

Several key areas of scientific literature give insight to the fundamentals behind the processes used in this research. The three areas of interest are biothermal heat transfer models, blood perfusion measurement, and application of parameter estimation techniques. Understanding this literature lends support to the methods used in the current research and gives a basis for comparison of the research to existing technologies.

2.1 Biothermal Heat Transfer Models

Much literature has been devoted to biothermal models, particularly those focused upon defining a blood flow or perfusion term. Most notable is the early work by Pennes (1948) who developed a general equation for tissue including a convective blood perfusion term and a metabolic heat generation term. The Pennes model has become the standard starting point for most biothermal analysis, and a benchmark against which more recent models are compared. Charney (1992) provides an excellent overview of several bioheat transfer models, starting with Pennes and including models by Wulff, Klinger, and Chen and Holmes. He includes model descriptions, experimental data, model shortcomings, and comparisons. These models all relate the blood perfusion or blood flow to convective terms within a combined conduction-convection transient heat equation with generation. It is interesting to note that the Wulff and Klinger models use a blood velocity within a temperature gradient for the convective term, as opposed to a perfusion term with some variable temperature used in the Pennes and other models. Because of this, Wulff and Klinger equations are very similar to the equations governing point source flow and heat generation through a porous

media (Ganapathy, 1994).

Some other models attempt a slightly different approach to arrive at working bio-thermal predictions. Weinbaum and Jiji (1985) developed a heat exchange model based upon the blood vessels acting as counter-current pairs. This, they argued, more closely resembles the actual geometry of perfused tissue, especially skeletal muscles. In another model, the constitutive behavior of porous solids was used to derive descriptions of fluid flow through such solids under deformation (Vankan et al., 1996). This method was applied to skeletal muscle to attain blood flow information based on pressure gradients and the resulting mass transport.

In a later paper by Weinbaum et al. (1997), a further analysis of the Weinbaum-Jiji equation saw that under certain general conditions, it reduced to the Pennes equation with the blood perfusion term multiplied by a geometry based factor. In fact, many recent bioheat transfer models, such as the one proposed by Brinck and Werner (1994) simply ‘improve’ the classical bioheat approach (that of Pennes) by establishing some efficiency or correction factor to be used with the Pennes convective blood perfusion term in a similar combined conduction-convection-generation equation.

2.2 Blood Perfusion Measurement Efforts

A historical record for the measurement of blood perfusion has been well documented by several authors, including Bowman et al. (1975); Eberhart et al. (1980); Bowman (1985); Chato (1985). The methods discussed in these papers are primarily invasive in nature. The most successful invasive method has been to utilize thermistor beads inserted into the tissue. Then one of two different methods of experiment can be applied.

One method of utilizing an embedded thermistor bead is to supply it with a controlled power sequence. This power is dissipated by the bead and the temperature response is recorded. The two most common heating methods, pulse decay and step heating, are compared by Kress and Roemer (1987). Valvano and Nho (1991) have also used multiple probes and sinusoidal heating. The temperature response is then input to an analytical model, such as one of the models discussed above, that determines blood perfusion. An example of data reduction for step heating in a thermistor bead is found in Newman et al. (1995).

In a second method, other work by Valvano et al. (1984); Bowman (1985) use the embedded thermistors as a control point. Here, the thermistors are kept at a constant temperature some increment above that of the surrounding tissue. The power required to maintain this difference is equal to the energy diffused from the bead, which is a function of blood perfusion. The power requirements are used in an analytical model to determine perfusion and effective conductivity.

While these methods have met with some success, they are undesirable due to their invasiveness. Invasive procedures cause discomfort and possible harm to a patient or act to disrupt the flow that is being measured. Also, a large thermistor bead increases the trauma to the tissue, but using a small bead will not allow the coverage of an effective area of tissue.

Because of these problems, several noninvasive methods have been developed. The most common are thermal clearance methods employing different heating and temperature sensors. Patel et al. (1987); Wei et al. (1995) both used thermistors covered with insulation placed on the tissue surface to simultaneously provide heating and measure surface temperature. Castellana et al. (1983) used a thin film resistor to do the same. Because of ambient heat loss to the insulation, Walsh and Bowman (1984) added a second active flake resistor to control the heat entering the tissue. Holti and Mitchell (1979) developed a thermal clearance probe based upon a heated copper disk connected to a surrounding non-heated copper ring by constantan wire. This thermopile device was then placed on the skin. Valvano et al. (1988) measured temperature response of skin in contact with a copper block using a thermal imaging system. Cui and Barbenel (1991) modeled the temperature response with different materials placed on the skin. The fundamental problems with these methods are the determination of the heat flux into the tissue, since the losses to ambient environment are unknown, and the unknown and variable contact resistance between the probe and tissue. Also, applying heat to the skin surface contains the potential for thermal tissue damage if the temperature rises above 42 degrees Celsius.

Other noninvasive methods include ultrasound and laser Doppler. Anderson and Burnside (1990) tried focused ultrasound as the heating source in a specific volume of tissue. Temperature response to heating was measured with a surface mounted thermistor. The limitations associated with focusing ultrasound on the micro-circulation led to use of laser light. Laser light is not used to heat the tissue, but rather to measure the blood flow directly using Doppler flowmetry. In basic operation, laser light delivered to tissue is

reflected back to a detector. Some of the laser light is intercepted by moving red blood cells and becomes Doppler shifted. This phenomenon has received significant attention and is reviewed in detail by Shepherd and Å. Öberg (1990). The earliest measurements of blood flow using this method were by Riva et al. (1972), with Stern (1975) going on to measure tissue perfusion. Instrumentation for this process was continually developed (Stern et al. (1977); Stern and Lappe (1978); Nilsson et al. (1980)) making laser-Doppler flowmetry (LDF) a marketable system for clinical perfusion measurements. This successful method does have a few drawbacks, however. One limitation of the method is that only relative, rather than absolute, perfusion can be measured. Secondly, the red blood cell motion is only measured in one direction, and is dependent on the optical properties of the tissue, which can vary with location and among different patients. A more practical consideration is the inherent high cost of the measurement equipment.

An alternate method that avoids the high cost and limitations of the LDF is the use of heat flux sensors to measure blood perfusion. Such methods have received scant attention. Michener et al. (1991) described a blood perfusion probe that measures heat flux and temperature at the skin surface. This work was furthered by Fouquet et al. (1993) and O'Reilly et al. (1996). The result of these authors' work was an air-cooled heat flux and temperature sensing probe. The heat flux and temperature data were compared to a model developed by Michener et al. (1991) based upon the Pennes equation.

2.3 Parameter Estimation

Parameter estimation and inverse methods, of which many exist, have been used in all types of applications. These methods use a model in conjunction with experimental data to determine information about a given system that may be directly unmeasurable. Parameter estimation involves determining system variables based on known boundary and initial conditions. Inverse methods are used to find boundary and initial conditions given known system variables. 'System variables' can include thermal and physical properties and geometry.

A common parameter estimation technique, the Box-Kanemasu method, has been successfully used to estimate thermal properties for a variety of materials, including composites (Scott and Beck, 1992a; Moncman et al., 1995) and biological material during freezing

(Saad and Scott, 1996). Other methods have been used in the area of biothermal heat transfer. For example, Wei et al. (1995) used a nonlinear least squares method to estimate blood perfusion based on their surface mounted thermistor model. Other biomedical applications have been subjected to parameter estimation and modeling, such as electrocardiography (Draghici et al., 1990; Walker and Kilpatrick, 1987), computerized tomography (Qin and Ciric, 1993; Iavors'kyi and Rafa, 1996), and biomagnetics (Scholz and Schwierz, 1994). For biomedical inverse problems, Clegg et al. (1988) applied Tikhonov regularization and Winget et al. (1986) applied the Levenburg-Marquardt method, both to hyperthermia studies. Both the parameter estimation and inverse studies all involved using experimental data in conjunction with a mathematical model to estimate some unmeasurable parameter based on measurements of the system conditions and response to certain stimuli.

Chapter 3

The Bioprobe

The concept of a heat flux probe to measure blood perfusion is based on the fundamental tenet that heat will flow along a negative temperature gradient. A temperature difference is created across a sensor that measures heat flux and temperature. This temperature difference is due to warm tissue containing warm fluid flow on one side of the sensor, and a cooling action on the other side of the sensor. In this research, jets of room temperature air provide convective cooling on the top sensor surface. The sensor then measures the heat flux response from the tissue and temperature response of the lower sensor surface. Both the amount of heat flux available to equilibrate and/or recover the cooling effect and the temperature response are related to the blood perfusion in the local region (this relationship is discussed in Section 4.1). Several different blood perfusion probes (bioprobes) have been built to accomplish this measurement process. These have all involved a heat flux sensor, temperature sensor, and air jet housing of some sort. A basic description of heat flux sensor technology, as well as a description of three relevant bioprobes, follows.

3.1 Heat Flux Sensors

3.1.1 Thermopile Core

The core of the heat flux sensor is a thin ($< 0.05\text{mm}$) thermopile. This thermopile is comprised of small bimetallic thermocouple junctions arranged in pairs across a thin resistive layer. Since the thermocouple junctions produce a voltage related to their temperature, the difference in voltages between two paired junctions represents the local temperature

difference across the resistive layer. The sum of these voltage differences between all of the junction pairs yields an average temperature difference across the entire thermopile. Based on Fourier's Law for conduction for a steady-state, one dimensional system,

$$q'' = \frac{k}{L}\Delta T \quad (3.1)$$

heat flux is directly proportional to the temperature difference. Therefore, the voltage output measured across the thermopile is proportional to the heat flux through the thermopile:

$$q'' = \frac{E}{S_q} \quad (3.2)$$

where q'' is the heat flux, E is the voltage output, and S_q is the sensitivity, or calibration coefficient, of the sensor. An example sketch of a thermopile is shown in Fig. 3.1.

3.1.2 Manufacturing Processes

Thermopiles for heat flux sensors are generally built by either foil, thin-film or sputtering processes. The foil process includes stamping out ultra thin foil legs of two thermocouple metals, copper and nickel for example. These legs are placed in an alternating pattern around the thermal barrier and overlapped at each end such that a pattern of upper and lower bimetallic junctions is created across the thermal barrier. At each junction, the metals are bonded together, usually by proprietary methods, in such a way that good electrical and physical adhesion is achieved without changing any of the properties of either metal. Sometimes several thermopiles can be used within one sensor by shunting them together in series with a foil leg.

The thin-film process creates a similar pattern of alternating thermocouples in series across a thermal barrier, but uses metal inks instead of foils. These inks can be deposited on a substrate using screening techniques similar to painting or printed circuit board generation. Layers of two thermocouple producing ink metals such as copper and nickel inks are deposited and cured in the desired pattern across a known thermal barrier. This barrier can be either a solid to which the metal inks are attached on both sides, or a layer of some polymer based dielectric ink deposited between the two metals. The size, sensitivity, and shape of a required heat flux sensor can be set by changing the size and pattern of the ink screens.

An ink pattern like the one manufactured with thin-film can also be made with sputtering processes. Sputtering processes create thermopiles that are an order of magnitude

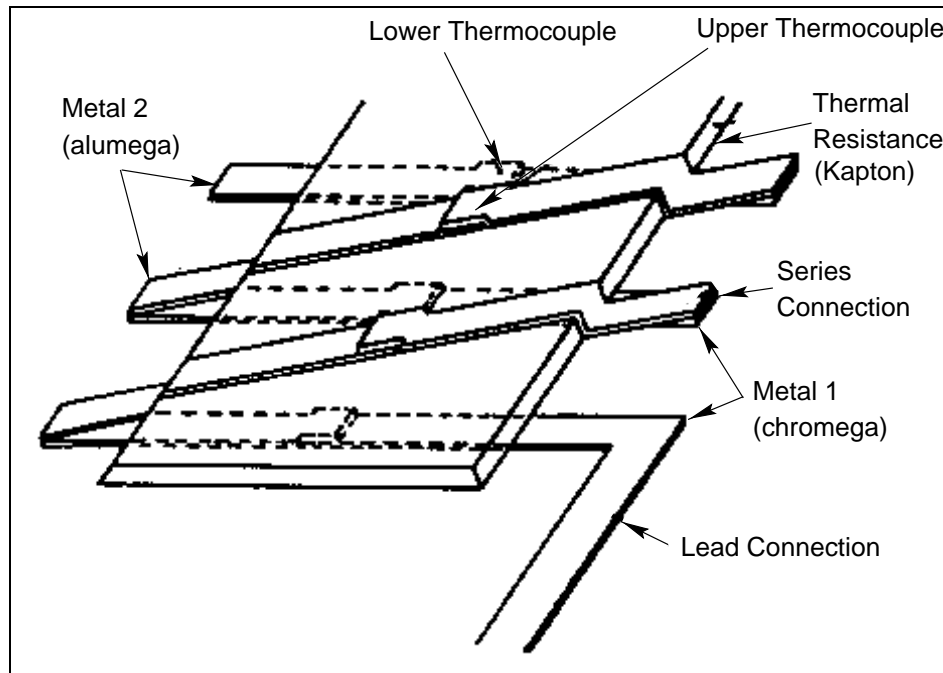


Fig. 3.1 Foil Style Thermopile Representation

lower in thickness than thin-film thermopiles. This increases the time response of the thermopile, but decreases the output (lower S_q). Such sputtered gauges were used in the work by Michener (1991). The bioprobe application does not require a fast response time and desires the highest possible sensor output. Therefore, the foil and thin-film thermopiles are used in the current research.

Based on these technologies, several different iterations of the bioprobe have been built, three of which are used in this research.

3.2 Bioprobe Designs

3.2.1 Early Designs, Bioprobe A

RdF with Kapton only, Probe A1

The first iteration of the bioprobe used in this research, Probe A1, consists of an Omega HFS-3 heat flux sensor manufactured by RdF Technologies using a foil process (RdF part number 27070-1). Figure 3.1 shows a representative cross section of the thermopile layout within the HFS-3. This is the sensor used in previous work by O'Reilly et al. (1996). There

are a total of 40 thermocouple junction pairs arranged in a square pattern within the RdF. Placed next to the thermopile is an independent type K thermocouple. Both the HFS-3 and the thermocouple are sandwiched between two Kapton sheets for protection. A picture of the A1 layout is shown in Fig. 3.2.

The output from the HFS-3 is carried by two copper wires in a Limo-cable configuration. There are type K thermocouple leads extending from the thermocouple bead within the Kapton, ending in a type K thermocouple plug. The overall dimensions of the sensor are 3.51 by 2.84 by 0.005 centimeters, as shown in Fig. 3.2.

RdF with Aluminum, Probe A2

Based on early tests and comparison of experimental output with a numerical model, it was noticed that the A1 probe had a different capacitance and transient response than expected. Also, the up and coming sensors using thin-film techniques were going to be mounted on thin aluminum sheets. To add a fairly well known capacitance to the probe and to simulate future sensors, a piece of aluminum sheet was added to one side of the A1 probe, and so called the A2 probe. A 15 mil sheet of aluminum (0.38 mm thick) cut to match the Kapton area was coated on one side with Omega thermal grease and placed on the upper side of the A1 sensor.

Air Jet Housing

The completion of the bioprobe assembly requires an air jet housing to force cooling on the upper side of the heat flux and temperature sensor. This is accomplished by flowing room temperature air at some set pressure through a grid of small holes to create jets that impinge on the sensor. The basic design for this housing is described in Gonzales (1995) and O'Reilly et al. (1996). Figure (3.2) shows this basic design. The plenum grid contains 16 evenly spaced holes of 0.79 mm diameter. The grid is set at a height of 7.62 millimeters above the sensor. For the current research, the six millimeter air hose as described in Gonzales (1995); O'Reilly et al. (1996) is replaced by a 1.27 centimeter hose and corresponding fittings (these are not shown in the figure). This change allows for larger mass flow of air, increasing the convective cooling action of the air flow. This higher convection (and consequently higher heat flux) is especially important with the addition of the capacitance to the sensor via the aluminum sheet. Higher convection ensures heat flux measurements within the region

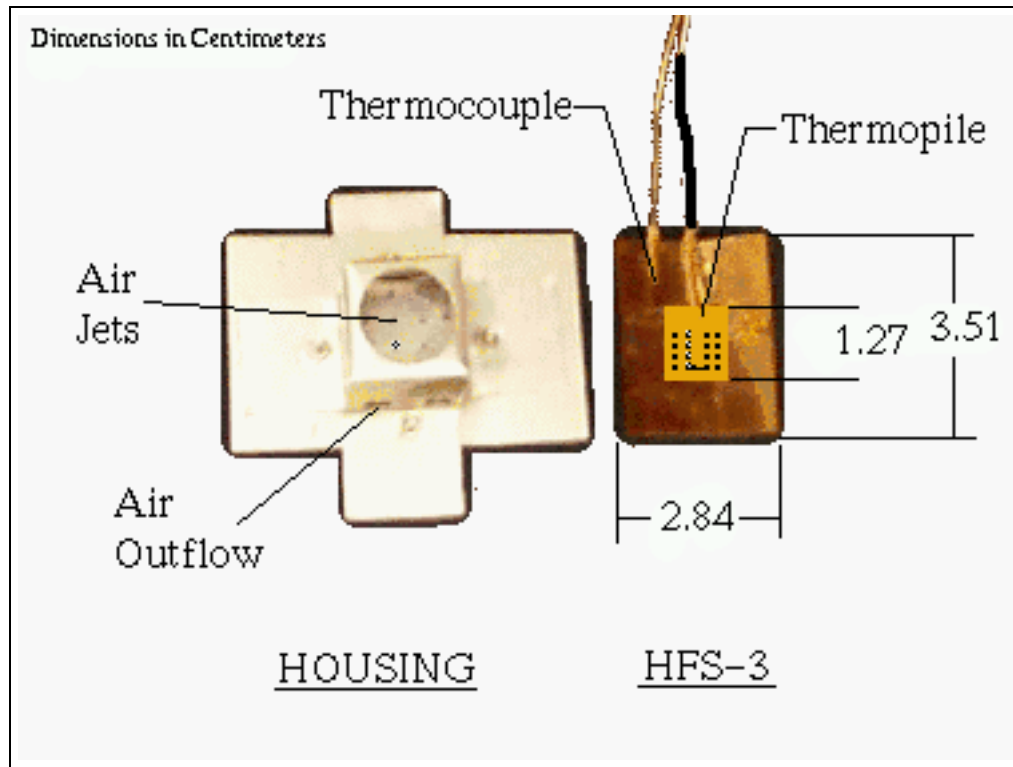


Fig. 3.2 Bioprobe A, Top View of Sensor and Air Jet Housing

where the model heat flux is sensitive to changes in blood perfusion.

3.2.2 Current Design, Bioprobe B

Episensor

The latest iteration of the bioprobe contains the Vatel Corporation's Episensor technology. This consists of a nickel and copper thermopile deposited by thin film processes on a square piece of anodized aluminum substrate. The 206 junction thermopile is arranged in a circular pattern 1.91 centimeters in diameter as shown in Fig. 3.3. A thin piece of aluminum foil was attached with some high conductivity thermal paste to create an isothermal layer over the thermopile. The end result is a sensor that attempts to create a uniform temperature distribution on both sides of a highly sensitive thermopile. Figure 3.4 shows a cross section of sensor B, including the thermopile pattern and substrate layers. Overall dimensions of this sensor are 2.97 by 2.95 by 0.07 centimeters as shown in Fig. 3.7.

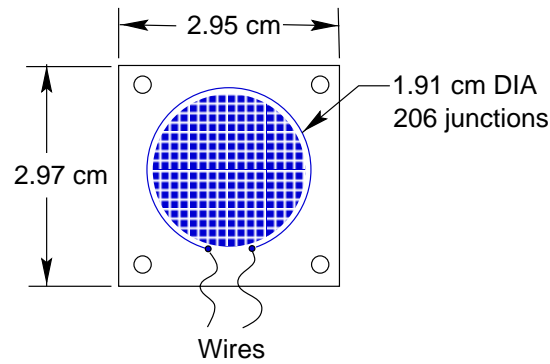


Fig. 3.3 Circular Thermopile Pattern of Bioprobe B

Thermocouple Placement

Several variations were tried in terms of the placement of a type E thin-foil thermocouple on the surface of the Episensor. It was desired to measure as best as possible the tissue side surface temperature of the probe. However, on the foil side, the heat flux sensor presents problems of both attachment and electrical isolation of the thermocouple. The thermocouple can easily be firmly attached to the anodized surface with no electrical shorting. This configuration requires that the anodized surface be placed on the tissue, causing the thermopile (foil side) to be on the air cooled surface. The heat flux measurement would then be convection off the probe instead of conduction from the tissue. While this heat flux is still related to blood flow, it will have a different magnitude and transient response than conductive heat flux.

A first attempt to place the thermocouple on the foil side surface was unsuccessful. The thermocouple would short out on the foil and attachment was poor. Not being attached to the surface made the thermocouple susceptible to folding and tearing, and indeed it did tear after only one test.

A second attempt included putting thermal paste on the foil and laying down the thermocouple while reinforcing the leads with some epoxy. This created a large hump on the probe surface that was unacceptable for practical application. The lump of paste was removed and the thermocouple placed down with a thin layer of polyurethane. This created an acceptable design from a physical standpoint.

A third design included the removal of a thin strip of foil in the probe center. The

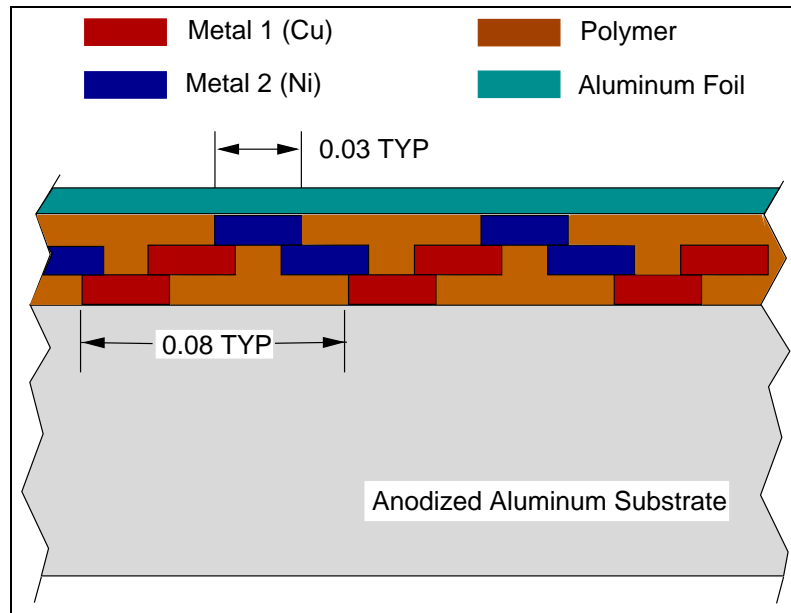


Fig. 3.4 Representative Cross Section of Episensor (Probe B)

thermocouple was placed down at the same time and on the same layer of paste as the aluminum foil. This created a flat, well attached thermocouple electrically isolated from its foil surroundings without disrupting the surface of the heat flux sensor. The progression of thermocouple placement configurations is shown in Fig. 3.5.

In the end, a design was produced where the thermocouple was on the same side of the Episensor as the thermopile so that conduction heat flux could be measured along with the tissue side surface temperature of the probe (Fig. 3.5, part (d)). Also, this final design included a shielded, twisted pair, insulated cable containing leads for both the Episensor and the thermocouple.

Air Jet Housing

Design for the bioprobe B air jet housing was based upon the previous housing design. The plenum size and air jet pattern were adjusted to match the Vatel biosensor and refinements were made in fitting type and air sealing. In comparison to the probe A housing, this plenum grid contains forty 0.52 mm diameter holes at a distance of 3 millimeters from the sensor surface. The new housings were professionally machined from aluminum except for the Plexiglas base that provides the spacing between the air jets and the sensor. This

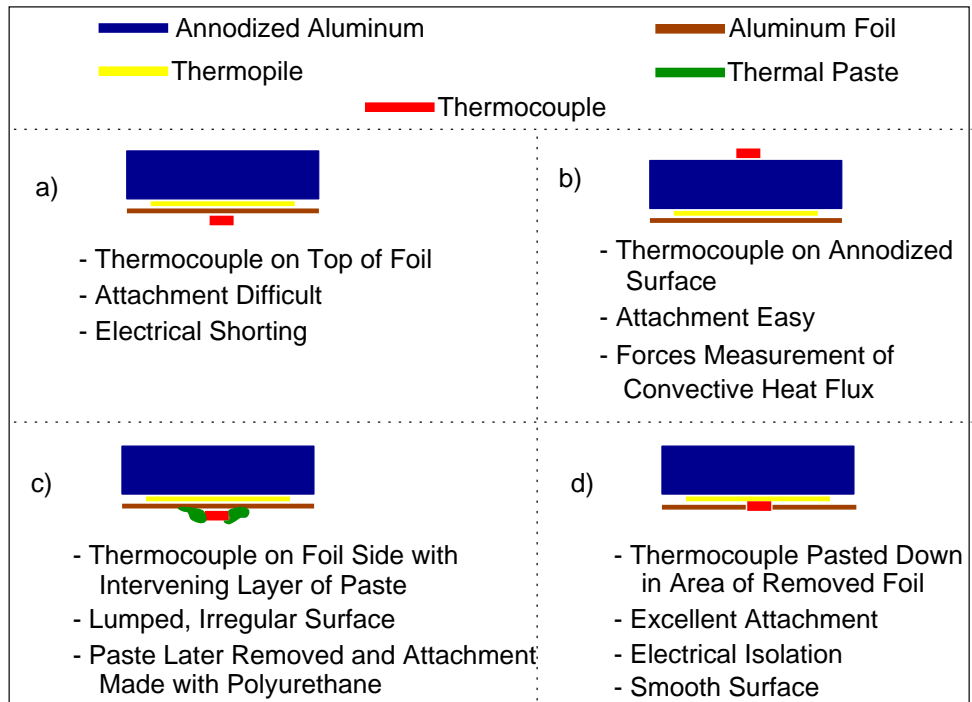


Fig. 3.5 Iterations of Foil Thermocouple Placement on Episensor

housing also contains a small hole in the upper chamber wall for the insertion of a wire thermocouple to measure air stream temperature. The resulting assembly is illustrated in Fig. 3.6. For most applications, the heat flux sensor was attached to this housing with thin strips of double-stick tape around the perimeter of the sensor.

Figure 3.7 displays the Episensor bioprobe and an isometric view of its associated air jet housing.

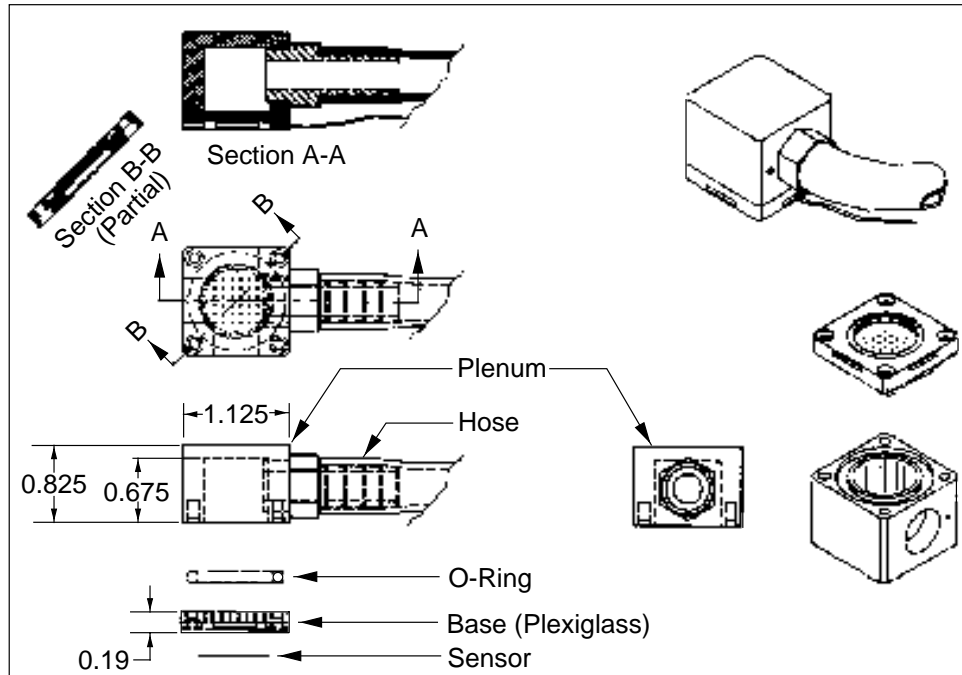


Fig. 3.6 Bioprobe B, Air Jet Housing Schematic

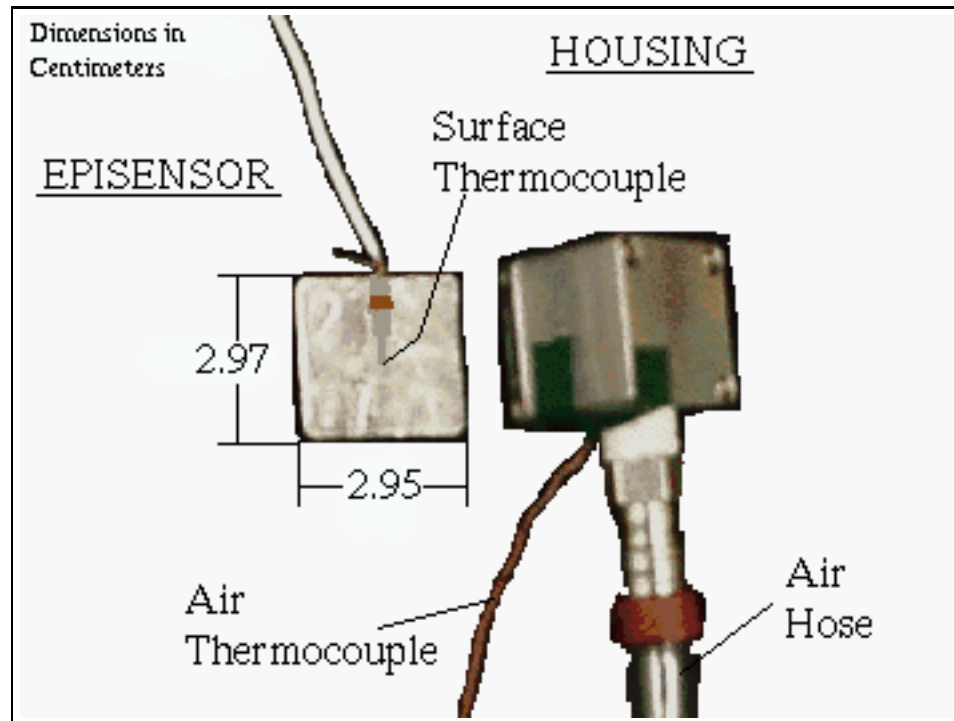


Fig. 3.7 Bioprobe B, View of Sensor Surface and Side of Air Jet Housing

3.3 Bioprobe Properties

3.3.1 Physical and Thermal

The overall dimensions for the various probe designs have been given in the previous sections. Several other properties of the sensors need to be known so that voltage data (output) can be incorporated into a biothermal model to measure perfusion. Namely, the physical properties of density, mass, volume, and the thermal properties of conductivity, specific heat, and diffusivity are required for the probe model.

The mass was found using a calibrated PB303 digital scale. Several measurements were taken with the probe placed on the scale in different orientations. In cases where wires were attached to the probe that were large enough not to be negligible in weight, only the probe body was placed on the scale and the wires were bent in such a way that their stiffness would not buoy the probe body and lead to an erroneous mass measurement. As before, this was repeated for several different probe and/or wire orientations. If any small discrepancy in mass was noticed, the measurements were averaged to obtain one fairly accurate mass for each individual probe.

The density was found by first calculating the volume of the probe. Measurements of length, width, and thickness were performed using fine calipers and triple checking each measurement. The volume was then calculated as the product of these three numbers. This volume was divided into the mass to obtain a density measurement. The exceptions to this procedure are the A1 and A2 probes. Here, nominal values for the density of the dominant material (e.g. Kapton or Aluminum) were taken from Incropera and Dewitt (1990).

The thermal properties of the probes were never experimentally analyzed. Instead, the properties of the substrate material were assumed to dominate the heat transfer characteristics of the probe. In the case of the A1 probe, this material is Kapton. For the A2 probe, the material is aluminum sheet; and finally for probe B the substrate material is aluminum shim. Nominal values of conductivity and specific heat at 300 K were taken from Table A-1 in Incropera and Dewitt (1990). For probe B the values of aluminum 2024 alloy were used since the specific material alloy was unknown. The thermal diffusivity was calculated by dividing the thermal conductivity by the product of density and specific heat, as per its definition.

Table 3.1 summarizes the resulting properties of each probe design. These properties

are used in the biothermal model and parameter estimation scheme except where changes are noted.

3.3.2 Calibration

Another important property of the bioprobes is the heat flux sensor calibration coefficient. As mentioned previously, the voltage output from the sensor is proportional to the average heat flux through the sensor as per Eq. (3.2). Before each sensor could be used, the coefficient, S_q , was found empirically.

The calibration of the HFS-3 sensor (Probe A) is performed in previous work by O'Reilly et al. (1996). The values obtained in that work are comparable to the manufacturer's calibration coefficients. Therefore, they are considered correct to use for the present research. Since both the Kapton and the thermal grease isolate the aluminum sheet from the HFS-3 in probe A2, it is assumed that no electrical or thermal interference exists between the aluminum and HFS-3 sensor. The calibration coefficient, then, is the same for both of the probe A designs. This coefficient for the HFS-3 is given as **10.19** mV/W/cm².

The Vatec sensors (bioprobe B) had to be calibrated to obtain a similar coefficient. This was accomplished using a R-Matic Guarded Hot Plate. First, however, the sensors were checked for any offset or erratic noise. They were placed in a thick book for approximately ten minutes to equilibrate to a zero heat flux situation (the book and contents were all at ambient temperature). The sensor voltage output was measured using a Hewlett-Packard 3468A multi-meter set to measure DC volts. All the sensors registered a zero voltage, indicating no original bias. The sensors were then placed within a R-Matic model 'Thermal

Table 3.1 Bioprobe Physical and Thermal Properties

Property	Probe A1	Probe A2	Probe B
Mass (g)	0.903	1.719	1.160
Length (cm)	3.50	3.50	2.96
Width (cm)	2.75	2.75	2.94
Thickness (cm)	0.00508	0.04320	0.06604
Density (kg/m ³)	1200.0	2720.0	2021.6
Conductivity (W/mK)	0.20	227.00	177.00
Specific Heat (J/kgK)	738.0	895.0	875.0
Diffusivity (m ² /s)	2.25×10^{-7}	9.32×10^{-5}	1.00×10^{-4}

Conductivity Instrument', made by Dynatech R/D Company, 1979, that maintains two constant temperature parallel plates, one hot, one cold. Padded insulation was placed on either side of the sensors to both eliminate air gaps (a cause for contact resistance and errors) and prevent direct contact of the sensors with either the hot or cold plate. A calibrated heat flow meter internal to the R-matic measured heat flux between the plates perpendicular to the plate surfaces. Figure 3.8 displays a cross sectional view of this setup. After allowing the system to stabilize for roughly twelve hours, the voltage output from the sensors was measured with the multi-meter. S_q was calculated as per Eq. (3.2). In some cases, the sensors were flipped over and the system left to stabilize again. A negative voltage measurement was made by the same multi-meter. Comparison of this measurement to the first positive heat flux measurement determined the dependence, if any, of sensor coefficient on heat flux direction. The resulting directional difference was less than ten percent, so it was considered statistically insignificant. In the cases of this directional study, the S_q 's were averaged to obtain one coefficient per sensor.

Table 3.2 shows the results of these calibrations for each individual bioprobe B. The table shows the steady-state heat flux as given by the R-matic, the voltage output of the sensor at that heat flux, and the corresponding coefficient. For the sensors that underwent more than one calibration, this table shows the average values. Although not calibrated alongside the B probes, the HFS-3 coefficient is given for comparison.

Table 3.2 Bioprobe Calibration Coefficients

Sensor	Heat Flux (W/m^2)	Voltage (mV)	S_q ($\text{mV}/\text{W}/\text{cm}^2$)
Probe A (HFS-3)	-	-	10.19
Probe B ^a			
1	205.5	0.154	7.57
2	205.5	0.158	7.68
3	190.3	0.132	6.91
4	190.3	0.1205	6.33

^aFour different bioprobe B sensors were calibrated
See section 3.2.2 for details

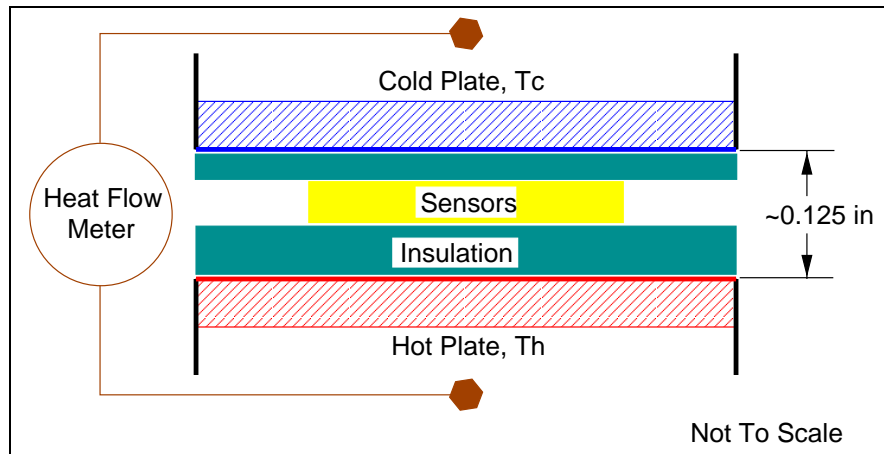


Fig. 3.8 Diagram of R-Matic Heat Flux Sensor Calibration

3.4 Anatomy of Bioprobe Heat Flux and Temperature Signals

As this point, some description of the typical heat flux and temperature signals obtained by applying these bioprobes on tissue is in order. Typical heat flux and temperature signals are shown in Fig. 3.9. The following chapters make reference to two different areas of these signals. The section between zero and ten seconds is referred to as the transient or beginning data area. This is because it shows the immediate, transient heat flux and temperature response of the probe to an abrupt change in environment. This area usually contains large slopes with respect to time. The heat flux curve characteristically has a rounded ‘spike’ as a part of its transient response. The section after ten seconds, to the end of the test, is referred to as the quasi-steady-state or end data area. This shows the long-term response of the probe to its environment after the initial shock. This area usually contains smaller slopes with respect to time.

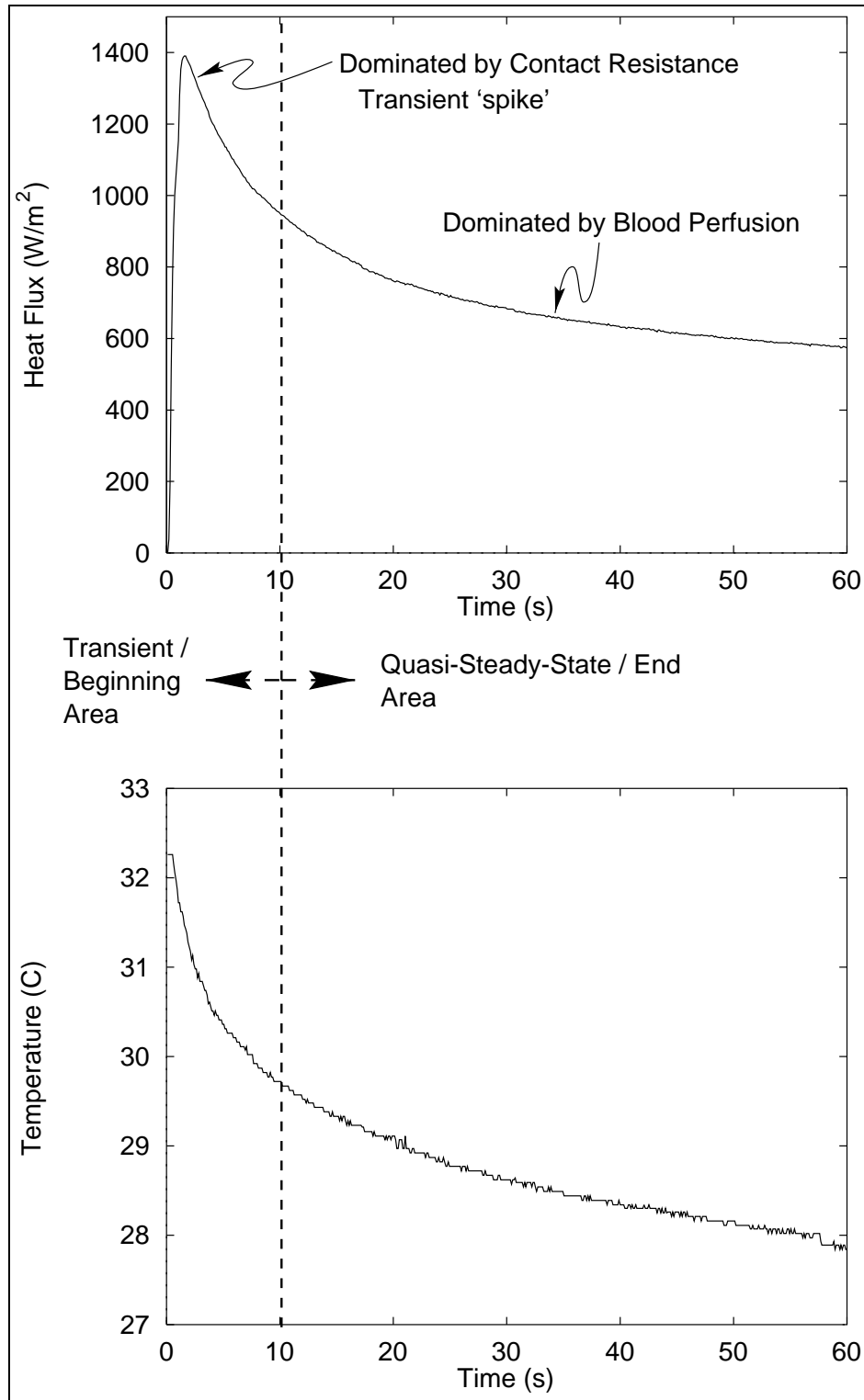


Fig. 3.9 Typical Heat Flux (Top) and Temperature (Bottom) Data from Bio-probe Showing Different Response Areas

Chapter 4

Biothermal Model and Parameter Estimation

The noninvasive estimation of blood perfusion requires the combined use of a theoretical model and experimental data. This chapter describes the former of these two and the parameter estimation technique that uses them both. A description of the biothermal model that describes probe and tissue is followed by a description of Gauss Minimization and the Box-Kanemasu modification. This includes a discussion of sensitivity coefficients and the objective function used to relate model and experiment data. Finally, some background is given on the statistical methods used to draw meaningful conclusions from all the results presented later in this document.

4.1 Biothermal Model

4.1.1 Theoretical Model

As mentioned before, the system under consideration consists of one of the various heat flux sensors placed on top of a section of tissue, with the air plenum housing placed over the sensor. A representation of this is shown in Fig. 4.1 and a sketch of the corresponding theoretical model shown in Fig. 4.2. Due to the small ratio between sensor thickness and skin thickness (approximately 0.3) the tissue is modeled as a semi-infinite medium. The expected thermal penetration depth of only a few millimeters from the tissue surface further supports the semi-infinite assumption. Also, the sensor can be considered symmetric about

its center. The forced air jets from the housing assembly create a convection boundary along the top side of the sensor. The housing itself is not included in the model; it is assumed to have no effect of the transfer of heat through the sensor other than its purpose of creating convection due to air flow. Further, the sides of the probe and the skin surface outside of the probe are modeled as an insulated boundary. This modeling is valid based on the thinness of the sensor leading to negligible surface area along the probe sides and, theoretically, an equilibrium between the skin surface and ambient environment leading to negligible heat transfer off the skin surface area not subjected to the probe.

Positive heat flux is defined as upwards, or from the tissue to the probe.

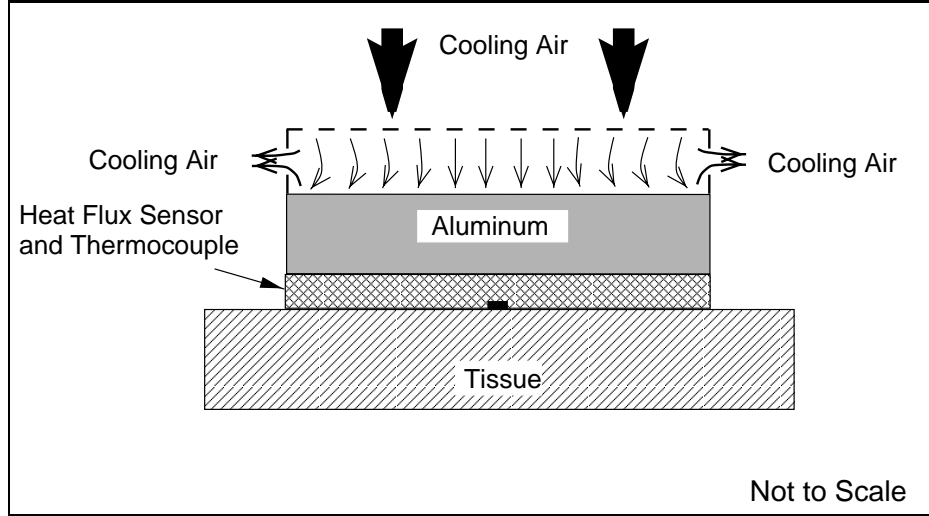


Fig. 4.1 Sketch of Bioprobe on Tissue, Side View

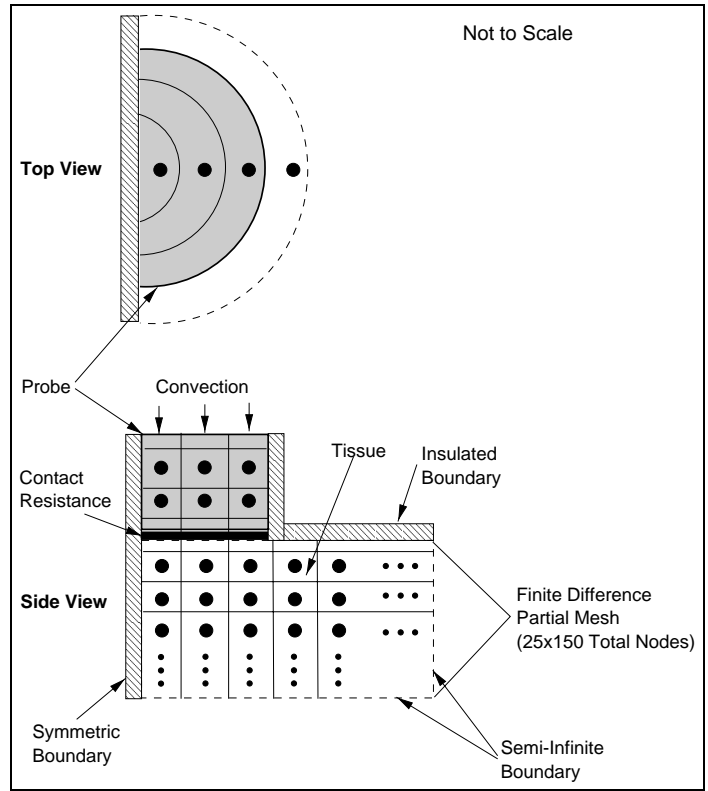


Fig. 4.2 Bioprobe Finite Difference Model

4.1.2 Mathematical Equations and Assumptions

As mentioned in the literature review, many models exist that attempt to explain heat transfer through biological tissue. One of the most basic and general of these is the Pennes bioheat equation. The general applicability of the Pennes model makes it useful as a test case and for research such as this where a model may be applied to a variety of tissue. However, for complex models, the bioheat equation requires a numerical solution technique.

The Pennes bioheat equation is based upon conservation of mass and energy within a homogeneous control volume of tissue. This control volume is fed by arterial core temperature blood on one side and drained by venous blood on the other side. Conduction from the core to the control volume also occurs. This basic system is shown in Fig. 4.3. It is assumed that the tissue within the control volume is a homogeneous porous matrix and the blood flow is uniform throughout. Another big assumption is that the thermal properties of the tissue and blood remain constant, even at different temperatures and pressures. With these assumptions, then, conservation of energy yields the following equation governing temperature of the control volume:

$$(\rho c_p)_t \frac{\partial T_t}{\partial t} = k_t \nabla^2 T_t + (\rho c_p w)_b (T_a - T_v) + q_m \quad (4.1)$$

where T_t is the temperature of the control volume (tissue), T_a and T_v are arterial and venous temperatures, respectively, q_m symbolizes metabolic heat generation, w_b is the blood perfusion rate and $(\rho c_p k)_t$ and $(\rho c_p)_b$ are the respective thermal properties of tissue and blood. For the purposes of this research, three other assumptions were made to simplify the model:

- (1) The temperature of the blood within the tissue is equal to the tissue temperature and likewise equal to the venous temperature.
- (2) The temperature of the arterial blood supply is equal to the core temperature, a constant.
- (3) The tissue under investigation has negligible metabolic generation. This is quite valid for normal skin and other protective tissues such as the epicardium and kidney cortex as well as phantom materials.

Adding these assumptions reduces the Pennes equation to:

$$(\rho c_p)_t \frac{\partial T_t}{\partial t} = k_t \nabla^2 T_t + (\rho c_p w)_b (T_a - T_t) \quad (4.2)$$

This, then, is the mathematical description of the heat transfer process used to

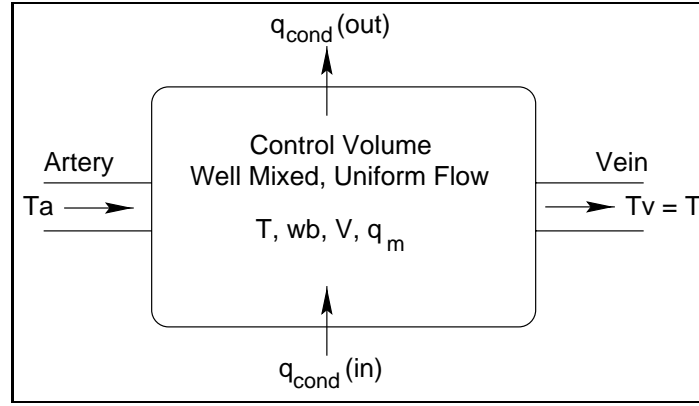


Fig. 4.3 Pennes Biothermal Control Volume

build a model for the effect of blood perfusion on temperature and heat flux within and from tissue.

The probe was mathematically described in much the same fashion. The probe is simplified to a homogeneous flat plate of representative material. In other words, it was assumed that the major material constituent (e.g. the substrate) dominates the thermal and physical characteristics of the probe, without regard to the differing layers or complexity of the probes as composite structures. In the case of probe design A1, this dominant material is Kapton and the thermopile itself, for the other designs the dominant material is aluminum. The sensor description contains no perfusion term and no heat generation. Assuming constant thermal properties the governing equation for temperature becomes:

$$(\rho c_p)_p \frac{\partial T_p}{\partial t} = k_p \nabla^2 T_p \quad (4.3)$$

where T_p is the probe temperature, and $(\rho c_p k)_p$ are the probe thermal properties based on the representative material.

The heat transfer between the sensor and skin at their interface is dominated by a contact resistance, R_c . The resistance can be due to both the macroscopic and microscopic differences in surface topography between the sensor and tissue. Also, this contact resistance can account for hair or skin imperfections. The heat flux across the probe-tissue interface is modeled as the temperature difference between the probe and tissue surfaces divided by the contact resistance.

$$q''_{cond} = \frac{1}{R_c} (T_t - T_p)_{interface} \quad (4.4)$$

This contact resistance can vary greatly between different applications, based upon characteristics such as individual sensor topography, type of tissue being monitored, or attachment pressure, for example. It represents an unknown within the model that must be calculated and changed with each individual application. Therefore contact resistance, a parameter of less interest to this study, but significant to the model, must be estimated along with the parameter of interest, blood perfusion.

Other heat flux quantities are also investigated, namely, convective heat flux off the top of the probe, and heat flux calculated within the probe. At times, convective heat flux, q''_{conv} , is measured experimentally instead of the above described conductive heat flux. The convective heat flux is modeled as the convection coefficient, h , times the temperature difference between the probe top surface, T_s , and the cooling air, T_∞ .

$$q''_{conv} = h(T_s - T_\infty) \quad (4.5)$$

Because the actual thermopile is sandwiched between a layer of foil and an aluminum sheet in the Bioprobe B configuration, it was theorized that calculating heat flux based on temperature differences within the probe might be more accurate than across the probe-tissue interface. Within the bioprobe model, this is found by

$$q''_{int} = \frac{k_p(T_L - T_{L-1})}{\Delta_L} \quad (4.6)$$

where q''_{int} is the internal heat flux, T_L, T_{L-1} the temperatures of the probe at positions L and $L - 1$, respectively, and Δ_L the distance between those two positions.

4.1.3 Solution Technique

The above model equations were solved numerically in two dimensions using a finite difference solution. Because of the nature of the problem and the complexity of the model (two different materials and noncontiguous boundary conditions) an analytical solution was not deemed practical. The finite difference technique used was an Alternating Direction Implicit method incorporating the Crank-Nicolson implicit procedure. As shown in Figure 4.2, the probe and tissue combination was divided into a cylindrical array of finite difference nodes, each surrounded by a control volume. Based on the symmetry of the sensor and physical model, it was assumed that the temperature is the same all along a particular radial position. Therefore the temperature field can be described in terms of temperature values at each value of radius from the probe center and depth from the probe top surface.

The derivation of non-dimensional nodal equations for this model is detailed in Michener (1991). The one difference in the current model is a change in boundary conditions over the probe surface. Michener (1991) based his model on a constant temperature boundary condition on the upper probe surface. The current model uses a convective boundary condition over the probe surface as explained in Section 4.1.1 above. This boundary condition was explored by O'Reilly et al. (1996), but mistakes were found in the coefficients for the finite difference equations. These mistakes were corrected to obtain the true, non-dimensional, coefficients for the nodes along the convective boundary. The finite difference equations can be solved implicitly using a tridiagonal matrix solution technique to obtain the temperature at each node for each moment in time. The heat flux across the interface is then calculated as per Eq. (4.4). The end result is a model that calculates the temperature field and heat flux based upon set values for the probe and tissue properties and the input of contact resistance and blood perfusion. The FORTRAN code for this model is given in Appendix A.

At this point some attention should be given to the treatment of convection in the model. In the ideal model, the convection is based on a convection coefficient between the cooling air and top sensor surface. This convection coefficient is a step function in time, being very low when no air flow exists and having some constant value h_{max} as soon as air flow is present. Experimentally, however, it can be seen that some finite amount of time exists over which the air flow rises from zero to the maximum amount of mass flow through the hose and jet housing. This implies some finite time during the beginning of air flow where the convection coefficient is less than its constant maximum value. Given the observation of a roughly linear progression of air flow from zero to maximum over the course of about 1.2 seconds, a piecewise function for the convection coefficient with respect to experimental time is incorporated into the model.

$$h = \begin{cases} 1.0 & : t < 0.0 \\ \frac{h_{max}-1.0}{1.2}t + 1.0 & : 0 \leq t \leq 1.2 \\ h_{max} & : 1.2 < t \end{cases} \quad (4.7)$$

Here, air flow is begun at time $t = 0.0$. This is an example of incorporating mathematics to ensure accurate modeling of the physical system. A true, robust theoretical model must account for experimental realities.

4.2 Parameter Estimation

The model described above is used in a parameter estimation scheme to calculate the input variables of contact resistance and blood perfusion based upon measurements of heat flux and surface temperature. Although many different forms of parameter estimation exist, the one described here is a gradient based method that has been successfully implemented for thermal applications. The parameter estimation process can be broken down into an evaluation of the model sensitivity to the desired parameters, definition of an appropriate objective function, and an iterative estimation procedure. While this document is not meant to provide thorough examination of such processes, brief descriptions of the mathematics and theory as they apply to the current problem are given in the following sections.

4.2.1 Sensitivity Coefficients

Of particular interest before starting any estimation procedure is the sensitivity of the theoretical model to various parameters. Sensitivity is defined as the effect that a change in a certain parameter has on the output variable. In this case, the output variables are heat flux and temperature. The parameters in question are blood perfusion, contact resistance, and the thermal and physical properties of the system. Sensitivities can be dependent on the state of the system and values of other parameters. These sensitivities are generally measured in terms of sensitivity coefficients, defined as the change in output due to a change in the parameter divided by that change in parameter. In other words, the sensitivity coefficient is the local partial derivative of the output with respect to the parameter. Mathematically, for the measurements discussed in this paper, the sensitivity coefficients for heat flux and temperature to some parameter β are:

$$X_{\beta,q} = \frac{\partial q''}{\partial \beta} \quad ; \quad X_{\beta,T} = \frac{\partial T}{\partial \beta} \quad (4.8)$$

For analytical models, finding X is a matter of applying the chain rule or some other formula to the continuous solution function. However, in a numerical solution that provides only discrete output, such as the one used here, the sensitivity coefficients must be found by a discrete perturbation. Namely:

$$X_{\beta,q} = \frac{\partial q''}{\partial \beta} \approx \frac{q''(\beta + \Delta\beta) - q''(\beta)}{\Delta\beta} \quad (4.9)$$

where the model is calculated with the parameter at some value β then calculated again at some value $\beta + \Delta\beta$ with $\Delta\beta$ being on the order of one percent of β . This is performed for both heat flux and temperature. In order to compare sensitivity to different parameters on a relevant scale, the X 's are nondimensionalized (normalized) based upon the maximum heat flux or temperature seen in the base case and the nominal value of the parameter.

$$X_{\beta,q}^+ = \frac{\partial q''}{\partial \beta} \left(\frac{\beta_o}{q''_{max}} \right) \quad ; \quad X_{\beta,T}^+ = \frac{\partial T}{\partial \beta} \left(\frac{\beta_o}{T_{max}} \right) \quad (4.10)$$

This allows the sensitivity coefficients to be plotted on the same axis and compared to one another, yielding information about the effect of each parameter on the model output.

Generally speaking, one would like the parameter perturbation to produce greater than a ten percent change in output ($X^+ > 0.1$) to be effectively used in a gradient method parameter estimation scheme. A low X^+ can lead to problems with convergence and resolution of accurate parameter estimates.

Another reason to inspect the sensitivity coefficients is to check for correlation among parameters. Correlation means that two or more parameters are linearly dependent upon one another. For example, say a heat flux is calculated with two parameters β_1 and β_2 by $q'' = a\beta_1 + c\beta_2$ where a,c are constants. Then for every change in β_1 there exists a comparable change in β_2 that will yield the same q'' . However, if $q'' = \beta_1 t + \beta_2$, t being a variable input, then this is not the case. There exist only certain combinations of β_1 and β_2 that will produce one q'' at each t. Sensitivity coefficient plots show linear correlation if one plot can be multiplied by a constant to produce the other. If two parameters are linearly dependent, or nearly so, they can not be estimated at the same time since no unique solution exists to the model. Also, problems can arise in estimating parameters that are nearly, but not completely linearly correlated. Programs for calculating X^+ and X for parameters in the previously described model are provided in Appendix B.

4.2.2 Estimation Procedure

Objective Function

As mentioned in the literature review, one of the more popular parameter estimation schemes for thermal analysis is Gauss minimization with the Box-Kanemasu modification. As with most parameter estimation schemes, this method attempts to adjust model parameters to obtain a match between model output and experimental data. This match is

achieved by the minimization of an objective function that relates model and experimental data. The objective function used for this purpose is a sum of squares error between calculated and measured data:

$$S = \sum_{i=1}^N \frac{(q''_{m_i} - q''_{c_i})^2}{\sigma_q^2} + \sum_{i=1}^N \frac{(T_{m_i} - T_{c_i})^2}{\sigma_T^2} \quad (4.11)$$

with q''_c, T_c and q''_m, T_m the calculated and experimental heat flux and surface temperature, respectively. The variance of the heat flux or temperature experimental data is denoted by σ^2 . Note that S is dimensionless, allowing the addition of heat flux and temperature terms. In most previous work (Walker and Kilpatrick, 1987; Scott and Beck, 1992a,b; Moncman et al., 1995; Saad and Scott, 1996; Park et al., 1997) only one dependent variable, namely temperature, is present in S . This research represents an innovation in that heat flux is also considered in the objective function.

Examination of the objective function is also an important step before using a parameter estimation procedure. A very flat S (corresponding to low X) means that a minimization routine will have trouble finding one distinct minimum value. On the other hand, if S is too curvaceous a minimization procedure might converge on a local minimum rather than the overall minimum of S . Ideally, S will contain a steep curve with one distinct minimum point. A program that uses the model to calculate S for inspection purposes is given in Appendix B.

Box-Kanemasu Parameter Estimation

The goal of any parameter estimation scheme is to minimize this objective function efficiently. Gauss minimization is a gradient based method that accomplishes this task. This method can be modified to produce the Box Kanemasu method which attempts to efficiate the Gauss minimization. Both of these methods are detailed in Beck and Arnold (1977). A brief overview is presented here.

The Gauss method finds the minimum of S by setting the derivative of S with respect to the estimated parameter vector, β to zero. For Eq. (4.11) this process yields:

$$\nabla_{\beta} S = \frac{2}{\sigma_q^2} [-\nabla_{\beta} \mathbf{q}_c''^T(\beta)] [\mathbf{q}_m'' - \mathbf{q}_c''(\beta)] - \frac{2}{\sigma_T^2} [-\nabla_{\beta} \mathbf{T}_c^T(\beta)] [\mathbf{T}_m - \mathbf{T}_c(\beta)] \quad (4.12)$$

Notice that $\nabla_{\beta} q_c(\beta)$ and $\nabla_{\beta} T_c(\beta)$ are the matrices of sensitivity coefficients for q

and \mathbf{T} :

$$\mathbf{X}_q(\beta) = [\nabla_\beta \mathbf{q}_c''(\beta)]^\top \quad (4.13)$$

$$\mathbf{X}_T(\beta) = [\nabla_\beta \mathbf{T}_c^\top(\beta)]^\top \quad (4.14)$$

Here, two approximations are made. First, the sensitivity vectors in Eqs. (4.11) and (4.12) are approximated by $\mathbf{X}_q(\mathbf{b})$ and $\mathbf{X}_T(\mathbf{b})$ respectively where \mathbf{b} is an approximate of β . Second, $\mathbf{q}_c''(\beta)$ and $\mathbf{T}_c(\beta)$ are approximated by the first two terms of a Taylor series expansion about \mathbf{b} . Substituting these approximations into Eq. (4.12) along with $\beta = \mathbf{b}^{k+1}$ and $\mathbf{b} = \mathbf{b}^k$ and solving for \mathbf{b} leads to the Gauss iterative estimate of \mathbf{b}^{k+1} given a previous value of \mathbf{b}^k as follows:

$$\mathbf{b}^{k+1} = \mathbf{b}^k + \Delta \mathbf{b}^k \quad (4.15)$$

where $\Delta \mathbf{b}^k$ is found by

$$\Delta \mathbf{b}^k = \left[\frac{1}{\sigma_q^2} \mathbf{X}_q(\mathbf{b})^\top \mathbf{X}_q(\mathbf{b}) + \frac{1}{\sigma_T^2} \mathbf{X}_T(\mathbf{b})^\top \mathbf{X}_T(\mathbf{b}) \right]^{-1} \cdot \left[\frac{1}{\sigma_q^2} \mathbf{X}_q(\mathbf{b})^\top (\mathbf{q}_m'' - \mathbf{q}_c''(\mathbf{b})) + \frac{1}{\sigma_T^2} \mathbf{X}_T(\mathbf{b})^\top (\mathbf{T}_m - \mathbf{T}_c(\mathbf{b})) \right] \quad (4.16)$$

In the Box-Kanemasu modification, the change in the parameter vector is modified by an iteration dependent scalar, d^{k+1} . This scalar attempts to increase or decrease the step size based on the distance of the system from a solution, allowing for quicker convergence. The iterations on \mathbf{b}^k are continued until the parameters converge or some predetermined maximum number of iterations is finished. The criterion for determining convergence is based on the change ratio of the current and previous iteration estimates.

$$\frac{\mathbf{b}^{k+1} - \mathbf{b}^k}{\mathbf{b}^k} \leq 0.001 \quad (4.17)$$

A general program was written to implement the Gauss minimization and Box-Kanemasu modification for any number of parameters and up to two dependent variables. The program reads in data from a formatted text file and uses the direct method of Gauss estimation to arrive at Gaussian parameter estimates. A flag in the program determines if these estimates are used or if the calculations proceed to the Box-Kanemasu modification. The output is a file containing the parameter estimates, confidence intervals, and the value of S at each iteration along with the measured and calculated data using the final estimates after convergence. The FORTRAN code for this general program, called 'BoxKan' is provided in Appendix C, as well as a sample format for the input file.

Sequential and Whole Domain Methods

Two common ways of implementing Gauss Minimization are the sequential and whole domain methods. In the sequential method, the parameter estimates are updated for every data point. In other words, the data and calculated values are considered one value at a time with the estimates being changed slightly based on agreement or non-agreement of that one comparison. This requires a sub-iteration to recalculate the model values at the current time step for each data point. The estimates at the last time step will have seen all the previous modifications and therefore represent the best estimates for the overall iteration. The flowchart in Fig. 4.4 illustrates this process.

In many cases the sequential method leads to quicker convergence of the system. However, it requires calculation of different model values not once per iteration, but as many times as there are time steps since the estimates are updated at each time step. For an analytical model, this is not a problem because current calculated values are independent of previous values calculated with different estimates. However, in an iterative model such as a finite difference or finite element solution the current time step calculations are dependent on previous values. Those previous values must be calculated using the same estimates. Therefore, the sequential method requires recalculation of the model from the beginning through to the current time step for each data point. For example, if 600 data points are used, instead of only calculating through the model once per iteration, an iterative model must be calculated close to 300 times by the end of just one overall Gauss iteration. This leads to large computational lengths of time.

The whole domain method uses all the data at once to derive one estimate per Gauss iteration. All the model values are calculated using the same estimates and then these values are used to find the appropriate change in estimates to lower the objective function. This allows for only one calculation of the model values per iteration. This may take a few more iterations to converge, but with an iterative model solution it is much faster because of the lesser required progressions through the model itself.

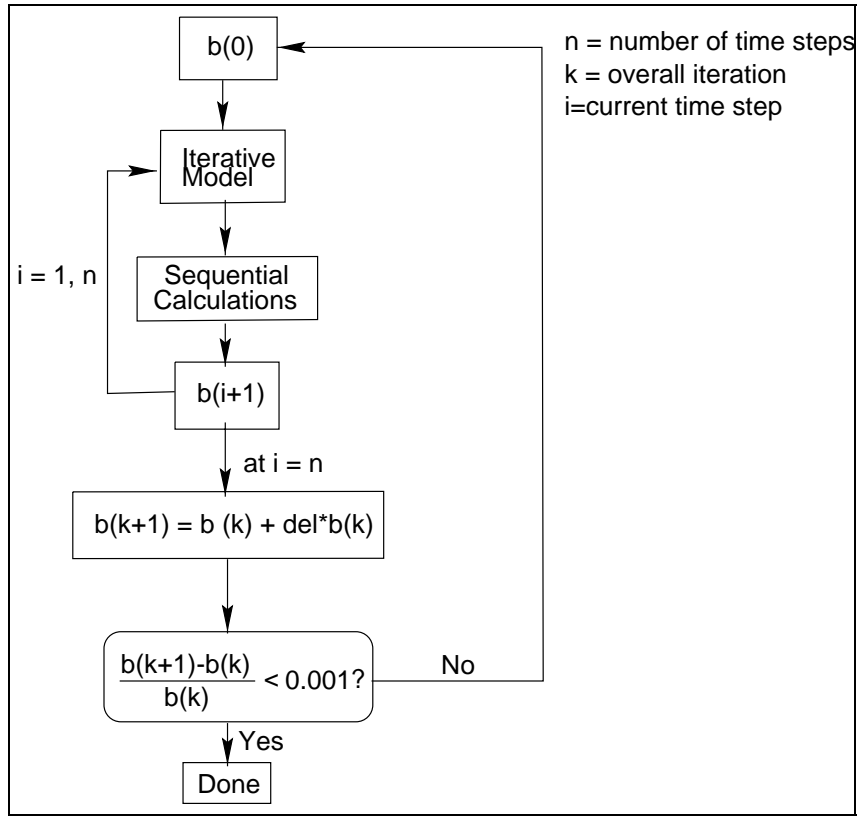


Fig. 4.4 Flow Chart of Sequential Estimation Process

4.2.3 Error Estimation and Confidence Intervals

Error Estimation

Confidence intervals for individual estimates obtained with the Gaussian or Box-Kanemasu method are calculated by the sensitivity coefficients and the probabilities within a normal distribution. For a 95 percent confidence interval around an estimate vector, this is:

$$\beta = \mathbf{b} \pm \left[\frac{1}{\sigma_q^2} \mathbf{X}_q(\mathbf{b})^\top \mathbf{X}_q(\mathbf{b}) + \frac{1}{\sigma_T^2} \mathbf{X}_T(\mathbf{b})^\top \mathbf{X}_T(\mathbf{b}) \right]^{1/2} \cdot 1.96 \quad (4.18)$$

where ‘1.96’ is the value of the 95 percent probability density based on the normal distribution. This formula describes the possible amount of variation in the estimates due to the estimation procedure and model. However, this formula assumes the only sources of error are changes in the parameters being estimated and the variance of the experimental data (noise). For a true measure of confidence in the estimates, possible errors from other areas must be considered. These errors can come from uncertainties in quantities set as

known in the model or uncertainty of the way in which certain phenomena are modeled. For example, the ‘known’ parameters of thermal properties for tissue and blood and the physical measurements of the probe are set as constants in the current model. But just like the unknown, estimated parameters, changes to these ‘known’ parameters can change the calculated output of the program. Uncertainty in these parameters must be included to gain a better measure of the error associated with each estimate.

The known parameter uncertainty is included by using the sensitivity of the model to the parameters in question to calculate an overall expected standard deviation for the model output. To obtain the standard deviation of model output based on one parameter, the uncertainty of the parameter, expressed as a standard deviation, is multiplied by the sensitivity coefficient of the output variable with respect to that parameter (Moffat, 1988). For example, the expected deviation of heat flux due to the i^{th} parameter is

$$\sigma_{b_i,q} = X_{b_i,q}^- \sigma_{b_i} \quad (4.19)$$

where X^- is a time averaged sensitivity coefficient. The sensitivity coefficients as described above are functions of time as well as the values of the other model parameters. The parameter estimation routine steps through a data set, revising its estimates with information taken from each discrete data point and corresponding model value. As such, it looks at the individual sensitivity coefficient values for each step in time. For Eq. (4.19) however, one averaged sensitivity coefficient over the entire time range is needed. This is found by time averaging the sensitivity coefficients using the time step between measurements, Δt and the overall time of the observed period, τ .

$$X_{b_i,q}^- = \frac{\Delta t}{\tau} \sum_{t=0}^{\tau} \frac{\partial q''}{\partial b_i}(t) \quad (4.20)$$

The expected standard deviations due to all the parameters in question are lumped into one overall standard deviation by taking the square sum of each individual contribution. For the heat flux example,

$$\sigma_{q,known} = \left[\sum_{i=1}^n \left(X_{b_i,q}^- \sigma_{b_i} \right)^2 \right]^{1/2} \quad (4.21)$$

where n is the number of known parameters under investigation.

The error estimate is arrived at by including the square of this standard deviation, σ_{known}^2 , in with the variance of the experimental measurements. This gives overall variances

of

$$\sigma_{q,tot}^2 = \sigma_q^2 + \sigma_{q,known}^2 \quad ; \quad \sigma_{T,tot}^2 = \sigma_T^2 + \sigma_{T,known}^2 \quad (4.22)$$

The quantities $\sigma_{q,tot}^2$ and $\sigma_{T,tot}^2$ are used in the parameter estimation process, especially for the calculation of the confidence interval, replacing σ_q^2 and σ_T^2 in Eq. (4.18) above. This then, gives a much more realistic measurement of the expected error attributed to each individual parameter estimate for the unknown parameters of interest. A much more detailed explanation of this process is given by Emery and Fadale (1996).

Confidence Intervals

Of further interest is determining the overall confidence interval for a group of parameter estimates. This is brought about by the need for estimation observations for many experiments under similar conditions in order to establish repeatability. Even under the same conditions, measurements from different experiments will exhibit some variation due to experimental error and random elements. For example, measurements of heat flux taken in nine different experiments for the same flow rate and initial temperature will be slightly different due to random error. These measurements will in turn lead to nine slightly different parameter estimates. Just as the error estimate gives a measure of the possible variability for an individual estimate, the confidence interval calculated for a group of like estimates gives a measure of the variability between experiments. This tells the overall expected range for an estimate around a particular true value.

The confidence interval for a group of estimates can be thought of as a probability region for the mean value of an estimate made under similar conditions. This value is calculated regardless of the error estimate for the individual observations since each observation is considered its own mean and the two are not correlated. The 95 percent confidence interval is found by the standard Student's-t formula:

$$CI = \bar{x} \pm t(.025, n - 1) \left(\frac{s}{\sqrt{n}} \right) \quad (4.23)$$

where \bar{x} is the average of all the observations, s is the standard deviation around the average, and n is the number of observations. The variability of each individual observation is slightly accounted for in the fact that with higher individual variability, the observations will naturally be more spread out. This leads to a larger standard deviation calculated for the group and likewise a larger overall confidence interval.

Chapter 5

Experiments

Six different types of experiments were completed in the course of this research. They included experiments to determine the convection coefficients of each probe, probe A1 and A2 experiments on live subject forearms, and experiments with probe B on live subject forearms and two different tissue phantoms. Two different data acquisition setups were employed, one for the probe A1 and A2 experiments, and a newer setup for the probe B experiments.

This chapter describes both data acquisition setups as well as the procedures and other equipment used to collect experimental data for a variety of situations. Two categories of experimental procedures are detailed; uncontrolled perfusion experiments on live subjects and controlled perfusion experiments with tissue phantoms. The relevant experiments are then described with information about the measurements taken and the test conditions including initial temperature, air temperature, and core fluid temperature. Also discussed within these sections are the derivation and sources of the property values used for the perfuse tissue in each of the experimental setups.

5.1 Setups

5.1.1 Data Acquisition

As the project under discussion progressed, several types of hardware were configured for the acquisition of heat flux and temperature data. Two data acquisition configurations were used, one for preliminary experiments with the A probes and one for more refined

experiments using the B probes. Although not much effort was given to comparing these two systems beyond relative user friendliness, a description of both set ups is given here for documentation purposes.

Previous System

The data acquisition system used for the preliminary tests with the A type probes is the same as that used in O'Reilly et al. (1996); Gonzales (1995). The RdF heat flux sensor leads are attached to a Vatell amplifier built specifically for heat flux sensors. Output from this amplifier is connected to a Hewlett Packard 3562A Data Acquisition System (HP DAS) that performs filtering, resolution, and analog to digital (A/D) conversion on the voltage signal. The HP DAS also contains a disk drive to record captured data, but in the HP operating system format (different from DOS or Unix). The leads from the type K thermocouple in the HFS-3 are connected to their own type K thermocouple amplifier, made by Omega. The output from this amplifier is also connected to the HP DAS. A type T thermocouple is connected to a stand-alone Doric Trendicator temperature measurement device. This thermocouple is inserted into the air jet housing to measure the cooling air temperature, T_∞ . The Doric has internal hardware that performs all the compensation and linearization necessary for the thermocouple so that the device's output is a digital display of the actual temperature reading to 0.1 degrees Celsius. Figure 5.1 provides a flow chart of this data acquisition set up.

Since no hardware was available to linearize and compensate the type K thermocouple, its voltage signal had to be referenced to some known prior to any experimentation. This was accomplished by linearizing the type K voltage output with the Doric output. However, assuming that the Doric is well calibrated, linearizing the type K output with the Doric output will produce decent absolute temperature measurements for a limited range. The linearization was performed by immersing both the type K and T thermocouples in first a cold water then a warm water bath. After being allowed to settle in the cold water bath until no noticeable changes in output signal remained, the temperature off the Doric and the voltage output of the type K thermocouple were recorded. This was repeated for the hot water bath. It was assumed that the voltage output with respect to temperature of the type K thermocouple is linear over this range. Then, based on knowing the voltage output and temperature (taken from the Doric) of the two endpoints, a liner relationship between

K thermocouple voltage, E_k , and temperature, T_k , was calculated as shown in Table 5.1

So now the voltage acquired from the type K thermocouple can be converted into temperature. The HFS-3 voltage is converted to heat flux as per its calibration coefficient given in Table 3.2.

Current System

A diagram of the current DAQ system is given in Fig. 5.2. This current system is a little more refined and user friendly than the previous. The purchase of a Pentium Pro Dual processor computer allowed for data acquisition, reduction, and model computation all within one system. For the purpose of the heat flux and temperature measurements, a Keithley DAS-TC board was purchased and installed in the computer. Along with this hardware, Test Point software was installed to control the board and data acquisition process. The DAS-TC board can be set to accept both thermocouple and small voltage input without the need for external amplification. The hardware performs cold junction compensation and linearization based upon thermocouple type. The board also performs the required A/D conversion. The heat flux sensor and surface thermocouple are wired directly into an isolated, isothermal terminal box which is connected to the DAS-TC board in the computer via a shielded ribbon cable. The board itself is insulated and shielded from interior computer noise. So for the current experiments, the DAS-TC board outputs a temperature value, in C, and a voltage value for each measurement in time. The Test Point software reads these values, formats the data, and writes the formatted data to an ASCII file on the DOS (Windows) system. Test Point also provides real-time graphs and control of the data acquisition process.

In addition to this hardware, an Omega thermocouple reader was used in the same

Table 5.1 K Thermocouple Linearization Data

Cold Bath	K TC Voltage	Doric (T TC) Temperature
Hot Bath	58.5 mV	21.0 C
	132.2 mV	38.9 C
Resulting Equation	$T_k = \frac{E_k - a}{m} + c$ with $m = \frac{132.2 - 58.5}{38.9 - 21.0} = 4.11 \text{mV/C}$ $a = 58.5 \text{mV}$ $c = 21.0^\circ\text{C}$	

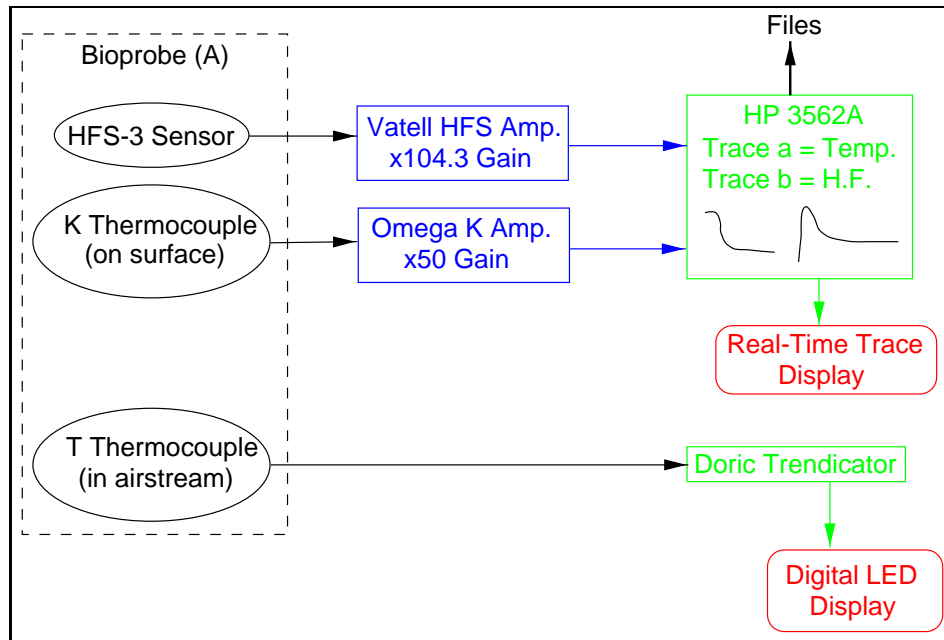


Fig. 5.1 Diagram of Previous HP Data Acquisition Set Up

capacity as the Doric Trendicator in the old system. A type-K thermocouple was placed in the air jet housing to measure the air flow temperature. The Omega reader contained a LED display of the temperature reading. Since both the thermocouples were calibrated fairly well on their own for absolute measurements, no cross linearization was deemed necessary as with the old system. In a truly proper system, the air temperature thermocouple would be of the same type as the surface thermocouple, and be wired into the DAS-TC board as well. However, the logistics of the supplied equipment did not make this feasible within a timely manner. Since air temperature is considered as an average value, its measurement separate from the other data should not largely effect the experimental results.

The following Table 5.2 compares the settings and/or defaults used when collecting data with both the HP-DAS and PC systems. The fact that a certain option may have been used on one system and not the other does not imply that the other system can not perform that function. Rather, that option was not designated necessary for the application. The sampling rates differ simply because the data acquisition hardware has preferred sampling rates and it was thought best not to change those settings. Windowing is a form of very high and low frequency magnitude adjustment that reduces the effect of certain frequencies on the signal, without taking them out entirely. Hanning is the standard windowing for

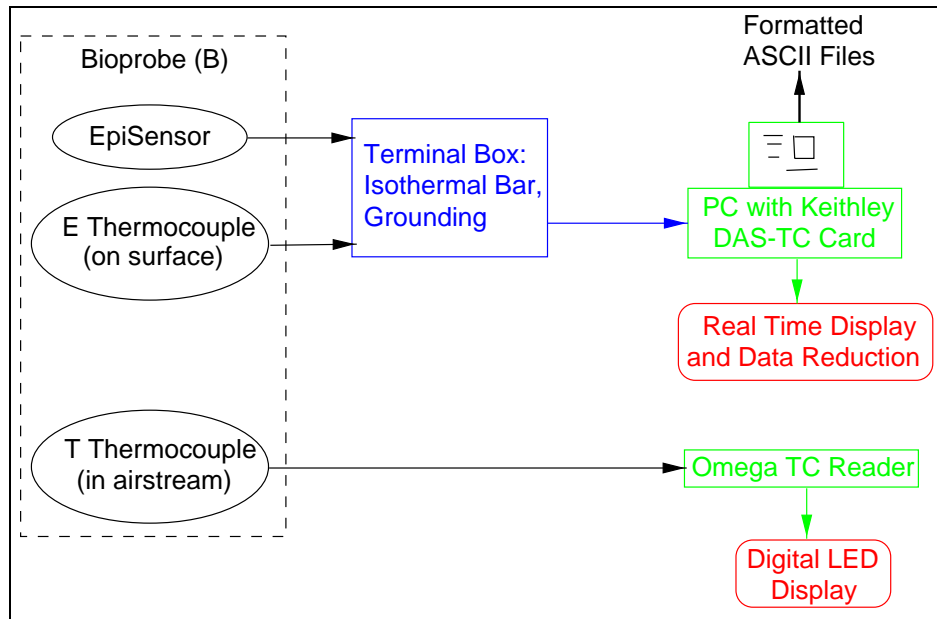


Fig. 5.2 Diagram of New, PC-Based Data Acquisition Set Up

data acquisition and is used here. These settings apply to all the following experimental discussions, unless explicitly otherwise noted.

5.1.2 Convection Coefficient Experiments

One important model parameter not dependent solely on material properties is the convection coefficient, h . The convection coefficient is a measure the effectiveness of the air jets at cooling the upper side of the sensor. This quantity is dependent on the geometry

Table 5.2 Comparison of Data Acquisition Settings

Setting	HP-DAS	PC-DAS
Sample Rate (Hz)	32.0	9.5
Windowing	Hanning	Hanning
Filtering	None	None
Anti-Aliasing	Yes	No
Averaging	None	None
Dynamic Range Amplification:	± 1.0 V	-6.25-25.0 mV
Heat Flux Sensor	104.3	None
Thermocouple	50.0	None

and flow characteristics of an individual system. Therefore, it must be calculated for each different probe design so that a correct convection coefficient can be included in the model calculations for the experiments.

The convection coefficient was measured empirically by using the bioprobes themselves. In the case of both probes A and B the sensors were flipped so that the heat flux gauges and surface thermocouples were on the upper side being directly impinged by the air jets. This allowed for the measurement of heat flux off the cooling surface, convective heat flux (as opposed to conductive heat flux measured when the sensors are on the lower side) and the cooled surface temperature. For the purposes of setting up a known, fairly steady-state process, the probes were placed on a hot plate kept at an approximately constant temperature. The air flow was turned on and measurements of convective heat flux (q''_{conv}), surface temperature (T_s), and air stream temperature (T_∞) recorded over time. The tests lasted about one minute. Only the quasi-steady-state data (after approximately 10 seconds) were used to calculate the convection coefficient according to the formula:

$$h = \frac{q''_{conv}}{T_s - T_\infty} \quad (5.1)$$

The convection coefficient of each test was taken as the average h from all the recorded data points. Two such tests were done using a heated copper block as the hot plate for the A2 probe. For convection coefficient tests with the B probe, a controlled hot plate (Fisher Scientific Porcelain-Top Stirring Hotplate) was used as the heat source with three successive tests performed with the hot plate control on different heat level settings. Table 5.3 summarizes the overall coefficient calculations for the probe A2 tests and each of the three different probe B tests.

Because these are average empirical estimates, and as will be seen later, small changes

Table 5.3 Convection Coefficients for Each Probe Type; Air supplied to the probe via the 1.27 cm air hoses at a wall pressure of 70 kPa.

Probe Type	Sample Rate (Hz)	$q''_{nominal}$ (W/m ²)	$h_{average} \pm$ STD (W/m ² K)
A: Overall	32 Hz	5,000	718.32
B: Test 1	9.5 Hz	600	466.00 \pm 12.70
B: Test 2	9.5 Hz	6,000	582.17 \pm 23.29
B: Test 3	9.5 Hz	12,500	588.85 \pm 21.24

in the convection coefficient do not have large contributions to the model output, some liberty was taken in choosing a ball-park figure to use as the h value in the model. The coefficient for the A probe was rounded off from the test averages. In the bioprobe B experiments the expected values for q'' were in the range of 1200 W/m². Therefore the convection coefficient for the B probe was calculated by linear interpolation between the lower and middle heat flux magnitude cases to find h at this q'' value. Based on these observations the convection coefficients used for all following calculations involving the biothermal model were set to:

Probe A: $h = 700$ W/m²K

Probe B: $h = 480$ W/m²K

5.2 Experimental Procedures

5.2.1 Arm Experimental Procedure

At this point, two general experimental procedures for the estimation of blood perfusion must be explained. One, experiments taken on live subjects and two, controlled experiments performed with phantom materials. These two procedures are explained in general here, with the details of particular experiments being added in later sections.

The live experiments were performed on human forearms. These were uncontrolled experiments in that no invasive procedure was performed alongside the noninvasive procedure discussed here, nor was any attempt made to physically alter the physiology of the subjects. The test procedure was similar to that of Fouquet et al. (1993); O'Reilly et al. (1996). The blood perfusion probe was held steady on the interior forearm, but with low enough pressure that the skin was not indented. The probe was placed on a spot away from excessive hair or any obvious large blood vessels. In some cases with Probe A, the probe was lightly held to the skin with tape. In tests with Probe B, the probe was lightly held to the skin by an elastic band around the arm and probe. Figure 5.3 displays a picture of the placement of probe B on a subject's forearm.

After a period of settling and/or equilibrium (different for some experiments), the cooling air was turned on for approximately one minute. During this minute, the heat flux and gauge surface temperature were recorded with the in use data acquisition system. Data logging was stopped prior to shutting off the cooling air. The temperature of the air within

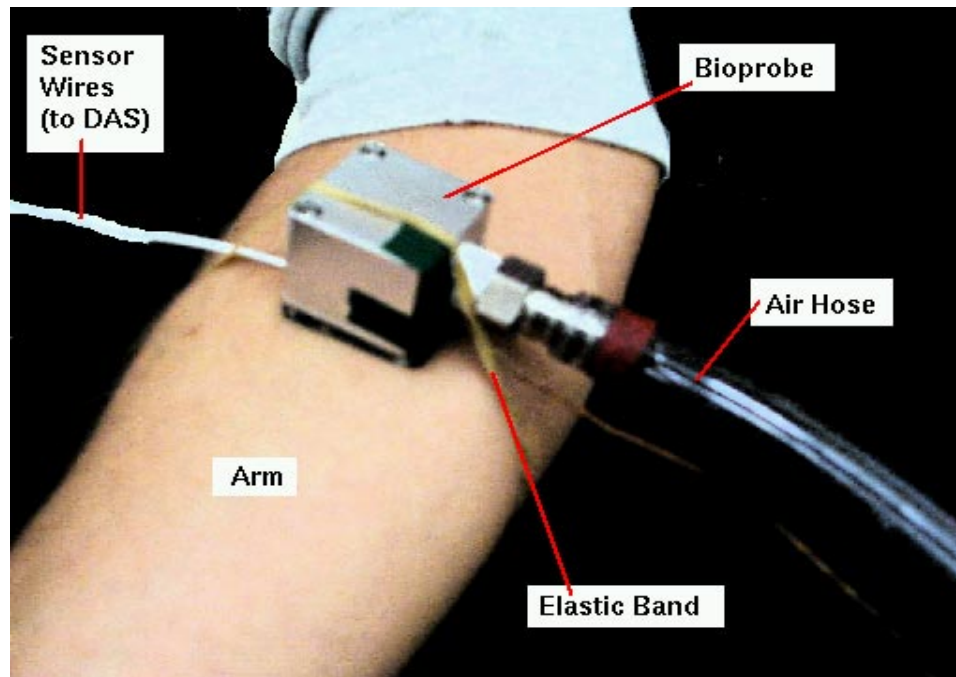


Fig. 5.3 Picture of Arm Experiment: Probe Placement

the housing was recorded by hand just after the cooling air was turned on and at the point that data logging was ended. These two measurements were used to compute the average air temperature during the course of the test. Also, the body core temperature was recorded at the end of the test by a thermocouple placed under the subject's tongue.

Tissue Properties

No experiments were performed to find true values for the physical and thermal properties of the subject's skin tissue or blood. Rather, reported averages were taken from literature for skin tissue conductivity and thermal diffusivity (Ott and Vari, 1979) and blood density and specific heat (Yang, 1989). The values used in this research for these quantities are summarized in Table 5.4.

5.2.2 Phantom Experimental Procedure

In order to verify the process of measuring blood perfusion with heat flux signals, a procedure had to be developed where the perfusion could be visualized and controlled. Controlling the perfusion rate and temperature of fluid through some media simulating tissue would

Table 5.4 Skin and Blood Properties

Property	Value	Units
Blood Density	1000.0	kg/m ³
Blood Specific Heat	4000.0	Jkg/K
Skin(Epidermis) Conductivity	0.50	W/mK
Skin(Epidermis) Diffusivity	1.5×10^{-7}	m ² /s

allow for a check of the process by observing if the heat flux signals change with a change in set perfusion rate. Also, if the parameter estimation scheme uses the experimental data to produce an estimate of perfusion, this estimate can be checked against the known rate to verify the process.

For this purpose, an experimental set up was designed to control the perfusion rate of heated water through some phantom material and allow dry surface measurements with the bioprobe. This set up is as follows.

A water-tight Plexiglas box holds a square sample of porous media acting as a phantom for a capillary bed or other perfuse tissue. The box sandwiches the media, about 2.54 centimeters thick, between a metal plate and a removable top piece. The metal plate is solid except for one hole in the center about 1.91 centimeters in diameter. The removable top is made of Plexiglas and acts to hold down the media. It contains a large hole in the center that allows for the placement of the bioprobe on the center top surface of the media. Four threaded rods with wing-nuts hold the box top-media-metal plate assembly together. Water flows in the bottom of the box and up through the hole in the metal plate that forces the flow up through the center of the media. The water then flows out holes along the top edges of the box sides. This creates a uniform flow of water upwards through the media then outwards from the center. This flow pattern attempts to simulate a uniform, multi-directional flow as assumed in the biothermal model, eliminating possible effects on the temperature field, and thereby the heat flux profile, due to directional flow patterns. The desired flow pattern is depicted in Fig. 5.4. The box extends below the metal plate for a distance of 7.62 centimeters to allow space for the water flow to become steady before it reaches the metal plate.

Water flow is provided by a peristaltic pump, such as the type used in dialysis and other biological, sterile pumping situations. A peristaltic pump uses rollers to pinch some

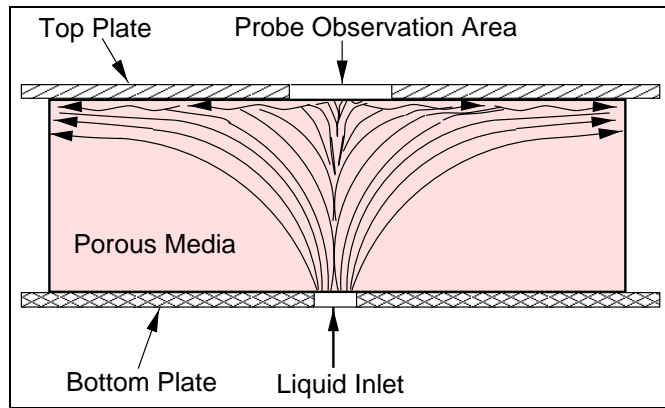


Fig. 5.4 Desired Flow Pattern Within Phantom Media (Two Dimensional View)

tubing. These rollers move along a small section of the tubing, causing fluid flow to follow the compressed area. This displaces all the fluid in the tubing creating a net movement that draws fluid in one end and pushes it out the other. The advantage of this pump is that no machine parts ever come into contact with the liquid. This eliminates the problems of contamination of the water flow and heating or cooling of the water by the pump. The one disadvantage of this pump is that the flow is pulsatile and not as steady as flow from an impeller or other style pump. The peristaltic pump has a motor control that allows the operator to set the pump speed, and therefore the flow rate. Flow rate is determined by both the pump speed and the size of the tubing used for the water flow.

The Plexiglas box assembly is immersed in a water bath kept at a constant temperature. To simulate in vitro conditions, this temperature is kept at around thirty seven degrees Celsius. The water bath is heated by an immersed resistance heater controlled by feedback circuitry. A thermistor monitors the temperature of the water and the circuitry triggers the heater on and off based upon the proximity of the measured temperature to the set point. The set point is adjusted by a variable resistor. The circuitry is designed to provide a constant temperature with minimal over and undershooting (high damping). The water bath is kept mixed by a magnetic pump that pulls water from the bottom of the bath and circulates it to the top of the bath. A stand alone thermometer is immersed in the bath so that the operator can monitor and record the true bath temperature.

Water is taken from the bath by the peristaltic pump to flow through the media/box

assembly. The outflow from the box flows freely back to the bath. The top of the media is covered by a layer of plastic wrap that prevents water flow from continuing out the top, simulating skin. The bioprobe is placed within the hole in the removable top and lightly held in place with some tape. The probe is further encased in a thin plastic bag to prevent wetting from any bath water that may spill over the top of the box. Holes in the top of the plastic bag allow for the escape of the cooling air.

The experimental set up, minus the water bath, is sketched in Fig. 5.5. The actual equipment is shown in the pictures of Figs. 5.6, 5.7, 5.8.

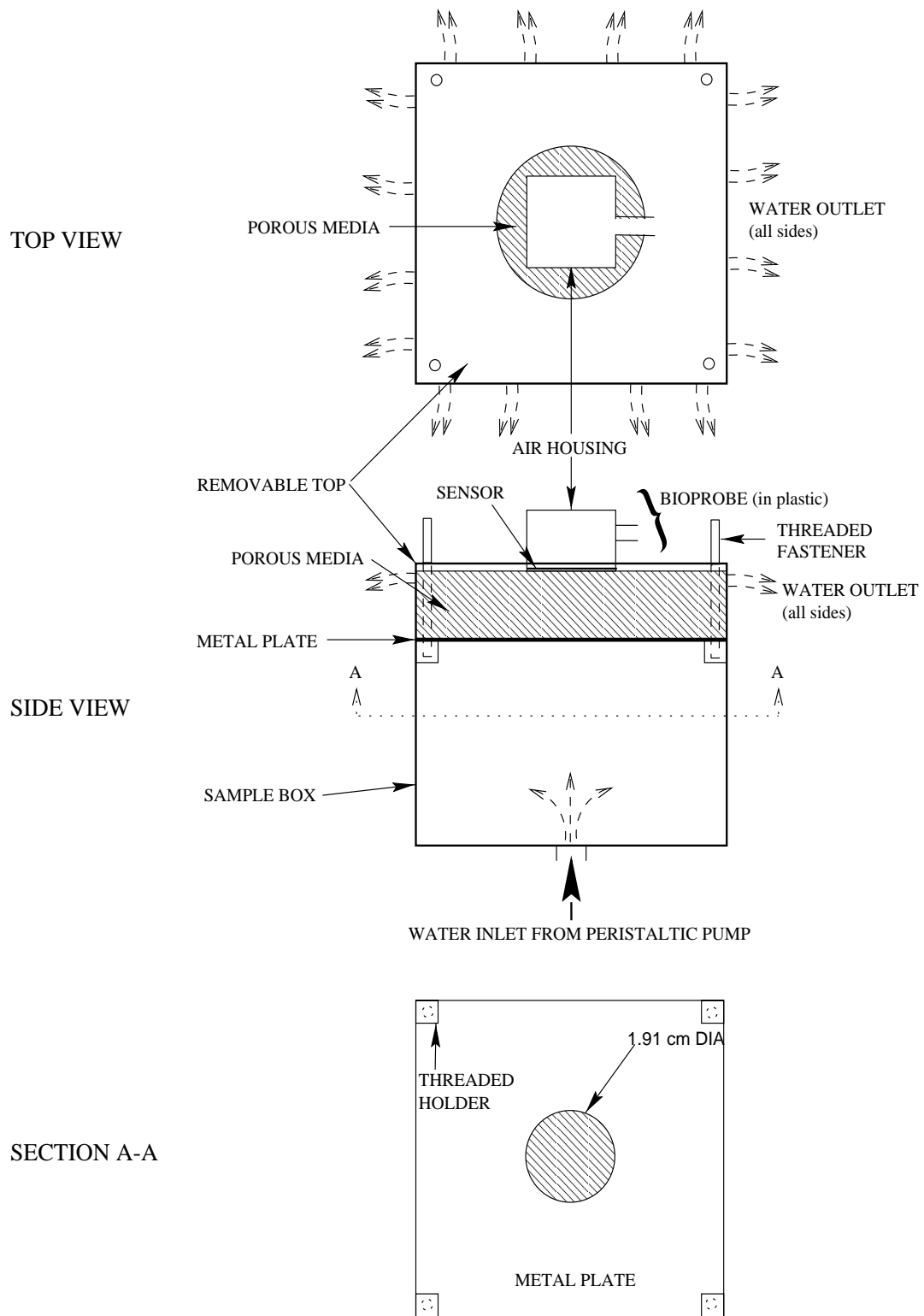


Fig. 5.5 Diagram of Phantom Experimental Set Up

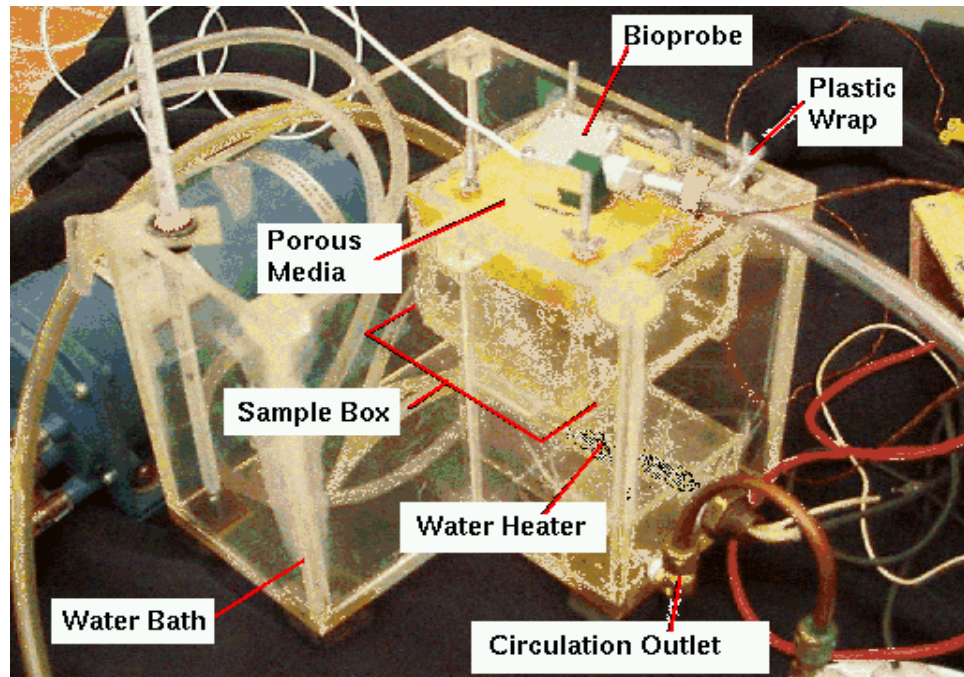


Fig. 5.6 Picture of Phantom Experimental Set Up, Water Bath

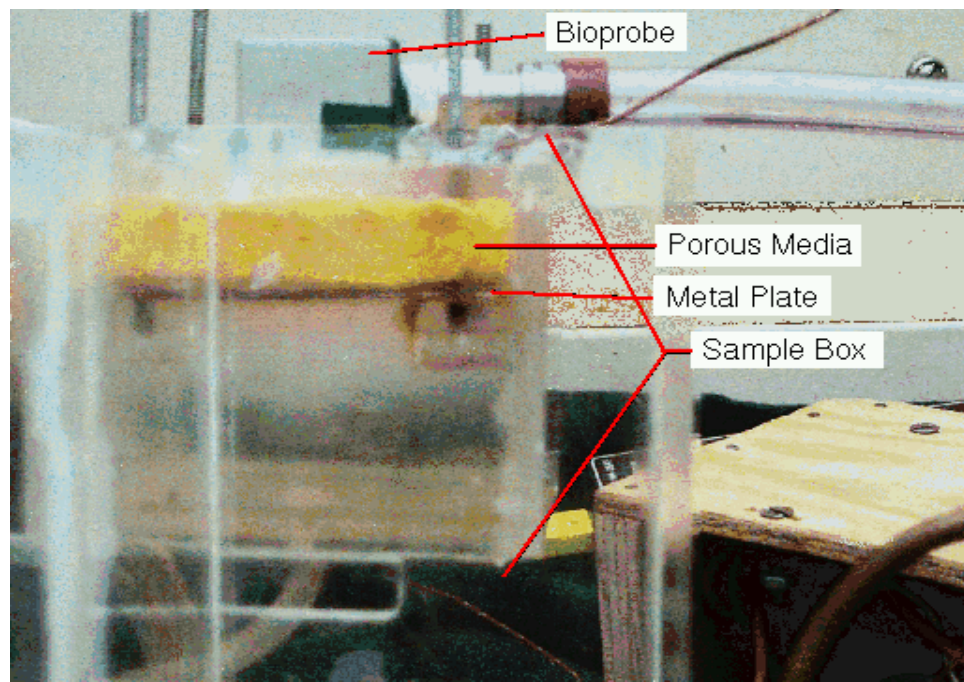


Fig. 5.7 Picture of Phantom Experimental Set Up, Sample Box

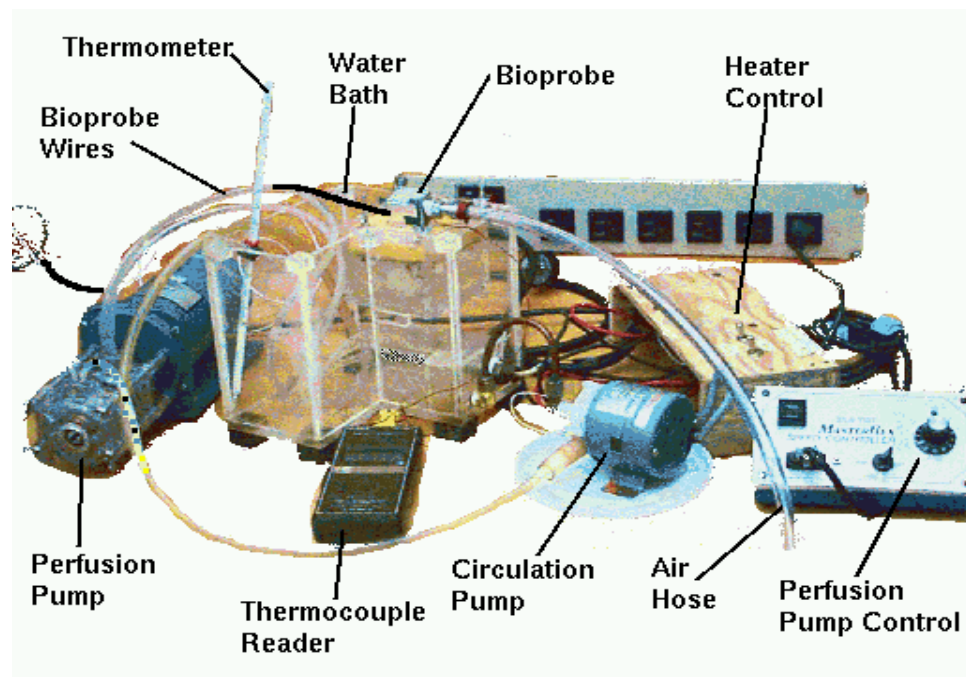


Fig. 5.8 Picture of Phantom Experimental Set Up, Equipment

5.3 Kapton Experiments (Probe A1)

Experiments were performed with the A1 probe configuration to gain repeatable and more detailed data of the type found in earlier work with the bioprobe (O'Reilly et al., 1996; Gonzales, 1995). Ten different tests with two subjects, five tests on each subject, were completed using the arm experimental procedure. Eight tests were one minute in duration and two were two minutes in duration. The two-minute tests were performed to check for any changes in system response at longer times. For each test, the probe was placed on the arm for at least five minutes and until the temperature and heat flux curves reached a steady value (thermal equilibrium). Then the air was turned on. For these tests, the original 0.635 centimeter air hose was used with an air pressure of 280 kilopascals. Data were collected using the HP-DAS equipment. The test names and initial conditions are summarized in Table 5.5 where T_i , T_{core} , T_∞ are the initial gauge surface temperature at equilibrium, the subject's core temperature, and the cooling air temperature, respectively.

Other experiments included trials with the settling condition to try and obtain heat flux curves similar in shape and magnitude to those reported by Gonzales (1995). Settling condition describes the time allowed for the probe to equilibrate on the tissue and any treatment of the probe prior to its contact with the measured tissue area. The previous experiments did not match either the Gonzales experiments or the model very well. No attention was given to the initial, air, or core temperatures in these experiments as they were not meant to be used as actual data. The goal was to find a settling condition leading to experimental data that more closely matched the model. Table 5.6 summarizes the initial probe application methods for these experiments, labeled as 'Trials'. These experiments led into the A2 probe configuration.

5.4 Kapton-Aluminum Experiments (Probe A2)

Three tests were completed with the A2 probe configuration. These tests were a continuation of the last A1 experiments to resolve a proper settling time procedure. It was also a step towards both checking the effect of increased probe capacitance and simulating the then being designed Episensor probe (probe B). For these three tests, the 0.635 cm hose provided air flow at 280 kPa. The HP-DAS was used for the data collection. Table 5.7 displays the settling conditions for these 'trials'.

Table 5.5 Conditions of First Kapton Experiments, Temperatures in °C

Test Name	T_i	T_{core}	T_∞
Run 1	31.86	36.60	23.80
Run 2	31.23	35.20	22.55
Run 3	30.69	36.45	21.85
Run 4	31.06	35.60	21.95
Run 5	30.72	36.20	22.50
Run 6	30.74	35.80	23.05
Run 7	30.50	36.00	23.30
Run 8	30.23	35.00	23.35
Run 9	30.55	36.20	22.30
Run 10	30.06	35.20	23.40

Table 5.6 Settling Conditions for Early Experiments (1)

Test Name	Settling Condition
Trial 1	No settling time; Probe placed on arm at the same time as the air was turned on
Trial 2	5 second settling time
Trial 3	Probe prewarmed on different part of arm
Trial 4	Probe placed on arm slightly after the air was turned on
Trial 5	Probe prewarmed on a hot plate to 40°C before application

After verification that those three tests better fit the model data, it was desired to change the experiment to achieve higher heat flux and larger temperature changes. Switching to a 1.27 centimeter air hose accomplished this by providing for a larger mass flow of cooling air. This created a larger convective cooling effect on the top side of the sensor. The air pressure was dropped down to 10 psi for this larger diameter hose arrangement. The convection coefficients reported in Section(5.1.2) are for this larger hose.

After computing the convection coefficient, four tests were run. For each of these

Table 5.7 Settling Conditions for Early Experiments (2)

Test Name	Settling Condition
Trial 6	Approximately 10 seconds settling time
Trial 7	Probe warmed by Subject 1 then placed on Subject 2 and allowed to settle for 2 minutes
Trial 8	Probe allowed to reach equilibrium (as with ‘Run’ data)

tests, the probe was warmed on one of the subject's arms until equilibrium. Then the probe was transferred to the opposite arm and allowed a few minutes to equilibrate. The idea here was to reduce the amount, if any, of thermal shock imposed on the area to be measured. The tests were one minute in duration and performed on three different subjects. The initial conditions for these tests are summarized in Table 5.8

Data Reduction

Data reduction for both the A1 and A2 experiments progressed as follows. The data recorded on the HP analyzer; voltages from the heat flux sensor and surface thermocouple, were converted into ASCII format via DOS based conversion programs called LIF and SDFTO63 (sdf format to DOS 6.3 format). These data were then imported into Microsoft Excell to convert the voltages into heat flux and temperature based on the coefficients and linearization equations found previously. Excel also facilitated the preparation of graphs, performance of statistical calculations, and comparison of the experimental to model data. The data files were formatted with time, variance, and header information so that they could be used as input files for the parameter estimation program. One file was created for each test. These files were saved in ASCII text format so that they could be transported to the Unix file-system required for running the parameter estimation codes.

5.5 Bioprobe Experiments (Probe B)

Experiments using the current bioprobe (B configuration) were many and varied. Many of the performed experiments were for tuning purposes or to develop protocols, or to check different probe generations. Therefore, not all of the performed experiments are included in this document, but only the experiments that are pertinent to the discussion.

Table 5.8 Conditions of A2 Experiments, Temperatures in °C

Test Name	T_i	T_{core}	T_∞
Alum 1	30.4	36.0	20.9
Alum 2	30.4	36.5	20.3
Alum 3	Not used, Probe moved during test		
Alum 4	30.4	36.0	20.3

The bioprobe was used in conjunction with the PC-DAS to collect heat flux and temperature data from both arm and phantom experiments. In most of these experiments, the probe surface temperature on the tissue (lower) side was measured. Due to different positioning of the surface thermocouple (See Section 3.2.2), one of two different heat flux quantities was measured; either convection or conduction. In the cases where the surface thermocouple was on the same side as the heat flux sensor, conduction of heat from tissue to the probe was measured. In the cases where the surface thermocouple was attached to the anodized surface opposite the heat flux sensor, convection of heat off the probe top surface was measured. Of these two cases, measuring conduction is the more desired since it may be more closely dependent on blood perfusion during transient times, and less susceptible to outside influences. However, because of limitations in probe design at different points in this research, sometimes convection had to be measured and used. Both heat fluxes are dependent on blood perfusion and can be manipulated with the numerical model, so their investigation was worthwhile.

5.5.1 Arm Experiments

Of the many experiments performed on living subjects' arms, four representative tests are discussed here. These four tests represent the typical data magnitudes and trends seen with measurements using normal, unperturbed forearm surfaces. These experiments also represent the four possible probe orientations with respect to the measured tissue using two different probe configurations. The possible orientations are: 1) the thermocouple on the anodized aluminum surface (opposite the heat flux sensor or foil side) with the thermocouple down against the tissue, 2) the thermocouple on the anodized aluminum surface with the foil side down, 3) the thermocouple and heat flux sensor on the same side with both down against the tissue, and 4) the thermocouple and heat flux sensor on the same side with both up exposed to the cooling air. The two probe configurations that produce these orientations are as shown in parts b and d in Fig. 3.5. These correspond to probes 2 and 3 in the calibration Table 3.2.

As with the A2 probe experiments, the probe was placed on a spot of the interior forearm away from excess hair or large blood vessels. The probe was allowed to sit on the arm until thermal equilibrium was reached, denoted by a negligible heat flux and constant temperature reading. Then the cooling air was turned on. As before, the air was provided at

roughly room temperature at a wall pressure of 10 psi. The tests were one minute in duration. Table 5.9 summarizes the orientation and initial conditions of these four experiments, labeled ‘episkin’ tests.

5.5.2 Phantom Experiments

The bioprobe B was also used to perform controlled phantom experiments using the setup described in Section 5.1.4. These experiments included using two different porous media, different probe positions, different flow rates, and varied water levels. The following sections highlight the experiments that led to important conclusions and revelations about the perfusion measurement system.

Aluminum Media

At first, it was desired to use a highly porous substance whose base material had well known thermal properties. This would allow for large and distinguishable perfusion rates as well as eliminate some experimental uncertainty regarding material properties. Porous aluminum was chosen as such a material. Porous aluminum is basically a reticular structure of open cells connected by solid aluminum alloy ligaments. A block of this substance appears like a metal sponge or foam, giving rise to the trade name of ‘foam metal’. Porous aluminum is manufactured for a variety of applications including filtering, structural enhancement with low added weight, and fluid applications. It can be formed to almost any specified size, shape, porosity, or average pore size. The manufacturers keep fairly reliable data as to the basic effective thermal properties of their materials. Also, porous aluminum can be machined and worked just like any metal.

Several samples of *Duocel* were obtained for free from Energy Research and Generation, Inc. (ERG) who manufacture this material. Some basic effective thermal properties

Table 5.9 Conditions of Bioprobe B Skin Experiments, Temperatures in °C

Test Name	Orientation	T_i	T_{core}	T_∞
Episkin 1	Thermocouple down, foil up	31.77	37.00	23.22
Episkin 2	Thermocouple up, foil down	31.77	37.00	24.06
Episkin 3	Thermocouple down, foil down	32.26	37.00	24.33
Episkin 4	Thermocouple up, foil up	32.15	37.00	24.42

were also obtained from this company. The samples obtained were made of 6101-F aluminum alloy with 16 pores per centimeter at a seven percent volume density. The sample standard size was 7.62 centimeters square by 2.54 centimeters thick, the size of the sample area in the experimental box (see Section 5.1.4). Four holes were drilled through the corners of the samples to allow passage of the sample box thread rods. The samples were machined down and smoothed so that they fit snugly in the sample box with room height-wise for the box top to be placed on and secured.

Several thermal properties of the aluminum are needed for the estimation program since these quantities are considered known constants in the biothermal model. The effective thermal properties of thermal diffusivity and conductivity for the porous aluminum are calculated based on a volume fraction addition of the properties of the base material and the fluid filling the pores.

ERG provided effective thermal conductivity information based on the porous aluminum in air. To back out the conductivity of the 6101 alloy, the volume fraction approach to composite properties was used where the property of a composite (in this case the effective property) is equal to the sum of the properties of its constituents multiplied by their volume fraction (in this case density percent). For thermal conductivity, k , this relation can be expressed as

$$k_{eff} = k_1(V_{f1}) + k_2(V_{f2}) \quad (5.2)$$

where V_{f1} and V_{f2} are the volume percents of material one and two respectively. A similar equation also applies to thermal diffusivity. Replacing k_1 and k_2 with k_{6101} for the aluminum alloy and k_{air} for air and solving for conductivity of aluminum yields

$$k_{6101} = \frac{k_{eff} - k_{air}V_{fair}}{V_{f6101}} \quad (5.3)$$

The calculated value for k_{6101} can then be used in the calculation of an effective conductivity based on the porous aluminum saturated with water according to Eq. (5.2) above. Thermal diffusivity is calculated with the same process, incorporating standard constant values for the specific heat and density of aluminum, air, and water.

Table 5.10 lists the values taken for different materials and the results of the above described calculations using those values. The values are for saturated water, aluminum, and air all at 310K. These numbers are assumed correct as tabulated in Incropera and Dewitt

(1990). The value of effective conductivity of the Duocel in air is from the manufacturer's documentation.

Before any true perfusion experimentation was begun, a simple test was performed to verify the flow pattern within the porous aluminum. The phantom experiments were set up as described except without the bioprobe. All the pumps were turned on to moderate flow rates. They were allowed to run for some time to observe that fluid was flowing through the system and all devices were working properly. Then the inlet hose to the perfusion pump was switched from the water bath to a beaker containing water colored with food coloring. The porous media was watched from the top view. As hoped, the color first appeared in the middle of the top surface and then slowly spread outward towards the side outlets of the sample box. Although no actual speed measurements were taken, this outward flow appeared uniform in all directions.

The system was then purged and filled with new water. After once again allowing the pumps to run at moderate speed, the perfusion pump was turned off. A few drops of food coloring were placed in the center top surface of the aluminum. With zero flow from the pump, this coloring stayed in place. However as soon as the perfusion pump was turned on, the spot of color diffused out towards the sides of the sample box. These two visualization tests lent confidence that the experimental set up produced the desired flow pattern of water up through the middle of the media then radially outwards (described in section 5.1.4). Then experiments with the bioprobe could begin.

The overall technique for all the phantom tests was similar to that for the arm experiments. The system was assembled with the bioprobe in place on the media and the bath water held at a constant temperature. The perfusion pump was set to the desired flow rate and allowed to flow freely. After the system reached thermal equilibrium, once again denoted by low, steady heat flux readings and constant temperature readings over the course of a minute, the cooling air was allowed to flow. As before, this cooling air was roughly room temperature and delivered at a wall pressure of 70 kPa. The tests lasted approximately one minute. All the experiments with the phantom media adhere to this overall technique. The differences between the following experiments include bath water level changes, probe location on the top surface, flow rates, and the differing plastic layers on the media and probe.

Several preliminary experiments were completed using the bioprobe B configuration

Table 5.10 Properties of Duocel Porous Aluminum Samples

Property	Value	Units
Effective Thermal Conductivity in Air	8.65	W/mK
Aluminum Density	2720	kg/m ³
Aluminum Specific Heat	895	J/kgK
Air Conductivity	0.026	W/mK
Water Conductivity	0.628	W/mK
Water Specific Heat	4178	J/kgK
Water Density	993.05	kg/m ³
Effective Thermal Conductivity in Water	9.21	W/mK
Effective Thermal Diffusivity in Water	3.68×10^{-6}	m ² /s

with the thermocouple on the anodized aluminum surface opposite the episensor. Because of this configuration, convective heat flux was recorded. Flow through the aluminum was provided with small tubing of 0.16 centimeter inner diameter looped through the perfusion pump. First tests at flow rates from zero to 1.67 milliliters per second (ml/s) ended up with the probe surface getting wet. The porous aluminum had punched small holes in the plastic wrap when the probe was placed on top with only moderate pressure. The probe was then encased in heavier, dual layer plastic to prevent wetting of its surface. Also, in the first tests not much attention was paid to bath water level. For the following tests, the water level in the bath was higher than the top of the porous sample, ensuring that water flow reached the top of the sample.

Unfortunately, the heat flux and temperature data recorded with this set up did not appear repeatable or sensitive to flow rate. The heat flux curves were very flat and had the same magnitudes and shape for different flow rates. At this point it was assumed that the flow rates were too small to be effective. Therefore the small hose in the perfusion pump was replaced with a larger 0.170 inch inner diameter hose to provide larger flow rates.

No flow meter was available for the ranges of flow rates seen with the larger hose. The flow rates at certain pump speed settings were determined by using a manual stopwatch to time changes in water volume in a graduated beaker. This ‘calibration’ was performed for ten different settings of the perfusion pump speed. The flow rates ranged from zero to 8.89 ml/s.

Once again the bath water level was overflowing the sample box and the bioprobe placed in a plastic bag in addition to the heavy plastic on the aluminum surface. Many tests were run to check for variation of heat flux and temperature both with flow rate and probe position. Three probe positions were used: 1) the probe in the center of the aluminum with the box top on, 2) the probe in the center of the aluminum with the box top off, 3) the probe on the side of the aluminum with the box top off. Data were recorded for three flow rates at each of the three probe positions. Noticeable variations in heat flux and temperature were observed for different flow rates. No noticeable difference in heat flux and temperature was observed for different probe placements. Three good tests resulted from having the probe placed in the center of the sample with the top on. Table 5.11 lists the conditions for these tests, which will be used in later analysis. T_i , T_{H_2O} , T_∞ represent the initial equilibrium temperature, the constant bath water temperature, and the average cooling air temperature, respectively.

Because of the initial success of these experiments, many others were performed under the same conditions for a larger variety of flow rates. In all, 34 experiments covering multiple tests at each of ten flow rates were completed. Four of these tests lasted two minutes in duration (instead of the usual one minute) with the air turned off after one minute. These two minute tests allowed for inspection of thermal recovery effects within the system. Once again, the probe surface temperature closest to the porous aluminum and convective heat flux were measured.

Aluminum-Arm Comparison Tests

At this point it was desired to compare the results obtained with the phantom with results under similar conditions on the arm. Data were recorded from the phantom set up using flow rates of zero and 1.95 ml/s. Newer generations of the bioprobe were available that

Table 5.11 Conditions of First Porous Aluminum Experiments, Temperatures in °C

Test Name	Flow Rate (ml/s)	T_i	T_{H_2O}	T_∞
18925	0.00	33.34	37.0	23.80
19925	4.94	33.90	37.0	23.58
20925	8.89	33.90	37.0	23.58

contained the surface thermocouple and heat flux sensor on the same side. This was used to measure the convective heat flux as before. Then the sensor was flipped over so that the foil side was closest to the porous media and two tests were run to measure conductive heat flux through the aluminum. The bioprobe assembly, including all the plastic, was removed from the porous aluminum and placed on a subject's forearm. Measurements of conductive and convective heat flux were taken in two different tests. By including the plastic wrap and bag on the arm experiments, these tests eliminated the effects of the plastic relative to the comparison of arm and phantom data.

The conditions of these experiments are shown in Table 5.12.

Sponge Media

After experimentation with the Duocel porous aluminum, it was determined that data should also be collected for another porous media with different thermal properties. A sponge was chosen as this material. Some fine pore sponge material was obtained from the local chemistry department. The sponge material was manufactured from natural cellulose by VWR Scientific. The sponge comes in a compact form that can be cut and shaped and then expands in contact with water. The standard thickness of the sponge material is about one inch. The provided material was cut to the 7.62 centimeter square dimensions of the sample box. Holes were punched by a nail into the corners of the sponge to allow for passage of the threaded holding rods. The result was a sponge block similar in size and shape to the porous aluminum described above.

The manufacturer provided no data on the thermal and physical properties of the sponge. These were derived in the lab by the moderate assumption that the properties

Table 5.12 Conditions of Aluminum-Arm Comparison Experiments

	Test Name	Type of Heat Flux Measured	Flow Rate (ml/s)	T_i (°C)	T_{core} (°C)	T_{H_2O} (°C)	T_∞ (°C)
Phantom	1116	convection	0.00	35.90	-	37.0	25.66
	2116	convection	1.95	35.75	-	37.0	26.06
	3116	conduction	1.95	35.75	-	37.0	25.28
	4116	conduction	0.00	35.95	-	37.0	25.56
Arm	7116	convection	-	31.15	37.0	-	23.75
	8116	conduction	-	30.74	37.0	-	23.75

of natural cellulose are close to that of the parent soft wood fiber. First, the density and volume fraction of the sponge material were calculated. Density of the cellulose fibers was found by weighing the sample in its dry, compressed state and dividing by its volume in this state. Then the sample was moistened and placed in the sample box as if in an experiment. It can safely be assumed that the volume of the cellulose fibers is the same in the expanded sponge as in the compact form so that the volume difference between expanded and compact forms is saturated with water. Thus the volume fraction of cellulose can be computed by dividing the volume of the compact sponge by the volume of the expanded sponge in the sample box. Using tabulated values for the conductivity and specific heat of both water and wood fiber with the density calculation and tabulated water density values, the effective thermal properties of the composite sponge-water media were calculated as per Eq. (5.2) similar to the Duocel calculations. The results of these measurements and calculations, as well as the tabulated values, taken from Incropera and Dewitt (1990), are summarized in Table 5.13. The tabulated properties were taken at 300K.

It can be seen in this table that the effective thermal properties of the sponge media are much lower than the properties of the porous aluminum and close to the properties used for skin tissue.

As with the porous aluminum, visualization of the flow through the sponge was done using food coloring in the perfusion pump supply. The results were the same. The color appeared first in the center of the sponge then spread outwards.

For the sponge experiments, the latest bioprobe with the thermocouple on the same side as the heat flux sensor and a shielded cable had been assembled. Therefore conduction heat flux was measured along with the media side probe surface temperature. The experimental procedure was the same as before. A thin layer of plastic wrap was placed between the sponge and box top to prevent flow of water out the top of the sponge and to simulate the uppermost layer of skin. The bioprobe was further encased in a plastic bag. The probe was placed on the sponge surface and allowed to sit until equilibration, denoted by low heat flux and constant temperature over the course of one minute. After observance of equilibrium, the cooling air was turned on, once again supplied at room temperature and 70 kPa. The air was left on for one minute while data were recorded. The water level in the bath was set to just at the top of the sample box, ensuring that the sponge was completely saturated.

Table 5.13 Properties of Sponge Samples

Property	Value	Units
Wood Fiber Conductivity	0.17	W/mK
Wood Fiber Specific Heat	2500	J/kgK
Sponge Length	7.62	cm
Sponge Width	7.62	cm
Sponge Thickness, compact	0.159	cm
Sponge Thickness, expanded in box	1.525	cm
Sponge Mass, dry	5.659	g
Volume Percent of Cellulose in Expanded Sponge	10.4	%
Water Conductivity	0.628	W/mK
Water Specific Heat	4178	J/kgK
Water Density	993.05	kg/m ³
Effective Thermal Conductivity in Water	0.58	W/mK
Effective Thermal Diffusivity in Water	1.46×10^{-7}	m ² /s

Several tests were run at each of four flow rates ranging from zero to 2.92 ml/s. Tests were also run on three different days with the setup being taken apart, cleaned and reassembled in between. In all, 36 sets of data were taken with the sponge media. The initial and environmental conditions of these experiments are given in Table 5.14.

Data Reduction

For all the experiments with the bioprobe using the PC-DAS system, the data were reduced in the following manner. The heat flux and temperature signals as recorded by the PC-DAS were downloaded directly into an Excel spreadsheet. Here, any offset bias present in the heat flux signal was calculated and then removed. During the data acquisition process, approximately ten seconds of ‘flat’ data (at equilibrium, prior to onset of the cooling air) were used to calculate the variance of the heat flux and temperature signals. This beginning data were then removed and the remaining data formatted as in Appendix C. The end result was an ASCII text file of heat flux and temperature data, for only the duration of air cooling, formatted for input to the parameter estimation program.

Table 5.14 Conditions for Sponge Tests

Test Name	Flow Rate (ml/s)	T_i °C	T_{H_2O} °C	T_∞ °C
Sp111	0.00	33.03	37.0	25.25
Sp211	0.00	33.10	37.0	25.36
Sp311	0.00	32.84	37.0	24.72
Sp411	1.01	34.75	37.0	24.81
Sp511	1.01	34.83	37.0	24.67
Sp611	1.01	34.98	37.0	24.61
Sp711	1.95	36.20	37.0	25.08
Sp811	1.95	35.98	37.0	25.64
Sp911	1.95	36.29	37.0	25.78
Sp1011	2.92	36.05	37.0	25.47
Sp1111	2.92	36.29	37.0	24.75
Sp1211	2.92	36.52	37.0	25.19
Sp119	0.00	32.85	37.0	25.22
Sp219	0.00	32.28	37.0	24.81
Sp319	0.00	32.25	37.0	24.50
Sp419	1.01	34.69	37.0	24.67
Sp519	1.01	34.79	37.0	24.86
Sp619	1.01	35.02	37.0	24.75
Sp719	1.95	35.88	37.0	24.47
Sp819	1.95	35.92	37.0	25.42
Sp919	1.95	35.79	37.0	25.92
Sp1019	2.92	36.62	37.0	25.53
Sp1119	2.92	36.49	37.0	25.19
Sp1219	2.92	36.18	37.0	25.08
Sp121	0.00	34.61	37.0	26.36
Sp221	0.00	33.05	37.0	25.97
Sp321	0.00	32.65	37.0	25.22
Sp421	1.01	34.90	37.0	25.58
Sp521	1.01	34.98	37.0	24.92
Sp621	1.01	35.06	37.0	24.83
Sp721	1.95	35.74	37.0	25.58
Sp821	1.95	36.10	37.0	26.08
Sp921	1.95	35.92	37.0	25.77
Sp1021	2.92	36.29	37.0	25.64
Sp1121	2.92	36.39	37.0	26.03
Sp1221	2.92	36.18	37.0	25.89

Chapter 6

Evaluations and Results

6.1 Biothermal Model Evaluation

Prior to and during experimentation and the development of the parameter estimation scheme, the model was evaluated against several parameters. Model outputs of various temperatures and heat fluxes were compared graphically after changing model parameters such as contact resistance, perfusion, convection coefficient, thermal properties, and geometry. The model was run alone based on user inputs for the parameter under consideration. The calculated temperature field and resulting heat fluxes with respect to time were graphed along side those calculated with other parameter values. The temperatures and heat fluxes of particular interest were: heat flux through the probe-tissue interface, heat flux calculated within the probe, convective heat flux (from the probe top surface), tissue-side surface temperature, top-side surface temperature. Also, some preliminary sensitivity coefficients were calculated. For times when certain parameters were held constant while others changed, the constant values were ‘guessed’ based on previous results and values found in literature.

These qualitative observations allowed the drawing of inferences about how various parameters effect the model output. This gave some predetermination of trouble areas or parameters that might need to be carefully controlled or measured during experimentation. Many of these evaluations were performed with either the type A or type B probe properties, not both. However, the qualitative trends seen with these properties hold true for all thermopile based probe designs.

6.1.1 Environmental and System Parameters

Model Position of Heat Flux Calculation

At this point, some discussion of the relative merits of q''_{int} , Eq. (4.6), and q''_{cond} , Eq. (4.4), is necessary. The internally calculated heat flux is derived because this quantity might better model the actual physical thermopile, where heat flux is measured. A representative graph of q''_{int} and q''_{cond} is shown in Fig. 6.1 for a 30 second simulation. Here, q''_{int} is calculated between the last two finite difference nodes in the probe. The two traces are very much the same, except for a very small difference in the initial response. The q''_{int} curve rises to a slightly higher peak value than the q''_{cond} curve, but not higher enough to be considered significant. This difference is most likely due to a small decrease in the contact resistance effect in the internal heat flux calculation. Beyond this, the two curves are equivalent.

Problems exist with the stability of the internal heat flux calculation. The changes in nodal temperatures are slightly oscillatory for the interior probe nodes, mainly because the thin probe creates very small distances between the nodes. Stability in a semi-implicit numerical method such as the one used in the model is achieved by modifying either the nodal distance or the calculation time step. Since the thickness in this model is fixed, the time step must be decreased. In order to gain a stable solution to produce Fig. 6.1, the time step in the model was decreased to 1/400 seconds - extremely small. This leads to large computation times and problems matching calculated data to experimental data recorded at much larger time steps. The stability issue worsens with modeling of thinner probes like the A1 bioprobe. Because of the problems with stability of the internal heat flux calculation and little difference between the two heat flux curves, the heat flux across the interface is a better choice for modeling. In further results and evaluations, only the heat fluxes either through the probe-tissue interface (q''_{cond}) or off the probe top (q''_{conv}) are considered.

Convection Coefficient

The graphs in Fig. 6.2 show the effect of convection coefficient, h , on the model output for the bioprobe B configuration. Large changes in h cause changes in the heat fluxes and temperatures. This is expected since the magnitude of h determines the amount of cooling applied to the probe. A higher h yields higher cooling, leading to higher heat flux and lower temperature values. This is supported by Fig. 6.2. As can be seen, if h is too low, no

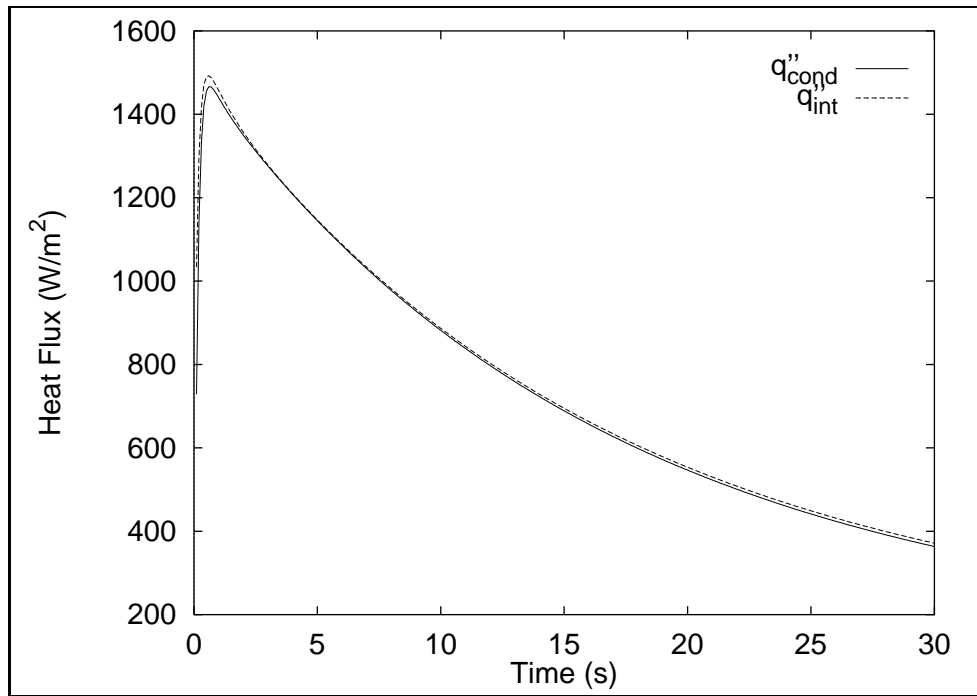


Fig. 6.1 Comparison of Conductive Heat Flux Calculated within the Probe and Across the Probe-Tissue Interface

net heat flux will exist. When h is large, the system will ‘top out’ and variations in heat flux and temperature are no longer functions of convection coefficient. Experimentally, the highest possible convection coefficient is desired since this increases the magnitude of the heat flux, which in turn increases the sensitivity of the system to blood perfusion (greater cooling equals larger effect on warm blood flow). The trends in Fig. 6.2 are for large (order of magnitude) changes in h . The model output does not change drastically for very small changes in convection coefficient, especially in the range of $1000 \text{ W/m}^2\text{K}$.

Contact Resistance

It is expected that the contact resistance, R_c , will be inversely proportional to the convection coefficient. Opposite to h , high R_c dampens out any heat flux response and low R_c increases the heat flux. The graphs in Figure 6.3 show these trends for probe B properties. Also, changes in contact resistance change the initial upward slope of the heat flux curves and initial downward slope of the surface temperature curves.

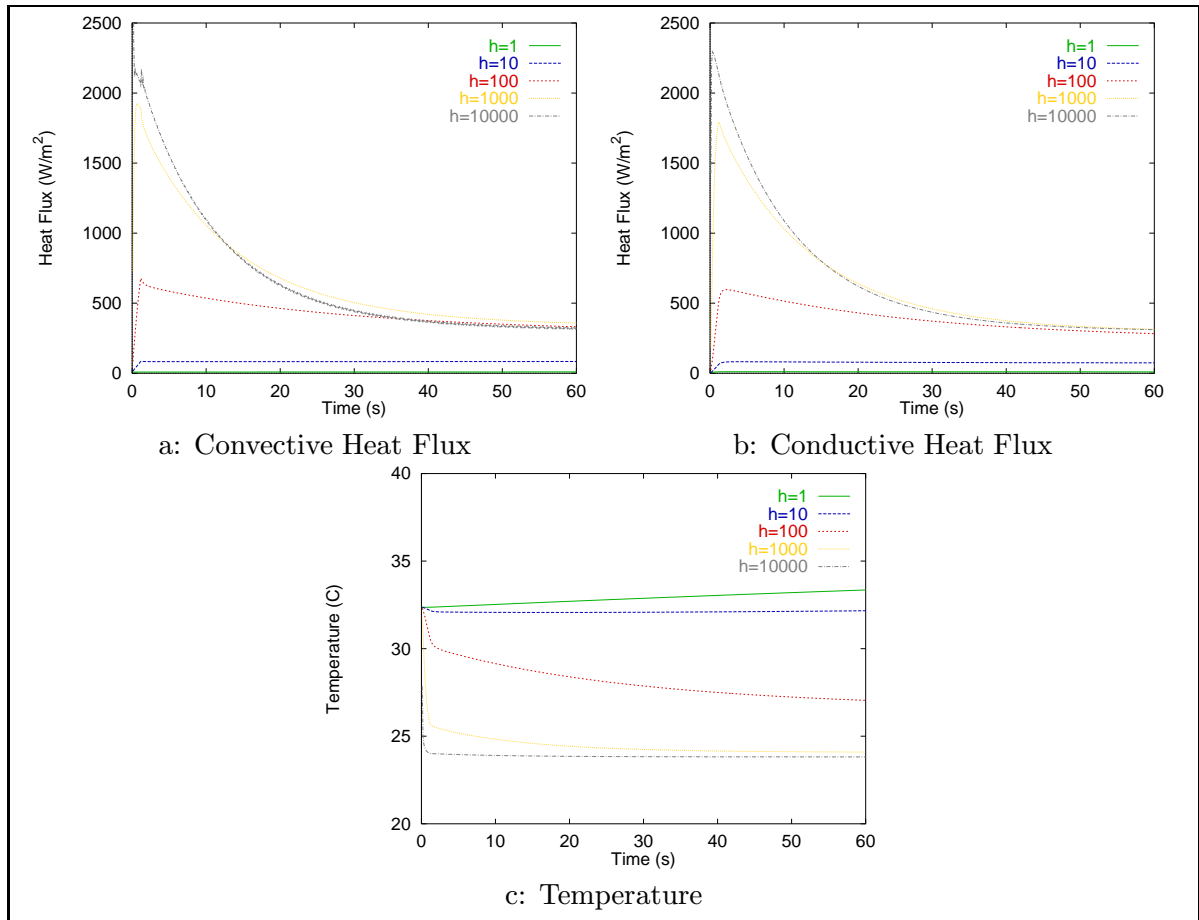


Fig. 6.2 Effect of Convection Coefficient on Model Output

Blood Perfusion

Blood perfusion, the main parameter of interest in this study, has a specific effect on the calculated heat flux and temperature. As described previously, the blood perfusion will try to recover the cooling effect on the probe by bringing heat to an area via new, warm blood. Blood perfusion, then, has little effect on the transient response of the output ($< 10s$), but has an effect on the end curve shape and quasi-steady-state values. This effect is seen in Figure 6.4 where the heat flux and surface temperature maintain a higher value at later times with higher perfusion. These graphs display the effect of w_b on both conductive and convective heat flux and interface and top sensor surface temperatures. As with contact resistance, the sensitivity of heat flux and temperature to blood perfusion for different probe types and experimental conditions will be investigated in following sections.

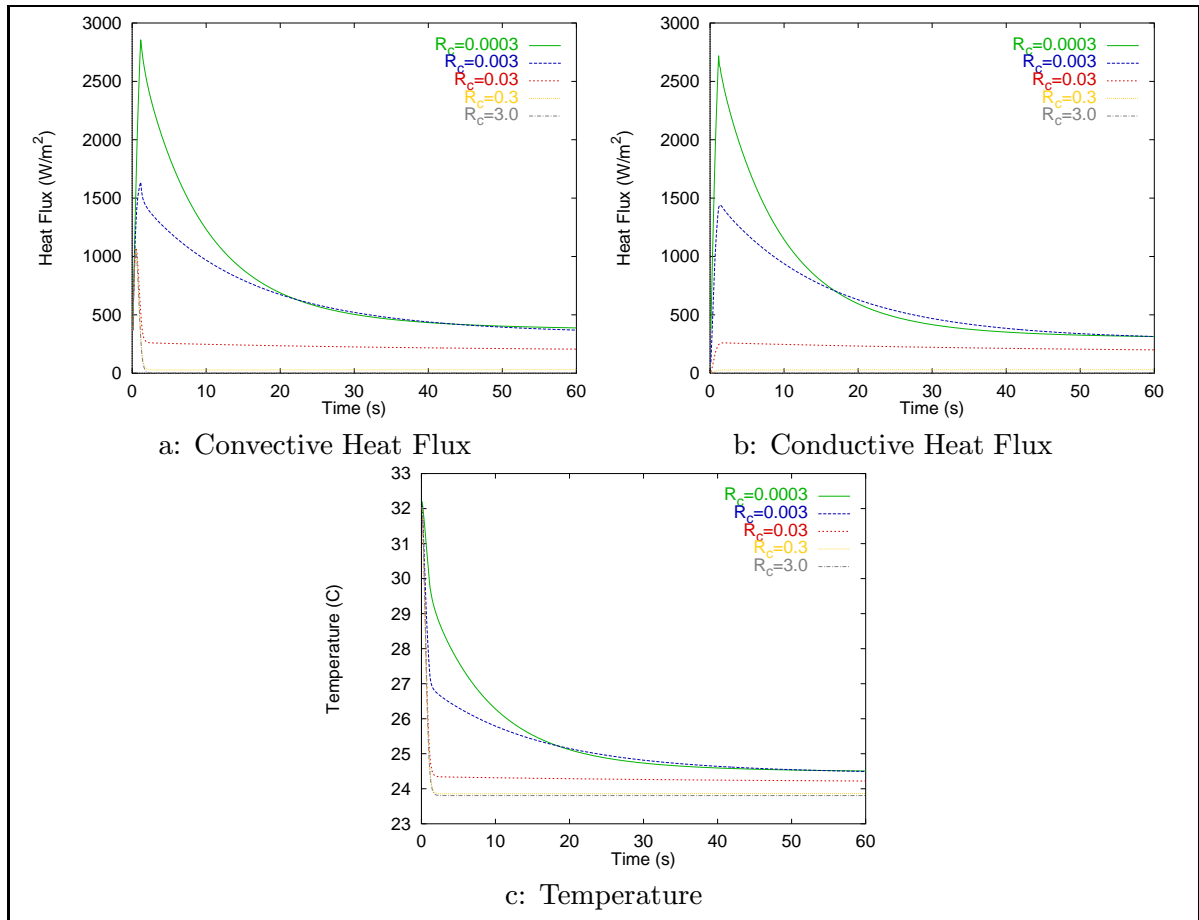


Fig. 6.3 Effect of Contact Resistance on Model Output

Required Nodal Geometry

Another model consideration is the number of nodes necessary to satisfy the semi-infinite boundary condition assumed in the solution. The distance between each node is determined by probe geometry and the desired number of nodes within the probe, an arbitrary setting usually equaling three nodes. But a finite number of nodes totaling some distance away from the probe is required to obtain semi-infinite conditions in the radial and depth directions. These conditions are considered met when there exists less than a 1.0 °C difference between each of the boundary nodes and the tissue initial temperature. This follows from the definition of a semi-infinite solid.

The model was run under ‘worst case’ conditions of a low contact resistance, high convection coefficient, and low blood perfusion with nominal guesses for environmental temperatures. A check was put in place to compare the temperature at each of the semi-infinite boundary nodes against the initial tissue temperature at each time step within a

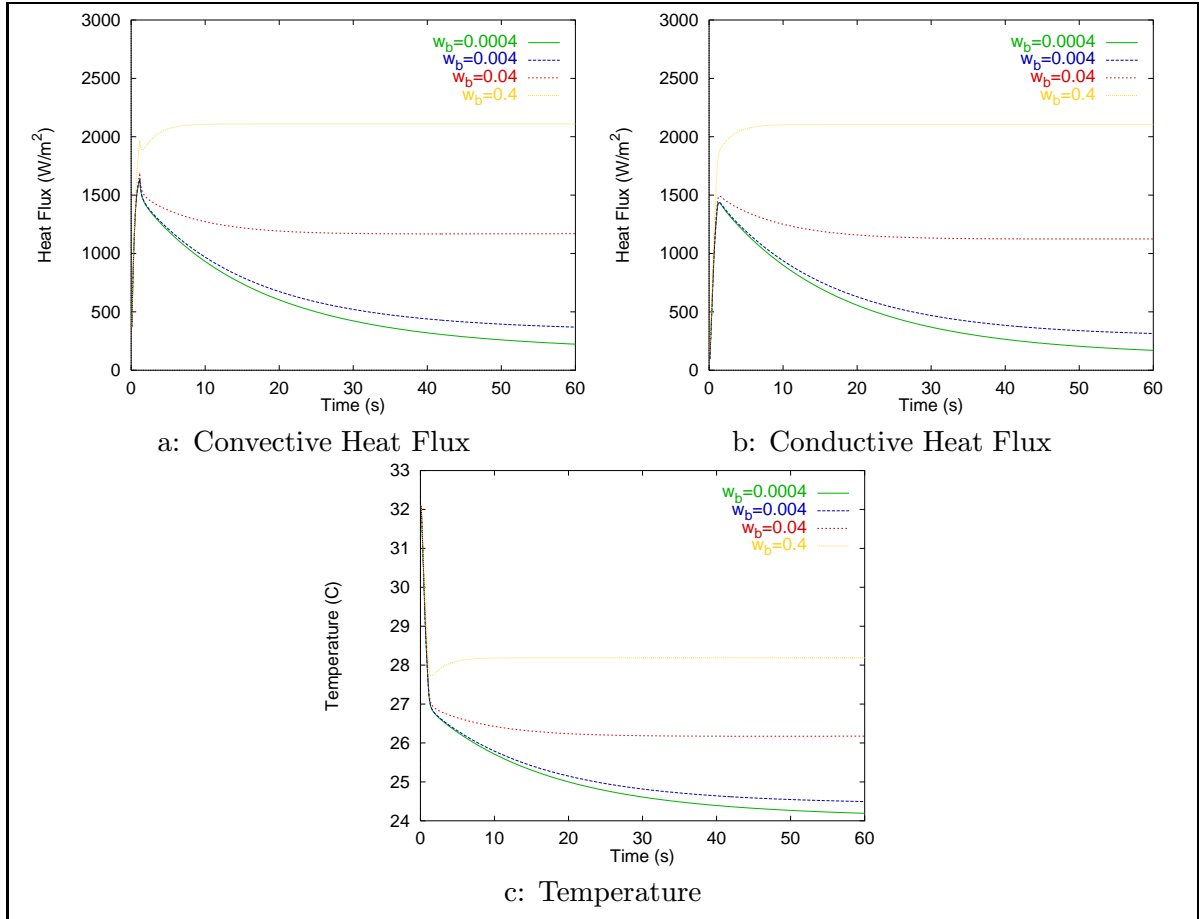


Fig. 6.4 Effect of Blood Perfusion on Model Output

virtual one-minute test. Maintaining the semi-infinite condition required about 150 nodes in depth and only 20 nodes in radial direction. This test was repeated for a variety of conditions, thermal properties, and R_c , w_b values. The end result was that the model should be used with **25 radial** and **150 depth** nodes.

Core and Air Stream Temperatures

The effect of the core temperature, T_{core} and temperature of the cooling air, T_∞ are similar. Raising the core temperature or lowering the air temperature acts to increase the temperature gradient across the probe, increasing the nominal heat flux through the sensor. The probe surface temperature increases with an increase in either T_∞ or T_{core} and decreases with a decrease in these parameters.

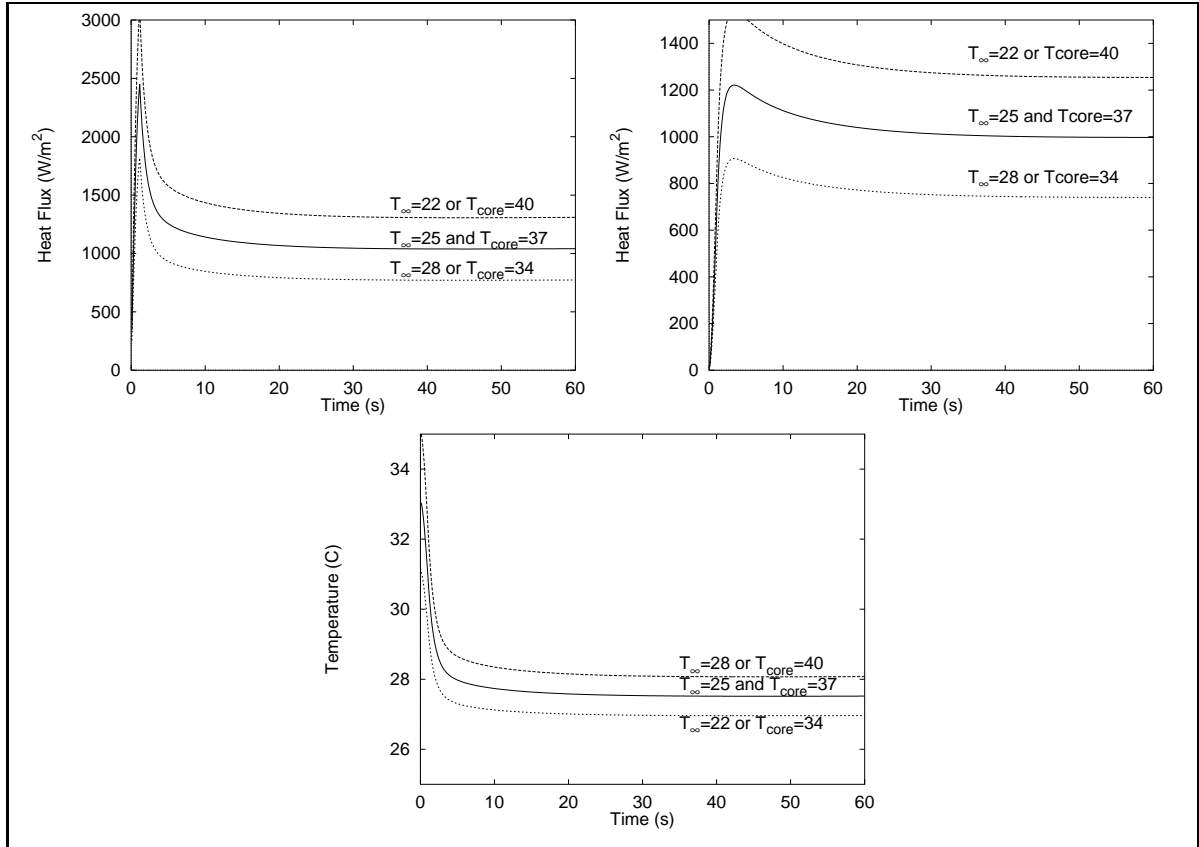


Fig. 6.5 Effect of Changes in Core and Air Stream Temperatures on Conductive, Convective Heat Flux and Probe Surface Temperature

6.1.2 Probe Parameters

Probe Density and Specific Heat

The density and specific heat of the probe, ρ and c_p , act much like the contact resistance in changing the transient portion of the heat flux and temperature curves. Density and specific heat effect the probe's ability to store energy. The more energy stored (higher ρ , c_p) the more heat flux it will take to produce a temperature change. Therefore, raising ρ or c_p will create a slower response of the system to the cooling effect. Just like contact resistance, a low density or specific heat will increase the magnitude of the transient slopes and a high density or specific heat will lower the slopes. These effects are displayed in Fig. 6.6 for the A2 probe properties. Of all the probe properties, density and specific heat have the largest effect on model output.

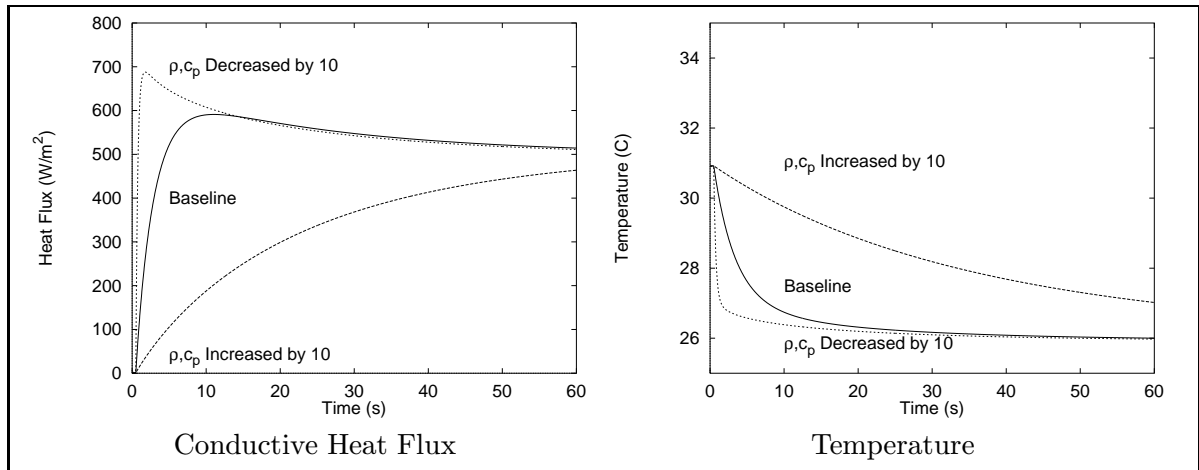


Fig. 6.6 Model Output Due to Changes in Probe Specific Heat or Density

Probe Thickness

The thickness of the probe, δ , also effects heat capacity much like density and specific heat. Large thicknesses lead to slower responses and small thicknesses lead to quick response times. The effects, graphically, of the thickness are almost exactly the same as for density and specific heat.

Check of Heat Capacity

Some concern was raised over the course of this research as to the correctness of the heat capacity ($\rho c_p \delta$) treatment of the probe within the biothermal model. To test this modeling, a separate and very simplistic model for the probe alone was developed. the probe was modeled as a lumped capacitance with a convective boundary on one side and a conductive boundary on the other. At either end of the boundaries was assumed some constant temperature equal to T_∞ and T_i . For this one-dimensional model, the temperature was calculated at a point in the center of the probe. The resulting model resistance network is shown in Fig. 6.7. The transient equations for temperature and heat flux through the lumped capacitance resulting from solving the energy balance equation for this network

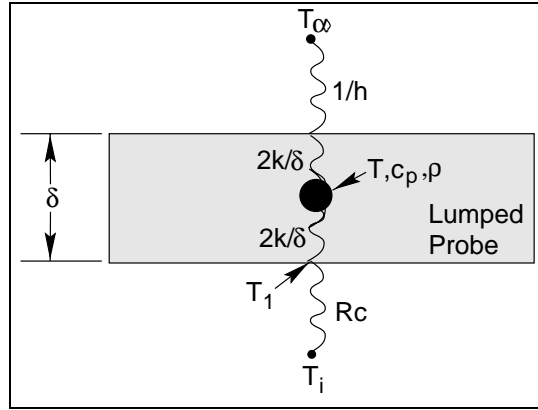


Fig. 6.7 Resistance Network for Lumped Capacitance Probe Model

were:

$$T(t) = T_i e^{-\lambda t} + \frac{1}{\lambda} \left(\frac{T_{\infty}}{c} + \frac{T_i}{a} \right) (1 - e^{-\lambda t}) \quad (6.1)$$

$$\lambda = \frac{1}{a} + \frac{1}{c} \quad (6.1a)$$

$$a = \rho c_p \delta \left(R_c + \frac{\delta}{2k_p} \right) \quad (6.1b)$$

$$c = \rho c_p \delta \left(\frac{1}{h} + \frac{\delta}{2k_p} \right) \quad (6.1c)$$

where $T(t)$ is the temperature of the probe lumped node at time t . The surface temperature was calculated as

$$T_1(t) = T_i - \frac{R_c \rho c_p \delta}{a} (T_i - T(t)) \quad (6.2)$$

and the heat flux through the probe calculated as

$$q''(t) = \frac{2k_p}{\delta} (T_1(t) - T(t)) \quad (6.1b)$$

This model gave a view of the transient nature of the probe which could be compared to the actual model in terms of shape and magnitude. Conductive heat flux and surface temperature were calculated for both models. A comparison is shown in Fig. 6.8. The fact that the shape and relative magnitude in the transient period were similar gave confidence that the heat capacity was modeled correctly in the more complex biothermal model.

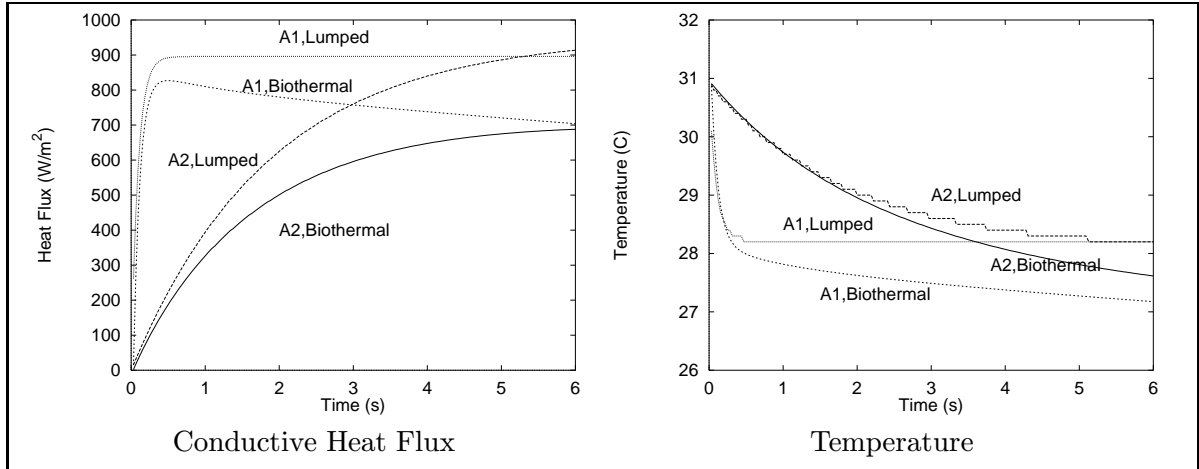


Fig. 6.8 Comparison of Biothermal Model and Lumped Capacitance Model for the Probe During Transient Times

Probe Conductivity

The graphs in Fig. 6.9 show that very large changes in probe thermal conductivity, k_p are required to effect the model output even slightly. Although slightly effecting the transient properties of the probe, k_p does not command as much of an effect as ρ or c_p .

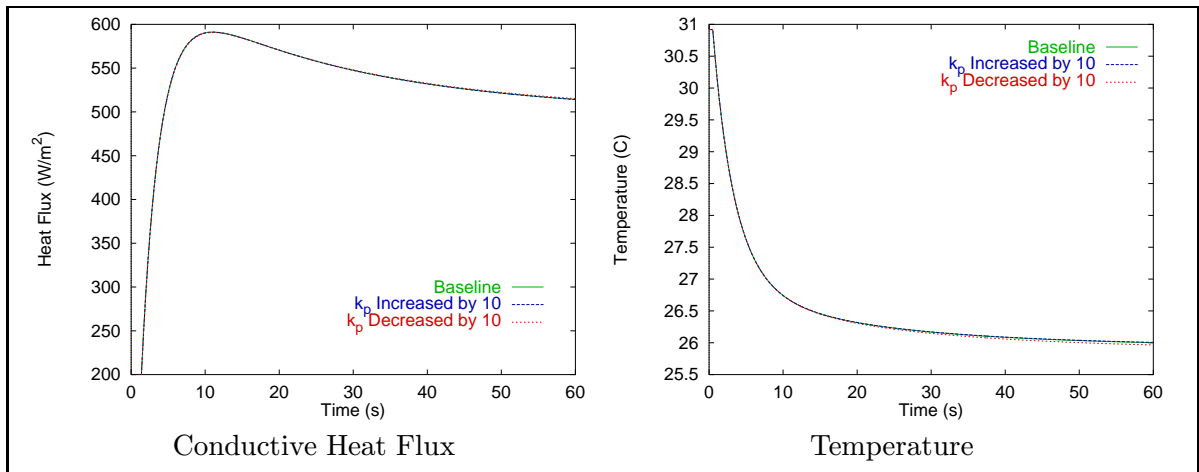


Fig. 6.9 Effect of Probe Conductivity on Model Output

Probe Radius

Another important question was the effect of probe radius on the calculations. The bioprobe B would have a different radius than previous bioprobe editions, and this size may be changed due to manufacturing or clinical restraints. To predict changes in system performance based on radial size and position, two tests were completed. First a test of the sensitivity of heat flux and temperature with respect to blood perfusion for different radial sizes. Second, the radial distributions of heat flux and temperature across the face of the probe were examined.

Figure 6.10 shows the sensitivity of heat flux to blood perfusion, $X_{q,w}$, calculated for different probe radii. As can be seen, not much variation exists, especially at short times. Some variation, about 12%, is evident at the end of the test between the lowest and highest radii. However, since the bioprobe will most likely have a radius in the 0.95+ range, it can be stated from Fig. 6.10 that no significant effect of radius needs to be considered.

The profile study had two purposes. One was to check changes in heat flux and temperature profiles for different probe radii. Secondly was to check for temperature uniformity or non-uniformity that might decide upon placement of the surface thermocouple. The heat flux and temperature at each node along the probe surface adjacent to the tissue were plotted against the ratio of radial position to overall radius. There were 10 radial nodes in the probe model. These profiles were plotted at 12 second intervals over a 60 second simulation. This was repeated for different radii under set initial and environmental conditions.

The results are shown in Figs. 6.11-6.12. The heat flux changes over the face of the probe by increasing at the last few nodes. The profiles become slightly flatter for larger radii because heat from the probe sides penetrates less far into the probe in terms of nodal position (the nodes are further apart in probes with larger radii). The overall difference between center and edge node heat flux is the same in all cases. This is acceptable since both the heat flux sensor and the model average the heat flux over the face of the probe. These small variations will average out.

The temperature profiles are fairly flat. The largest difference between center and end node temperatures is 0.2 °C. The usual temperature difference between tissue and environment ($T_t - T_\infty$) is 10 °C. Based on this, the variation across the probe surface is

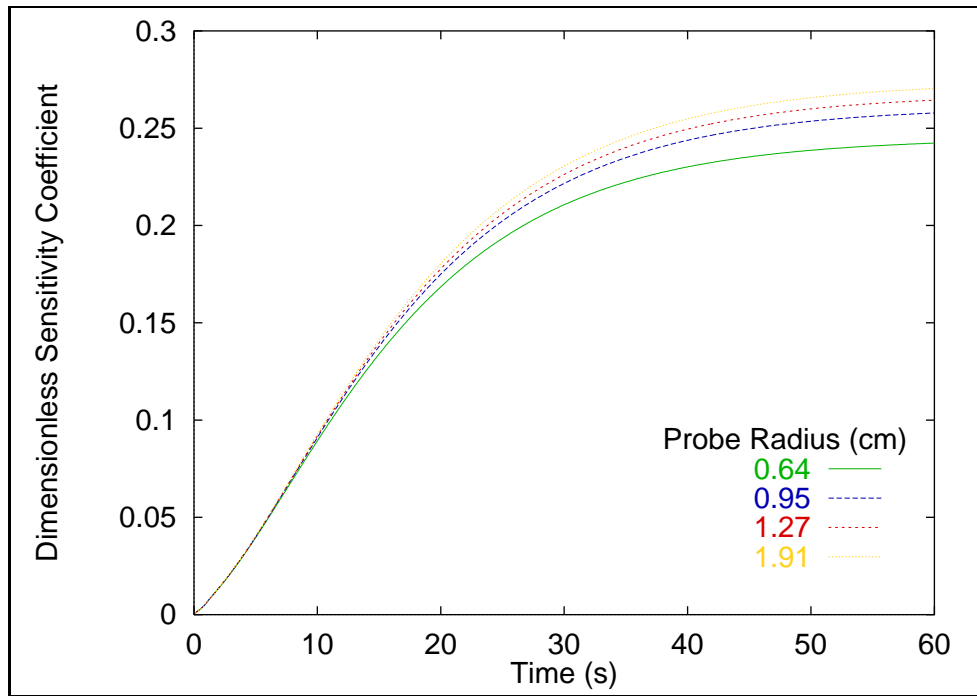


Fig. 6.10 Effect of Probe Radius on Heat Flux Sensitivity to Blood Perfusion; Four lines represent $X_{w,q}^+$ over time for probe radii of 0.64, 0.95, 1.27, and 1.91 centimeters

2.0% of the measured quantity, small enough to be neglected. Also, no real difference exists between temperature profiles calculated with different radii. Therefore, exact placement of the surface thermocouple in the center or off to the side of the probe is not crucial. The temperature at one point on the probe surface can be considered representative of the temperature at all points on the probe surface for the purpose of comparison to environmental temperatures.

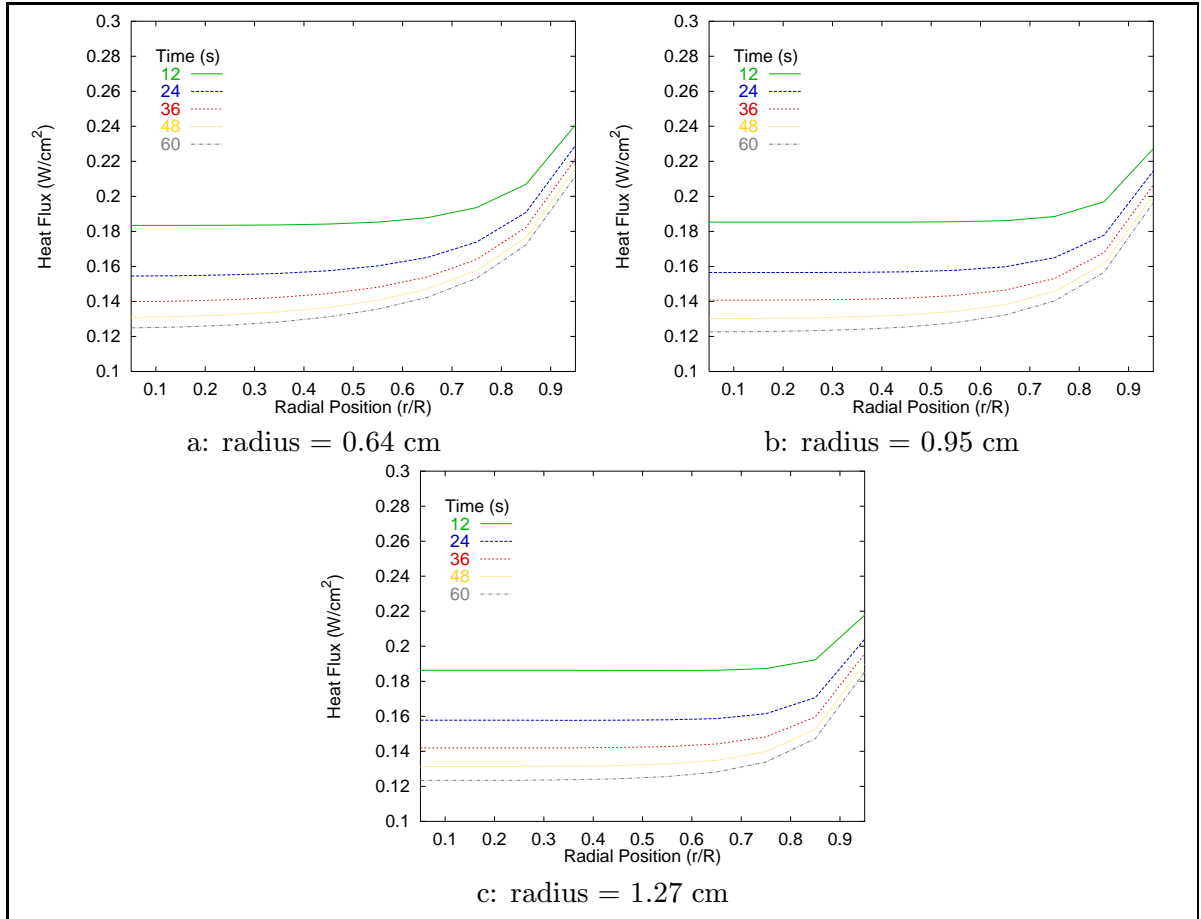


Fig. 6.11 Heat Flux Distribution Across Probe Surface for Different Probe Radii

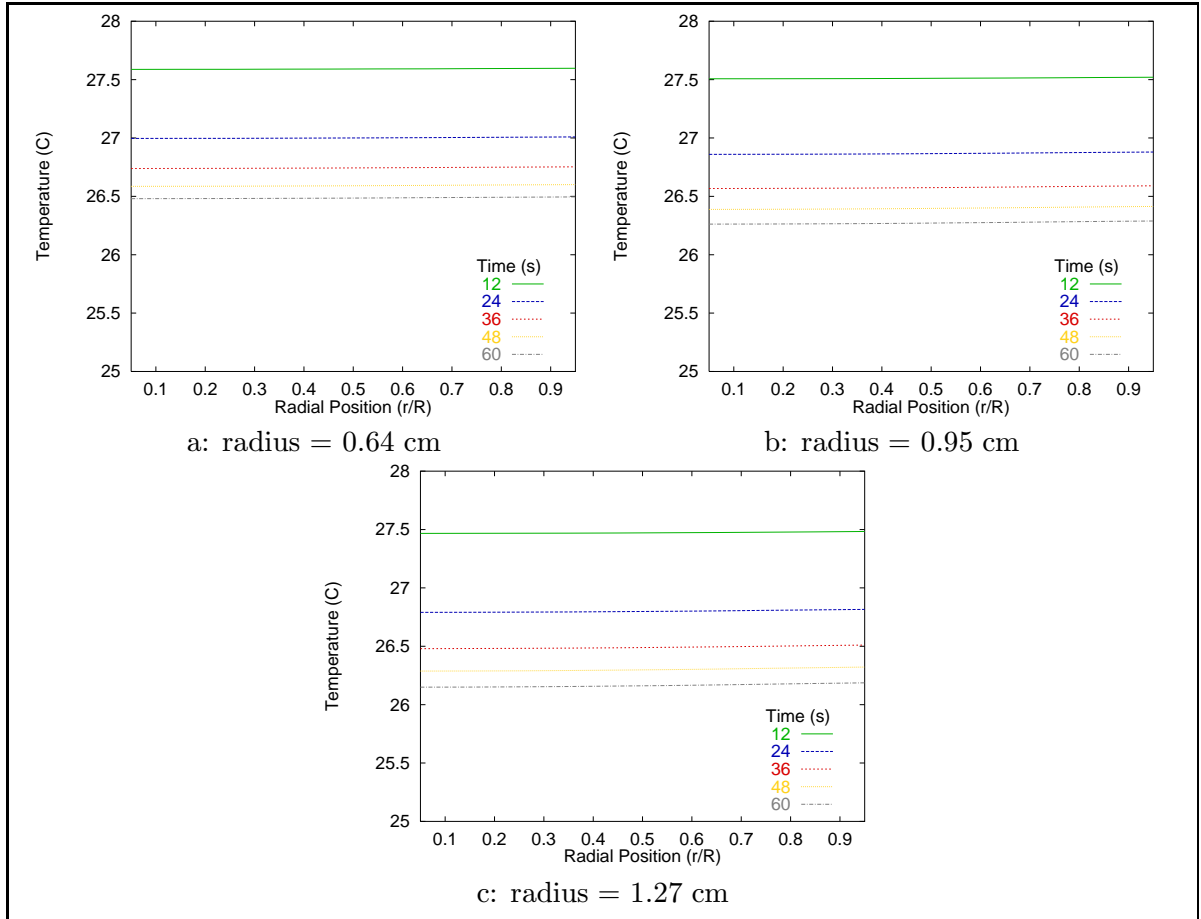


Fig. 6.12 Temperature Distribution Across Probe Surface for Different Probe Radii

6.1.3 Probe Surface Temperature Evaluation

During the course of this research, it was observed that the model and experimental temperature did not coincide. Figure 6.13 shows a representative comparison of calculated and experimental surface temperature. The curves have a different shape and slope, especially during the transient times. The model predicts a much larger initial drop due to the cooling than is experimentally observed. At first, it was thought that errors were in the temperature measurement with the A probes. But as surface temperature measurements were made with the B probe and more reliable equipment, the results were similar. Based on the curves in Fig. 6.13, it was conjectured that some energy storage was occurring experimentally that was not in the model calculations. This led to the belief that some capacitance existed in the thermocouple that was not included in the biothermal model.

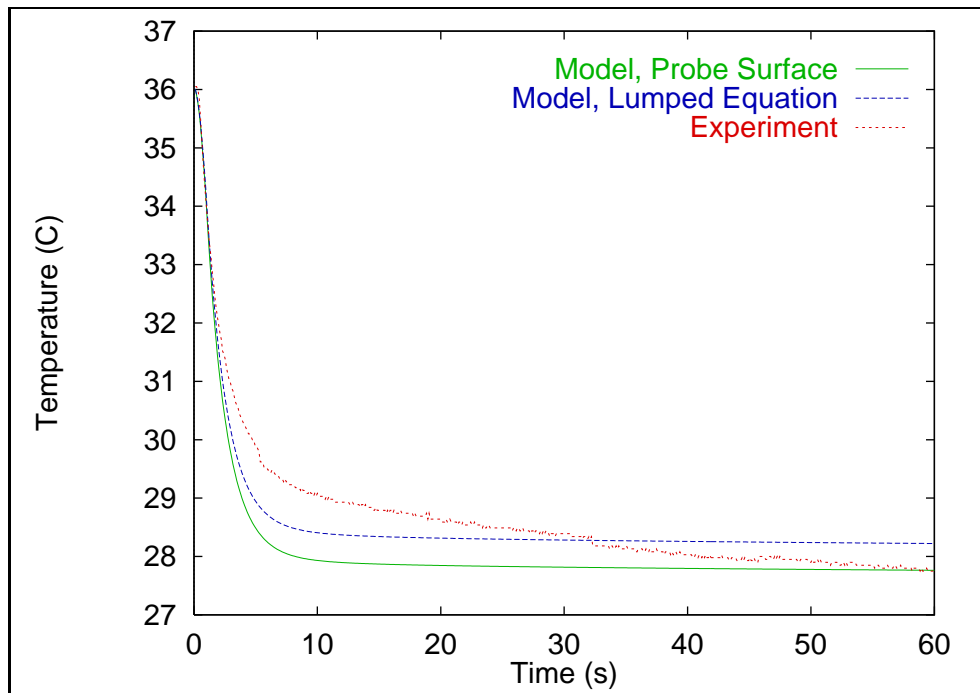


Fig. 6.13 Bias Between Experimental and Model Probe Surface Temperature

This capacitance could be due to the thermal paste used to attach the thermocouple or the finite thickness of the thermocouple itself. A one-dimensional, transient, lumped capacitance model for the thermocouple was developed much like the probe capacitance model described in section 6.1.2. Adding this lumped capacitance should account for the paste layer and change the transient response of the model temperature.

The thermal resistance network for this thermocouple model is shown in Fig. 6.14. Here, the probe surface temperature and skin temperature are treated as constants for each time step. Between the skin and thermocouple lies the contact resistance and between the thermocouple and probe lies the glue resistance. Solving the transient energy conservation for this system yields the following equations for temperature as a function of time:

$$T(t) = (T_{skin} - C) e^{at} + C \quad (6.3)$$

$$C = \frac{R_{glue}T_{skin} + R_cT_{gs}}{R_c + R_{glue}} \quad (6.3a)$$

$$a = \frac{R_c + R_{glue}}{\rho c_p L (R_c R_{glue})} \quad (6.3b)$$

where T_{gs} represents the true probe surface temperature, L the thickness of the thermal paste, k_g the conductivity of the glue and ρ, c_p the density and specific heat of the thermocouple composite.

Based on information from the manufacturer and ‘educated guesses’ for other properties, the values in Table 6.1 were used for the variables in Eq. (6.3). This equation, then is used to calculate the thermocouple temperature based on probe and skin surface node temperatures at each model time step. The results of using this new method are shown in Figure 6.13 as the ‘lumped equation’.

This new method does not solve the temperature difference problem. The model still predicts a larger, quicker cooling response than experiment while reaching some steady value

Table 6.1 Property Values for Thermocouple Capacitance Model

Variable	Value	Units
L	0.127	mm
k_g	0.1	W/mK
ρ	1000.0	kg/m ³
c_p	4000.0	J/kgK
R_{glue}	0.00125	m ² K/W

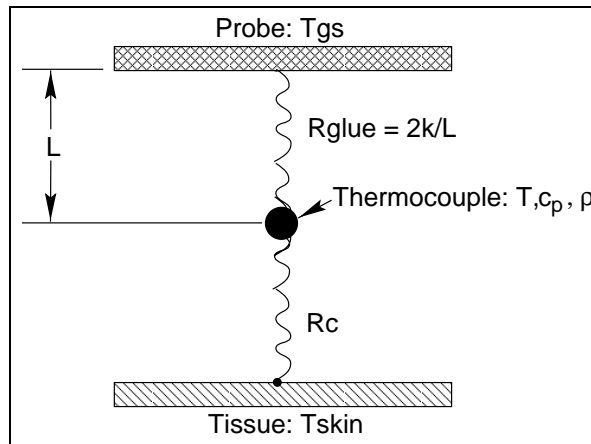


Fig. 6.14 Resistance Network for Lumped Thermocouple Model

not reached in experiment. Different values for L , k_g , ρ , c_p still do not bring the model and experiment curves into agreement. Therefore, in many cases, the temperature curves are not used in the parameter estimation process. The temperature measurement is still important in order to set the initial conditions of the probe and determine thermal equilibrium. Even with the model calculation and experimental data not matching for the singular quantity of surface temperature over the course of time, the initial conditions can be assumed correct so that the model starts at the same conditions as experiment. The temperature difference, independent of the absolute values, can be used for heat flux calculations, which do match well with experiment.

6.2 Evaluation of Parameter Estimation Program

In order to gain confidence and check for errors in the parameter estimation scheme described in Chapter 4, the program was run with simulated data. Random errors of $1.0 \text{ (W/m}^2\text{)}^2$ for heat flux and $0.05 \text{ }^\circ\text{C}^2$ for temperature were added to output from the mathematical model to create a simulation of experimental data. The model was run with specified values for contact resistance and blood perfusion. These data were then used in the estimation procedure to determine contact resistance and blood perfusion based on the simulated data. The estimates from the parameter estimation procedure should equal the specified values used to create the data. Also, since the model was used to both create the data and estimate the parameters, any bias error should be eliminated. The variances for

heat flux and temperature should be approximately equal to the sum of the squared error divided by the number of data points minus degree of freedom. Thus, the expected value of the Root-Mean-Squared error, defined as

$$RMS_{q,T} = \sqrt{\frac{S_{q,T}}{N-p}} = \sqrt{\frac{\sigma_q^{-2} \sum (q_m - q_c)^2 + \sigma_T^{-2} \sum (T_m - T_c)^2}{N-p}} \quad (6.4)$$

is equal to $\sqrt{2}$ or 1.41. The specified parameter values, parameter estimates with 95% confidence intervals, and resulting RMS value are given in Table 6.2. The exact estimates along with RMS value of 1.73, on the same order of magnitude as the expected value, give confidence in this estimation procedure.

Shown in Table 6.3 are results of this same method performed with various ranges of random error added to the model output. Here, only heat flux is used to estimate the contact resistance and blood perfusion, so that the expected RMS_q value, calculated by

$$RMS_q = \sqrt{\frac{\sigma_q^{-2} \sum (q_m - q_c)^2}{N-p}} \quad (6.5)$$

is 1.0. Adding higher random error tests the ability of the procedure to handle experimental data with a large amount of noise or other variance, and how that may effect the estimated values. The random errors added were 25 W/m² and 100 W/m², corresponding to variances of 625 and 10000 (W/m²)² respectively. The estimates changed somewhat, but remained within 3% of the specified values, with RMS_q values well below the expected value. Also, the RMS_q values were much lower than the $RMS_{q,T}$ values, indicating that most of the error came from the temperature comparison. These simulations gave confidence that experimental noise would not have a detrimental effect on the estimation procedure, just increase the root-mean-squared error and likewise the confidence intervals surrounding the individual estimates.

Table 6.2 Results of Estimation Procedure on Simulated Data, Heat Flux and Temperature

Test	R_c (m ² K/W)	w_b (ml/ml/s)	$RMS_{q,T}$
Specified Values	0.003	0.002	-
Estimated Values	$0.003 \pm 2.0 \times 10^{-7}$	$0.002 \pm 1.9 \times 10^{-6}$	1.73

Table 6.3 Results of Estimation Procedure on Simulated Data, Varying Error

Error (W/m ²)	R_c (m ² K/W)	w_b (ml/ml/s)	RMS_q
Specified Values	0.003	0.019	-
1.0	0.003	0.019	0.005
25.0	0.003	0.0189	0.08
100.0	0.00299	0.0185	0.20

6.3 Sensitivity Analysis: Bioprobe A

The sensitivity coefficients, as described in Chapter 3, for both the A1 and A2 probe configurations are compared. Figure 6.15 shows the non-dimensional sensitivity coefficients for heat flux and temperature with respect to blood perfusion. The corresponding coefficients with respect to contact resistance are given in Figure 6.16. Note the scales on the graphs; the sensitivity with respect to contact resistance is much higher than that for blood perfusion. The temperature sensitivity is very low for both cases. This low sensitivity of the system to the calculated surface temperature gives support to not using this quantity in the estimation procedure if the temperature relation or experimental data are suspect. The A2 probe has an increased heat flux sensitivity to both contact resistance and blood perfusion over the A1 probe. However, the magnitudes of the sensitivities to blood perfusion remain relatively small.

A comparison of Figs. 6.15, 6.16 shows that the parameters are not linearly dependent over the entire range of experiment. Some correlation may exist at later times, but as long as the estimation procedure is carried out over the entire test time, linear dependence effects should not pose a problem. What may cause convergence problems, however, is the relative dominance of contact resistance over blood perfusion within the estimation scheme.

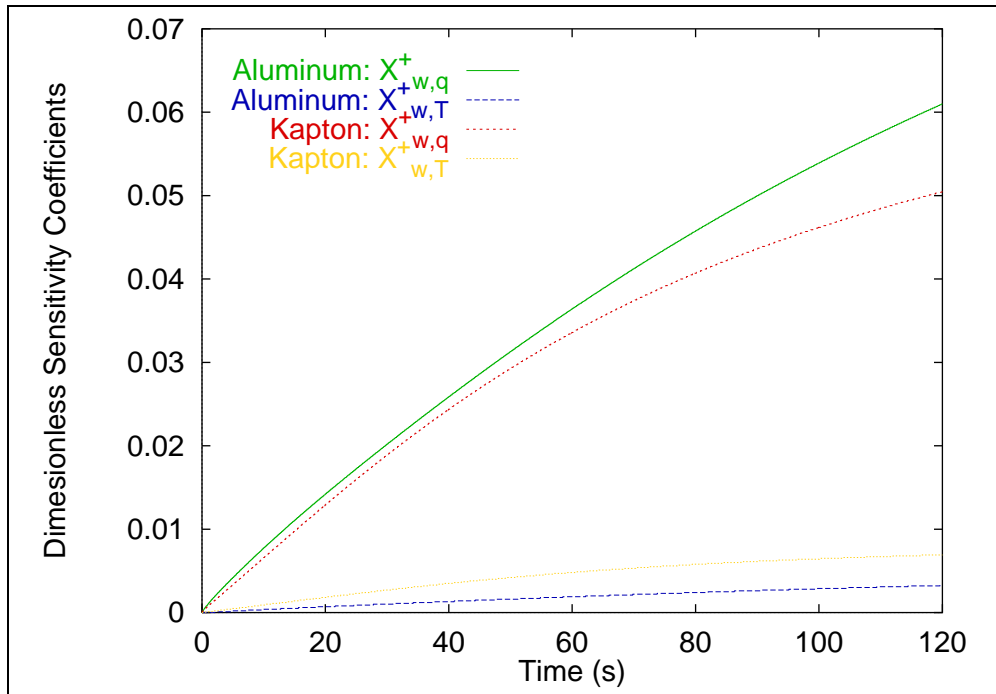


Fig. 6.15 Non-dimensional Sensitivity Coefficients of Heat Flux and Temperature to Blood Perfusion for the Type A Probes

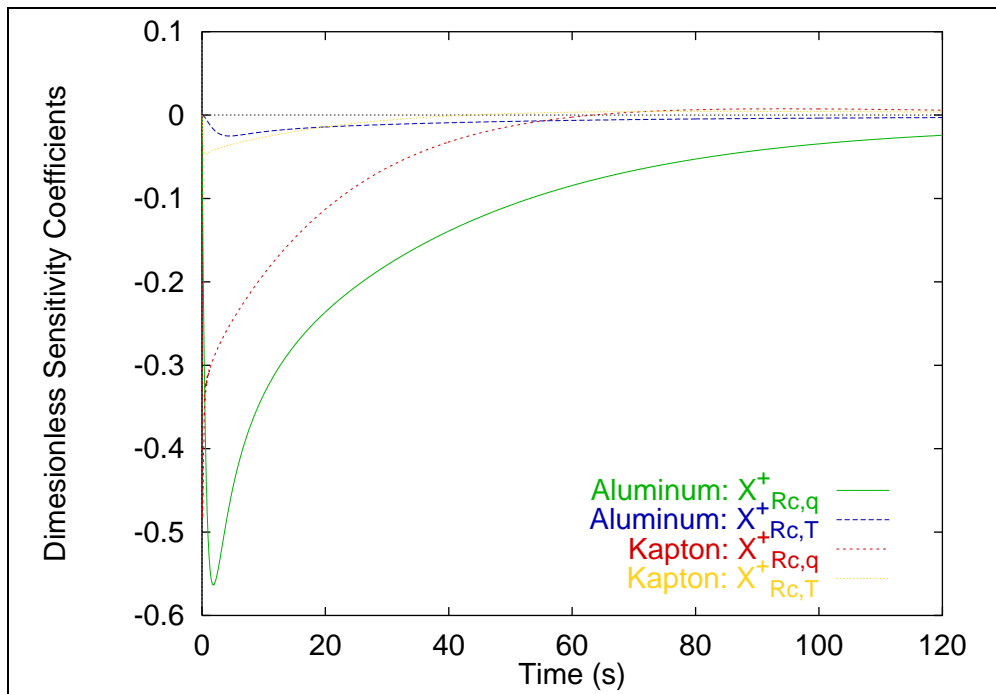


Fig. 6.16 Non-dimensional Sensitivity Coefficients of Heat Flux and Temperature to Contact Resistance for the Type A Probes

6.4 Results with Previous Data

The estimation procedure was applied to two sets of heat flux data from previous studies (O'Reilly et al. (1996), Figure 6). These two experiments were run under similar conditions using the A1 probe configuration. Trial-and-error attempts at finding contact resistance blood perfusion had been made, but no formal attempt of parameter estimation.

The results of performing the estimation scheme with this data and the corresponding A1 and tissue properties are shown in Table 6.4. The variance of the experimental data, σ_q^2 was 0.0015 W/m^2 , very low. This variance combined with low bias between the experiments and model led to the low 95 percent confidence intervals for the individual estimates as reported in table 6.4. This is also reflected in the low RMS_q values.

Figure 6.17 compares the experimental heat flux to model heat flux calculated with the parameter estimates for contact resistance and blood perfusion. The curves match well over the course of the data. Note, however, that for both tests a small bias is present during the beginning, transient portion of the test. This bias is further evident upon inspecting the residuals for heat flux, e_{qi} , defined as $e_{qi} = (q_{mi} - q_{ci})$ for each of the i^{th} measurements, illustrated in Fig. 6.18. The bias is denoted by the residual mean not equaling zero for the beginning portion of the plot. However, in the case of these experiments, the bias is relatively small compared to the overall residual variance. This beginning bias will become more pronounced in the results of the following sections.

Table 6.4 Estimation Results; Previous Data

Test	Estimated Properties		RMS_q
	R_c ($\text{m}^2\text{K/W}$)	w_b (ml/ml/s)	
Test 1	$(6.5 \pm 0.00005) \times 10^{-3}$	$(18.0 \pm 0.0005) \times 10^{-3}$	5.8×10^{-7}
Test 2	$(7.7 \pm 0.00005) \times 10^{-3}$	$(17.0 \pm 0.0005) \times 10^{-3}$	1.5×10^{-6}
Mean	7.1×10^{-3}	17.5×10^{-3}	-

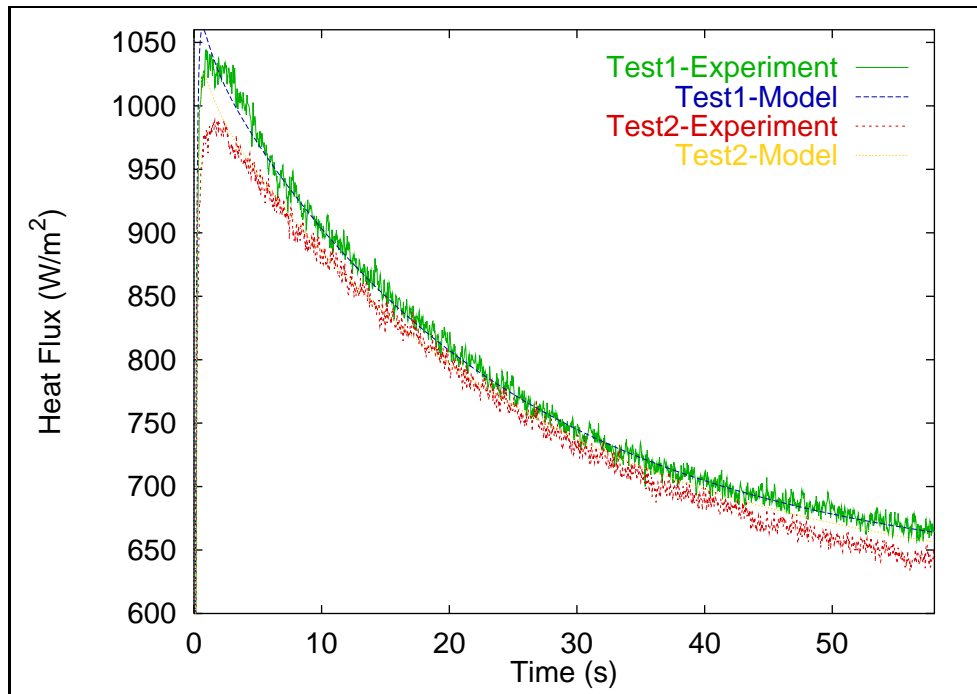


Fig. 6.17 Experimental Data and Model Output for Previous Tests

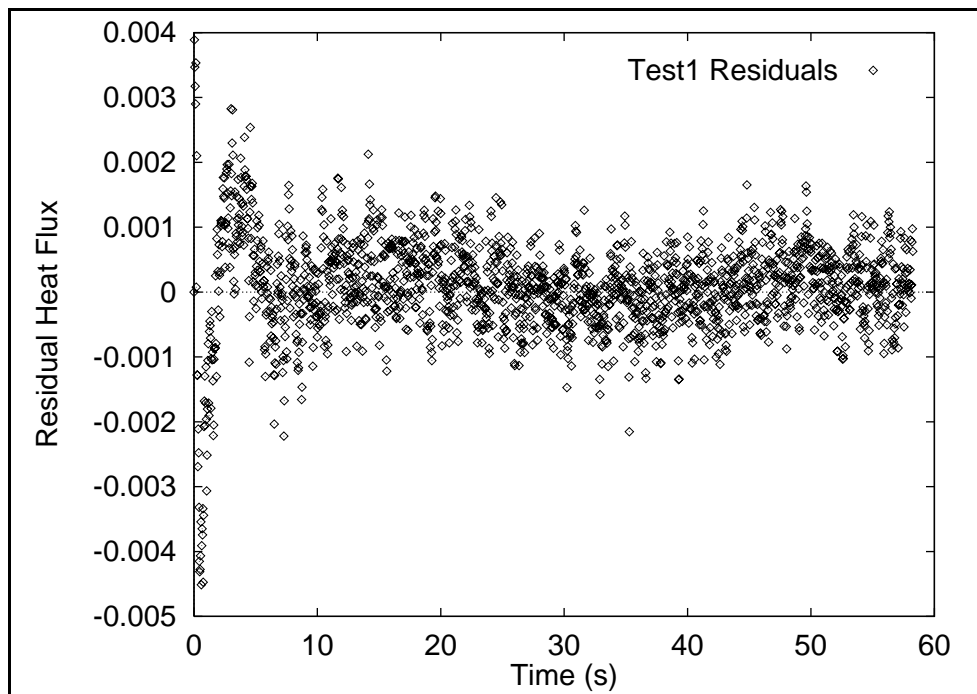


Fig. 6.18 Heat Flux Residuals from Previous Test 1

6.5 Results of A1 and A2 Experiments

6.5.1 Runs and A1 Trials

The parameter estimation scheme used in the preceding section was not so successful with the first Kapton experiments (Run 1-10). As mentioned in Section 5.2, the data from these experiments did not coincide with the previous data or with model output. The major difference was in the transient region, shown in Figure 6.19. Here, a comparison between the previous experimental tests and model output with Run 1 conditions shows that the current experiments do not contain the heat flux ‘spike’ observed before or expected based on the model. This created enough bias that the estimation process would not converge properly.

Further tests, Trials 1-5, were performed with the A1 probe to try different settling techniques to repeat the previous data. None of the techniques as described in Table 5.6 produced heat flux data of similar shape to the previous tests. All of the heat flux responses contained much lower and flatter transient ‘spikes’. No method existed that proved the repeatability of the previous data with the current experimental set up. Worse, the Trials data did not match with the biothermal model.

6.5.2 A2 Trials and Alums

This failure to resolve the heat flux transient ‘spike’ led to the addition of a known capacitance to the probe for more accurate modeling. Thus the A2 probe configuration was born. It was also a step towards simulating the then-in-design bioprobe B (Episensor).

The heat flux data from the settling procedure trials using the A2 probe, Trials 7-8 better matched the bioprobe model. The addition of the capacitance of the aluminum to the biothermal model flattened out the ‘spike’ and lengthened the transient probe response. This was also seen experimentally. Trial 8, letting the probe equilibrate before turning on the air, provided a good match in shape and magnitude to the typical model output for heat flux. Also, as previously noted, the A2 probe has a higher heat flux sensitivity to blood perfusion. Therefore, using the A2 probe to model a known probe capacitance and allowing thermal equilibrium before cooling, as in the Run experiments, is the best experimental protocol.

This experimental protocol was used to run several experiments (Alums) as described

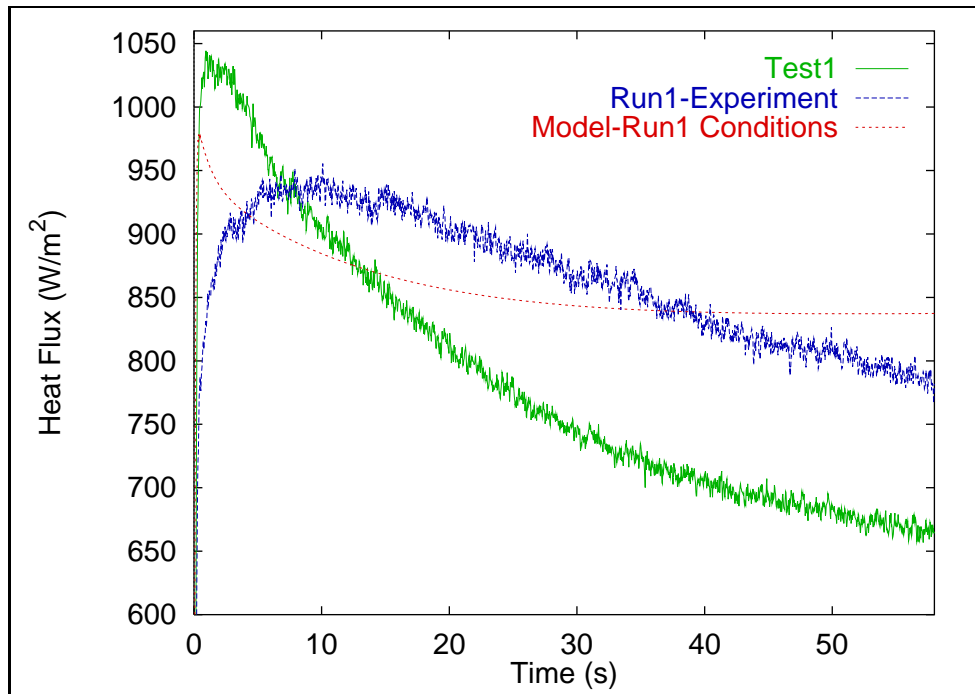


Fig. 6.19 Comparison of Run1 Data and Previous Test Heat Flux

in Section 5.3. Recall that here the air hose size was increased over that used in the Run and Trial experiments. This provided larger cooling that led to higher heat flux, seen in the comparison the the maximum heat flux in the ‘Run 1’ curve (1000 W/m^2) to the maximum in the ‘Alum’ curves (1600 W/m^2). The estimation procedure was applied to this data to simultaneously estimate blood perfusion and contact resistance as before. Here, however, the estimation scheme did not converge. This lack of convergence was blamed on both the bias still present between model and experiment and the imbalance in sensitivities of the system.

Therefore the estimation procedure was restructured to avoid the effects of the sensitivity imbalance. An iterative scheme was developed where the Box Kanemasu method was used to estimate perfusion based on a fixed value for contact resistance. The blood perfusion was then held fixed at the previously estimated value and the contact resistance estimated. This two-step ‘switching’ procedure was repeated until the individual estimates converged. Convergence generally was achieved within four iterations.

Because of the poor agreement between calculated and experimental surface temperatures, the temperature was removed from the estimation process. As the sensitivity

analysis showed, the heat flux was much more responsive to blood perfusion and contact resistance than the temperature, by an order of magnitude. So the temperature data does not add much value to the estimation process. The ‘switching’ estimation procedure was carried out using only heat flux measurements.

The resulting estimates, 95% confidence intervals, and RMS_q values are given in Table 6.5. The step-by-step iterative estimates for Alum 1 are given to show the convergence of the switching procedure. Figure 6.20 displays the experimental and calculated heat fluxes for each ‘Alum’ experiment based on the estimates in Table 6.5. Note the continued presence of bias in the transient portion of the curves. If the RMS_q is calculated over the last portion of the curve, neglecting the first 10 seconds, the value reduces almost in half. This is important since this portion of the curve is under the effect of blood perfusion. Regardless of the beginning bias, dominated by contact resistance, a good match of the curves (low RMS_q values) during the later times is more important for producing a good blood perfusion estimate. The end-time error values are given in Table 6.5 as RMS_q^* .

It should be noted that Alums 2 and 3 were performed on a different subject than Alum 1. Hence, the difference in magnitude of the perfusion estimate between these tests. All three estimates are still within expected ranges for skin tissue blood perfusion under various conditions (cited as 0.0005 to 0.005 ml/ml/s by Johnson et al. (1986)).

6.6 Results of Aluminum Phantom Experiments

The positive results obtained with the bioprobe A experiments led to advancement to the bioprobe B configuration and experimentation with this probe on both biological and phan-

Table 6.5 Estimation Procedure Results; Alum Experiments

Test Name		Estimated Parameters		RMS_q	RMS_q^*
		$R_c(\text{m}^2\text{K}/\text{W})$	$w_b(\text{ml}/\text{ml}/\text{s})$		
Test 1	Iteration 1	0.003	0.00164		
	Iteration 2	0.0037	0.00102		
	Iteration 3	0.0036	0.00081		
	Iteration 4	0.0035	0.00070		
	Iteration 5	$0.0035 \pm 3.9 \times 10^{-7}$	$0.00070 \pm 1.3 \times 10^{-6}$	44.7	25.4
Test2		$0.0023 \pm 3.6 \times 10^{-7}$	$0.0044 \pm 1.7 \times 10^{-6}$	45.2	24.1
Test3		$0.0032 \pm 2.1 \times 10^{-7}$	$0.0035 \pm 0.8 \times 10^{-6}$	73.2	45.6

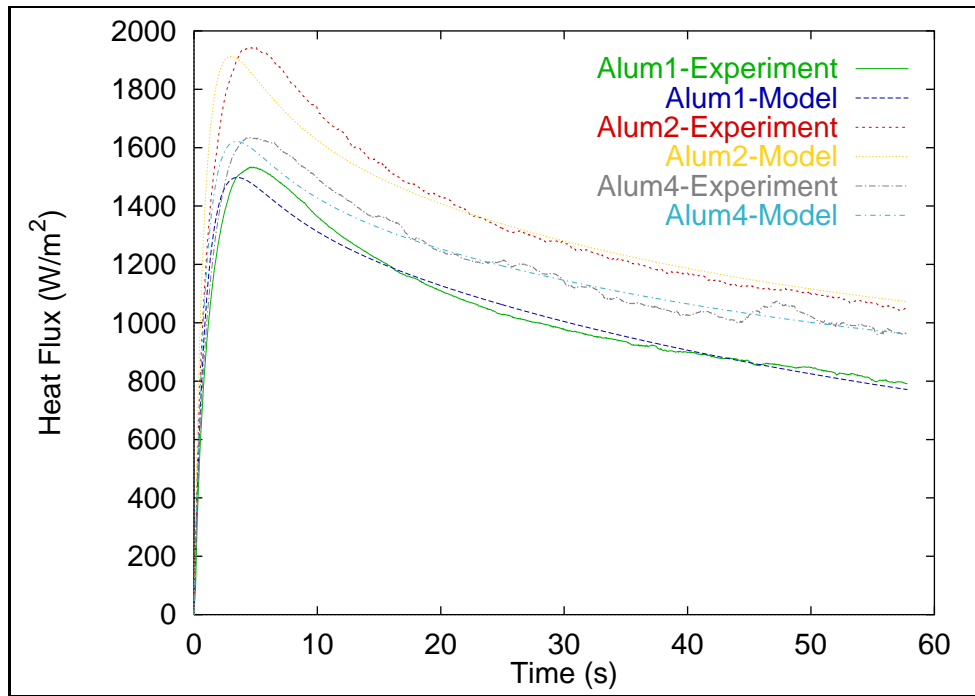


Fig. 6.20 Comparison of Experimental and Model Heat Flux Outputs; Alum Tests

tom media. These experiments were described in Chapter 5. The results of those measurements and the parameter estimation efforts that followed are described here.

6.6.1 Convective Heat Flux Experiments on Aluminum Phantom

The heat flux and temperature curves, along with the corresponding contact resistance and perfusion estimates and model output for the first aluminum experiments are shown in Figure 6.21. The flat nature of these conductive heat flux curves is not exactly the desired response, but variation between the curves at different flow rates is evident. The estimates for contact resistance and perfusion show this difference as well. The sensitivity coefficients for this system are given in Figure 6.22. Note that the imbalance between contact resistance and blood perfusion sensitivity still exists as before. These three tests appear successful in that differences in heat flux and temperature response are observed as well as increasing perfusion estimates with increasing flow rates.

This provided the basis for more experiments with greater flow rate variation. The initial success, however, was not repeatable. Representative heat flux from the 34 tests

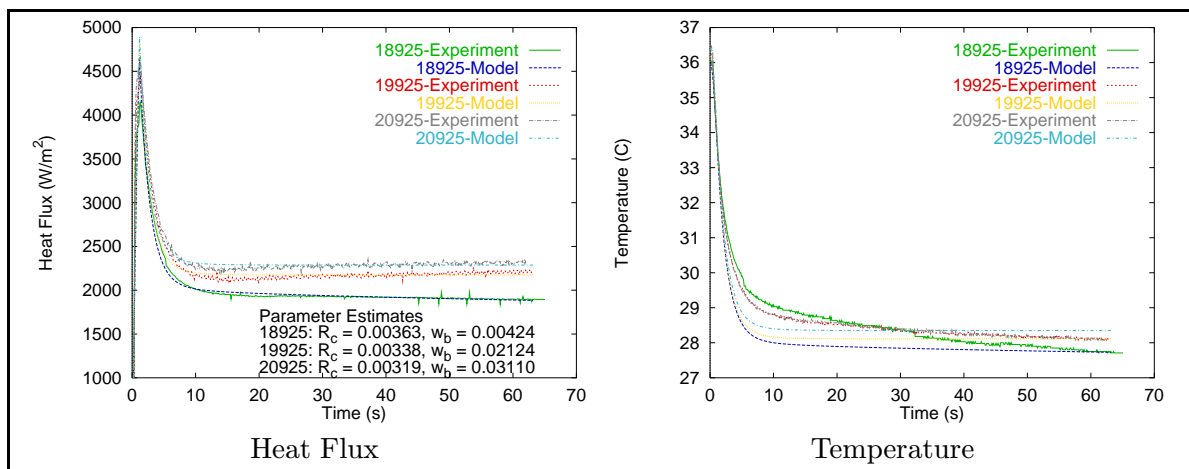


Fig. 6.21 Heat Flux and Temperature Output for First Aluminum Phantom Tests

performed at each of 8 flow rates showed no distinct variation in heat flux or temperature (Fig. 6.23). Also, data from repeated tests with the same flow rate (Fig. 6.24) were not consistent. At first, this could be explained by variation in environment conditions or contact resistance from test to test. The exact value of air and initial temperature were not able to be controlled experimentally. Also, contact resistance could change due to small changes in probe settling on the media. Differences in these quantities would shift the heat flux curves along the heat flux axis (See Section 6.1.1). This would mean the experimental data at different flow rates could overlap yet still lead to different perfusion estimates.

This could not be effectively checked due to problems with the estimation procedure using these data sets. Bias between model and experiment along with the low sensitivities contributed to non-convergence in most cases. At this point, the estimation procedure was modified to try and account for the bias. Trial and error attempts at finding R_c , w_b showed that the model was still biased during the transient portion of the experiment. This was also evident in the first experiments. The model output and estimation procedure were being dominated by contact resistance effects. This was reinforced by the fact that in trying the ‘switching’ method used above, the program converged on R_c estimates, but generally failed to converge on estimates for perfusion.

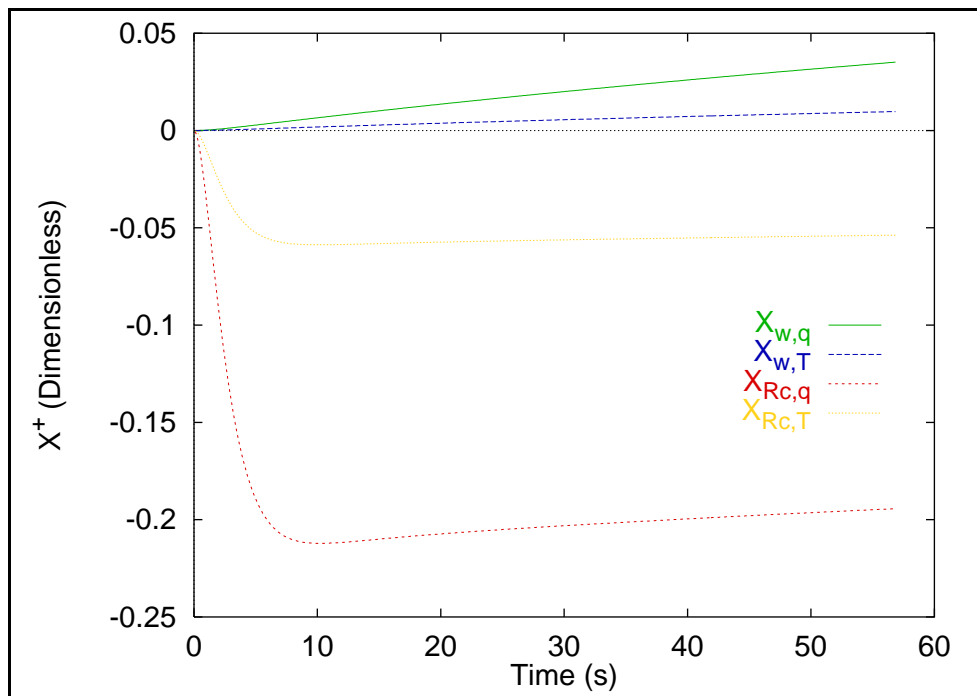


Fig. 6.22 Dimensionless Sensitivity Coefficients of Convective Heat Flux and Surface Temperature to Contact Resistance and Perfusion for Bioprobe B on Aluminum Media

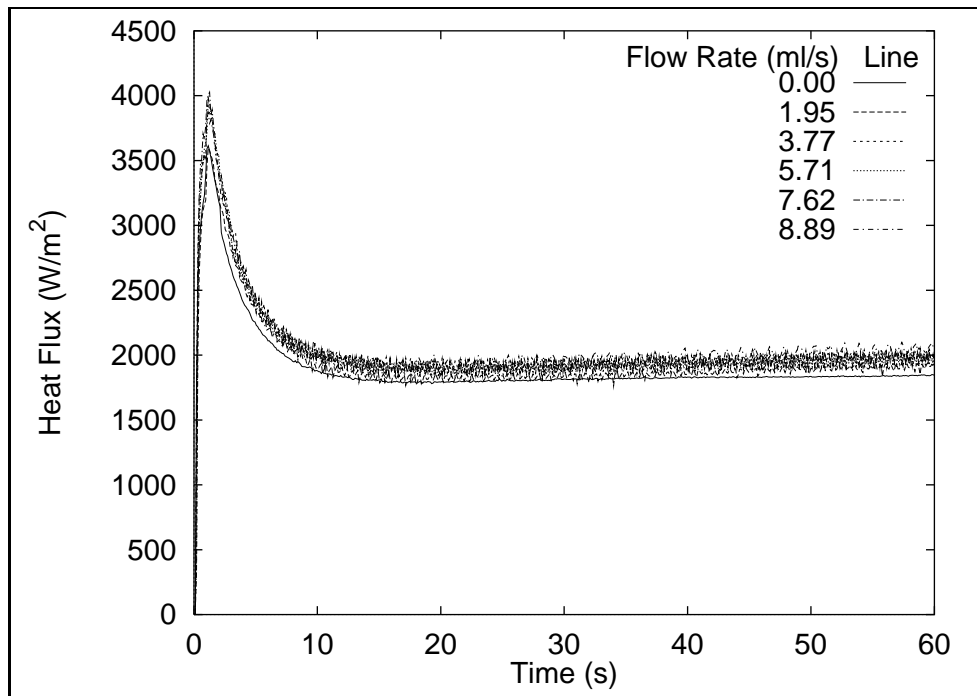


Fig. 6.23 Heat Flux Data from Aluminum Media Tests at Different Flow Rates Showing No Correlation with Flow Rate

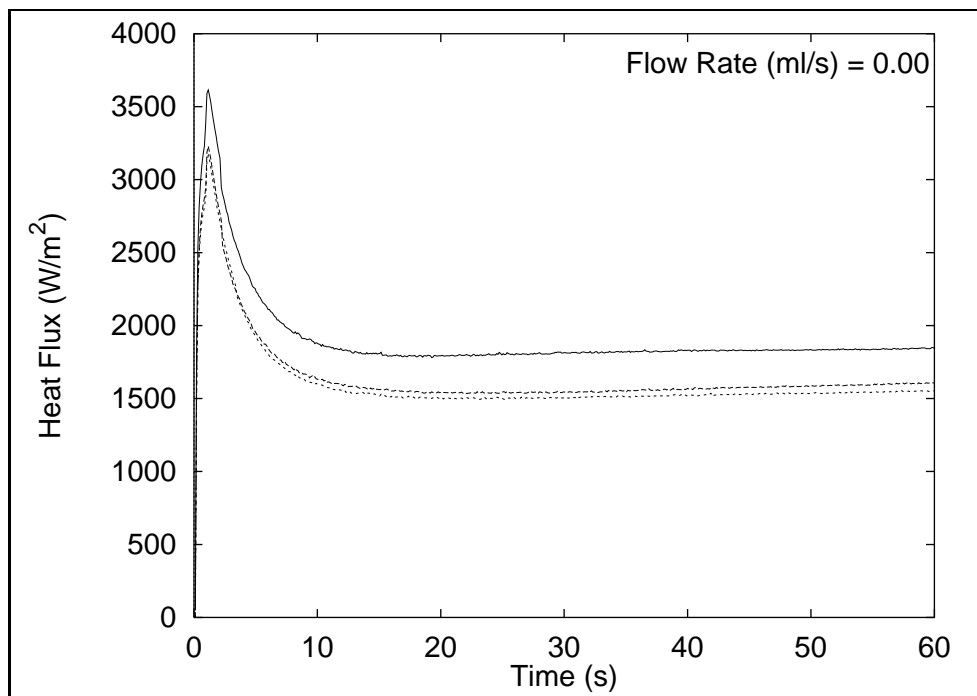


Fig. 6.24 Heat Flux Data from Aluminum Media Tests at the Same Flow Rate Showing Non-Repeatability

Two changes to the estimation program were attempted as a way to rectify this situation. One, estimation was performed using the end portion of the data ($> 10s$) where the data is more dominated by perfusion. Second, the beginning portion of data ($< 10s$) was scaled by increasing the experimental variance by a factor of 10. This effectively lowered the importance of this data compared to the end data, but still used all the data in estimating the unknown parameters. These two methods were attempted with the switching scheme, with estimating both parameters at once (B-K Method), and with just Gaussian estimation (no B-K modification). For these estimation attempts, only the heat flux data were used since the temperature issue was never properly resolved and the sensitivity of temperature remained low.

After validation of these processes with simulated data, they were applied to tests 18925-20925 (Table 5.11) since these ‘worked’ before. The results for 19925 compared to earlier estimation are tabulated in Table 6.6. Similar results are seen for Tests 18925 and 20925. In general, the end data case provided estimates where the model agreed slightly better with experiment, but not so remarkably as to justify using this method over the more theoretically correct program incorporating all the experimental data.

While these estimation procedures worked for some experiments, not one was found that provided converged estimates in all cases. In the experiments that did converge, the values of contact resistance and perfusion did not differ with respect to experimental flow rate. The end conclusion, then, was that the initial success of Tests 18925-20925 were not repeatable. Using absolute heat flux measurements in conjunction with the current model would not provide decent perfusion estimates.

Table 6.6 Results of Varied Estimation Procedures on 19925 Data; *BK* denotes concurrent estimation using the Box-Kanemasu Modification, *Gauss* denotes concurrent estimation using just the Gauss Method

Estimation Type	R_c (m^2K/W)	w_b (ml/ml/s)
All Data, Unscaled, BK	0.00338	0.02124
All Data, Unscaled, Gauss	0.00338	0.02122
All Data, Unscaled, Switching Method	0.00338	0.02124
All Data, Scaled, Gauss	Did Not Converge	
End Data, BK	0.00357	0.04388
End Data, Gauss	Did Not Converge	
End Data, Switching Method	0.003314	0.01704

Another tactic could be employed, however. It was previously investigated (Fouquet et al., 1993) that changes in contact resistance or blood perfusion changed the *slope* of the heat flux output over the beginning and end regions, respectively. Therefore, instead of fitting absolute values, using the estimation scheme on slope calculations from the data over these two regions might lead to favorable results. Looking just at slopes in terms of $\Delta q/\Delta t$ would eliminate the problems of offset in absolute heat flux values due to environmental factors. So, while the heat flux curves in Fig. 6.24 might not lie on top of one another, the slopes may be the same, leading to the same perfusion estimates.

The model was evaluated for slope evaluations to support this possible avenue of estimation. The forward model was run using the aluminum media and bioprobe B properties. In addition to heat flux and temperature output, the slopes of these curves over time were calculated using the endpoints at particular times during the simulation. These times were determined by observations of where the blood perfusion and contact resistance began to effect the slopes of conductive and convective heat flux and surface temperature, and where such effects stopped. The conditions used in the simulation were as follows:

$$T_i = 36.28 \text{ }^\circ\text{C}$$

$$T_{core} = 37.0 \text{ }^\circ\text{C}$$

$$T_\infty = 25.0 \text{ }^\circ\text{C}$$

$$h = 480.0 \text{ W/m}^2\text{K}$$

Simulation Time = 60 seconds

The times used for the slope calculation are given in Table 6.7. The simulation was run for all 40 combinations of $R_c = 0.0001, 0.0005, 0.001, 0.005, 0.01$; and $w_b = 0.00, 0.0001, 0.0005, 0.001, 0.005, 0.01, 0.05, 0.1$. This process was also repeated using skin tissue properties instead of the aluminum media properties.

Figure 6.25 shows graphs of heat flux output for varying blood perfusion at two

Table 6.7 Calculation Times for Determining Heat Flux and Temperature Slope with Respect to Contact Resistance and Blood Perfusion

Model Output	Time from Simulation Start (s)	
	R_c ($\text{m}^2\text{K/W}$)	w_b (ml/ml/s)
Conduction, q''_{cond}	0.0-1.5	15.0-60.0
Convection, q''_{conv}	1.5-2.0	15.0-60.0
Temperature, T_p	1.0-2.0	15.0-60.0

constant contact resistance values for aluminum properties. For lower values of R_c and w_b , the curves show obvious slope differences, but at higher values, no real difference in slope for varying w_b appears. This is reinforced by looking at the slope values plotted against perfusion in Fig. 6.26. For $w_b > 0.01$ this graph is a horizontal line, indicating no change in slope with respect to perfusion. The same trends are also seen for contact resistance. Note the similarities in curve shape and magnitude of the high R_c, w_b curves and the experimental data for 18925, 19925, 20925 given previously. The experimental curves coincide with the model areas of insensitivity to blood perfusion. These trends are less evident in the simulations using skin properties. Figures (6.27) and (6.28) show that with skin properties, especially in the range of expected physiologic blood perfusion (0.0005-0.005 ml/ml/s), slope variations do exist.

This shows then, that the aluminum phantom experiments are in a range of high R_c , w_b , and thermal properties ($k_t = 9.21$ W/mK) that make the thermal response of the system insensitive to flow rate. The earlier estimation procedure is not wrong, but rather the experimental data are invalid for making estimations based on heat flux measurements. A different media must be used that has thermal properties similar to biological tissue ($k_t = 0.5$ W/mK).

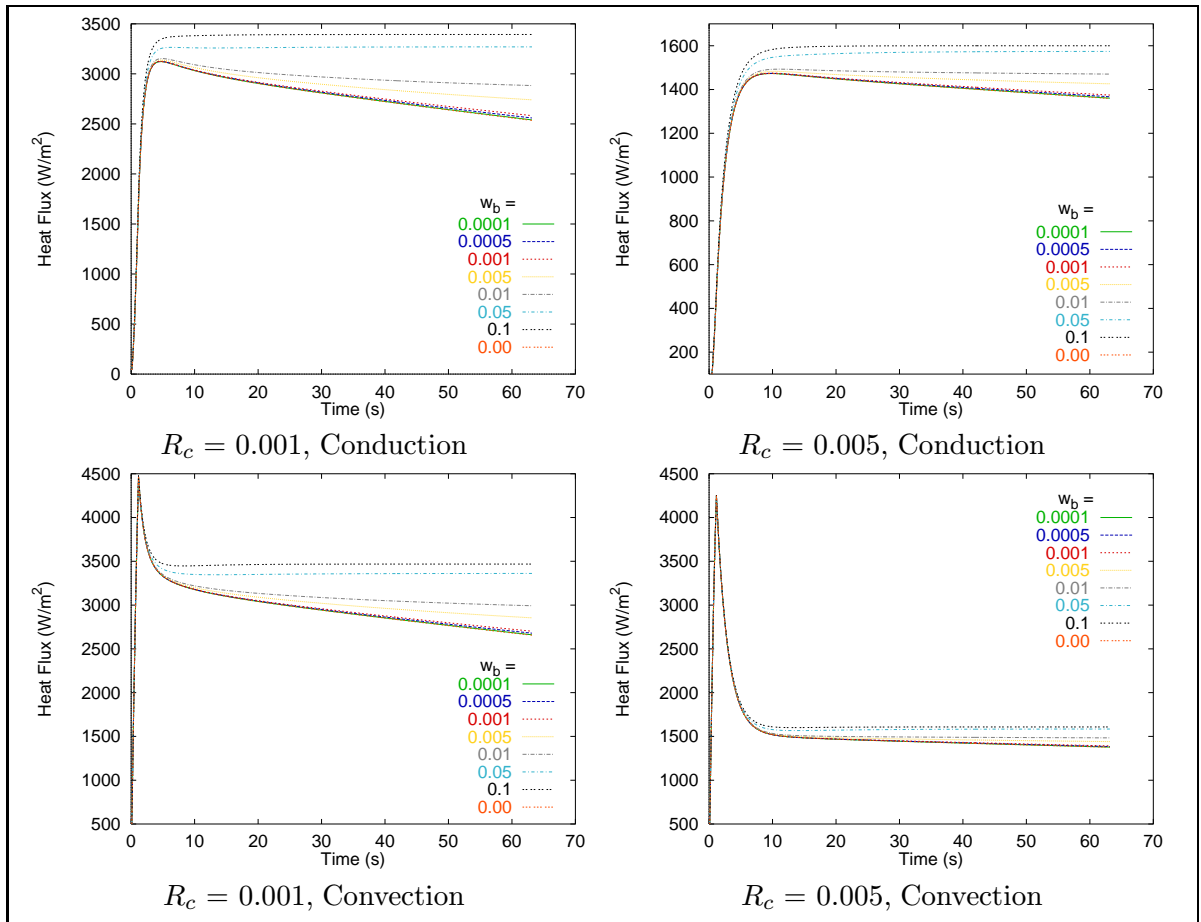


Fig. 6.25 Model Heat Flux Output for Varying Blood Perfusion Values at Constant Contact Resistance. Trends are shown for two set contact resistance values for both conductive and convective heat flux for Bioprobe B on aluminum porous media. Values for R_c are given in m²K/W.

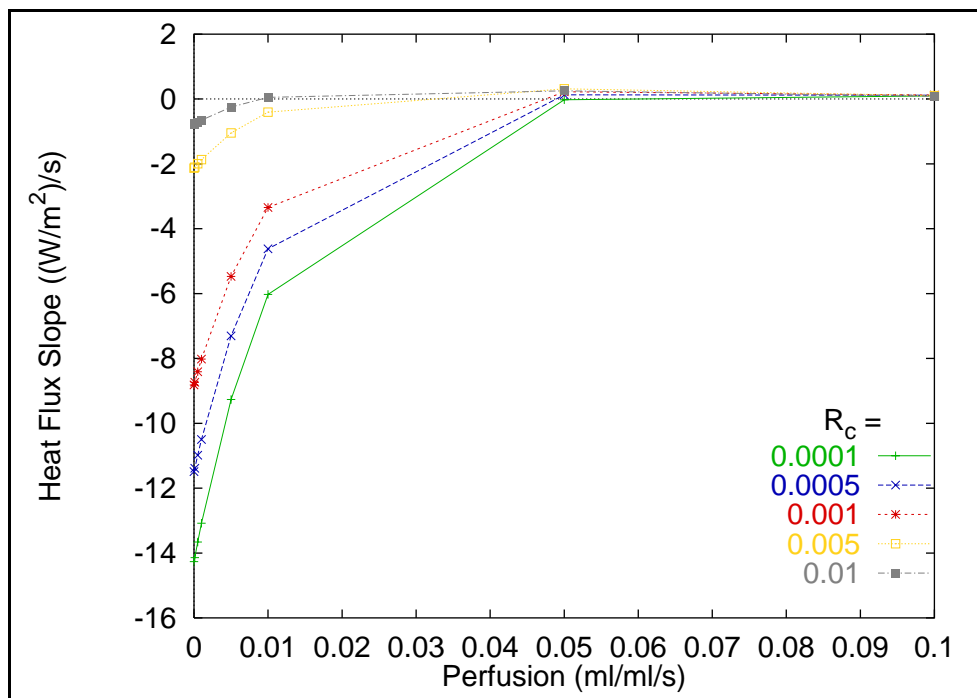


Fig. 6.26 Conductive Heat Flux Slopes over Time Plotted Against Blood Perfusion

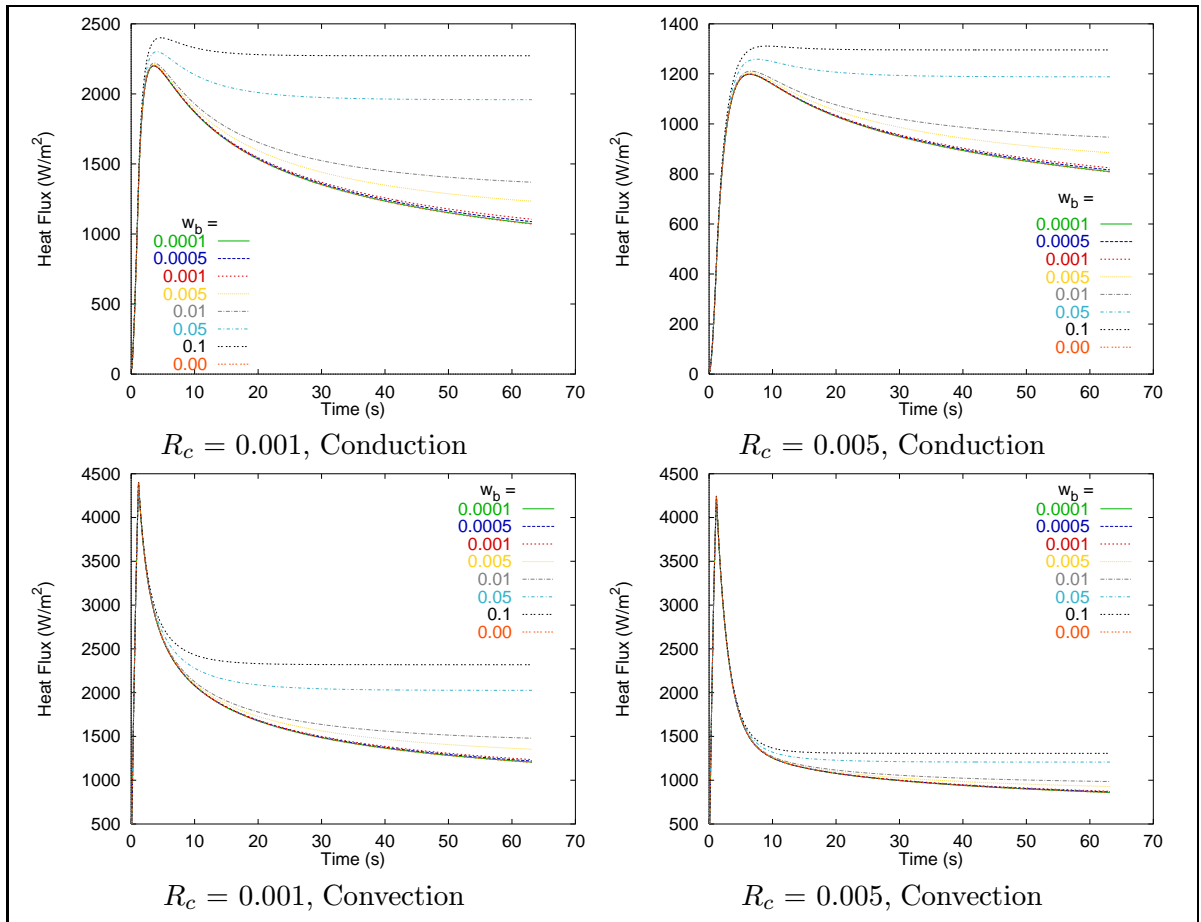


Fig. 6.27 Model Heat Flux Output for Varying Blood Perfusion Values at Constant Contact Resistance. Trends are shown for two set contact resistance values for both conductive and convective heat flux for Bioprobe B on skin tissue. Values for R_c are given in $\text{m}^2\text{K}/\text{W}$.

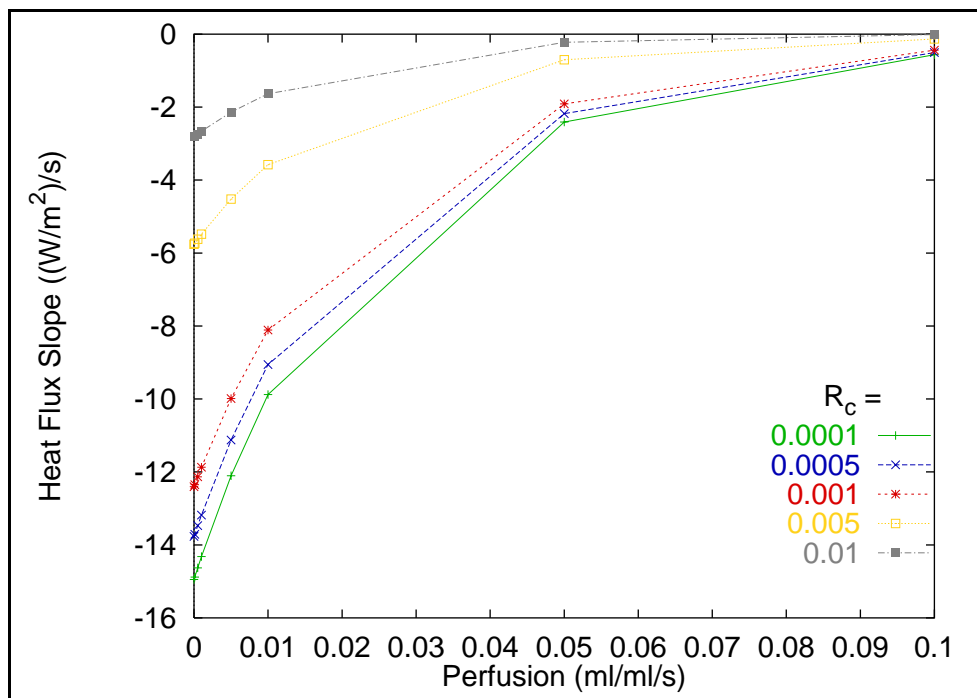


Fig. 6.28 Conductive Heat Flux Slopes over Time Plotted Against Blood Perfusion

6.6.2 Aluminum-Arm Comparisons

The above observations of poor heat flux variability to flow rate led to checking phantom experimental data with similar experiments on the forearm as described in 5.4.2 and Table 5.12. Figure 6.29 shows a comparison of heat flux from these six tests. The results between phantom and real tissue are quite different. This further enforces the conclusion that the aluminum media set-up incorporates a combination of R_c , w_b , and thermal properties that make it invalid as a phantom or direct simulation of the physiologic process of perfusion in cutaneous tissue.

6.7 Results of Arm Tests with Bioprobe B

The heat flux and corresponding estimate values and model output for the arm experiments in 5.4.2 are shown in Fig. 6.30. Here, estimates for R_c and w_b were calculated concurrently using the most recent, correct version of the parameter estimation program incorporating all of the heat flux data, unscaled, with just Gaussian estimation. Once again, bias is present between model and experiment. The parameter estimation process converged, but the process is dominated by contact resistance and the match of model and experimental heat flux during the end times are off. These results are still better than the previous attempts that provided no actual estimates.

Estimates for Episkin 2,3 were calculated using the parameter estimation scheme both with just end data and with scaling the beginning data. Once again an attempt to minimize the dominance of R_c on the estimation process. The results were not any closer to the experimental data. So, the best results stand as shown in Fig. 6.30. The perfusion estimates are higher than expected for physiologic values of blood perfusion, 0.01 versus 0.004 ml/ml/s, but consistent with the values found in the low flow rate phantom cases discussed in the next Chapter.

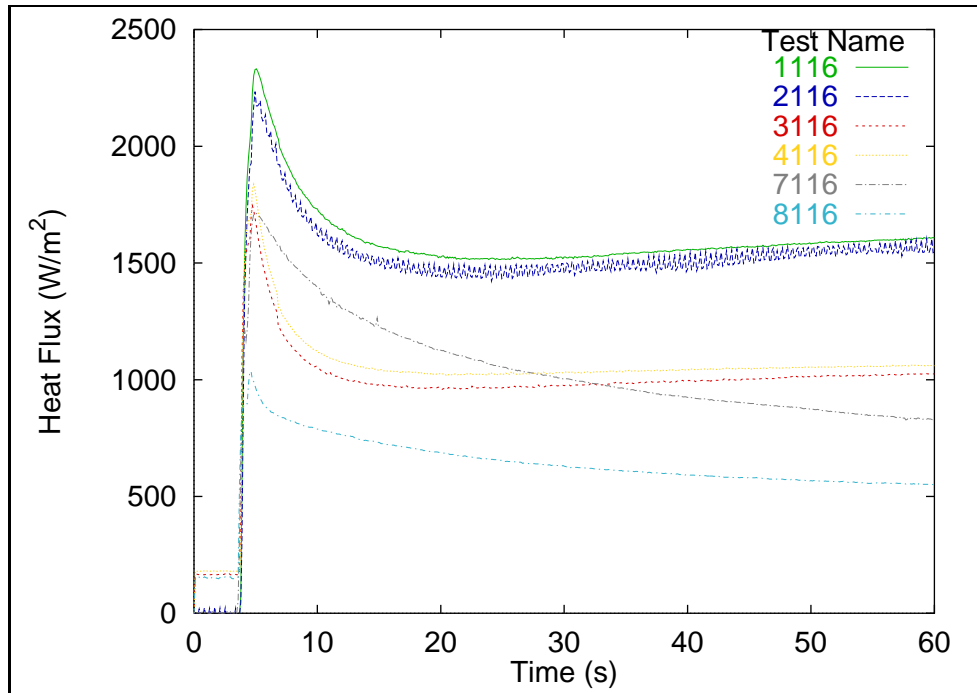


Fig. 6.29 Comparison of Aluminum Phantom and Arm Heat Fluxes; The aluminum phantom experiments (1116-4116) have a much different shape and magnitude than the corresponding arm experiments (7116-8116)

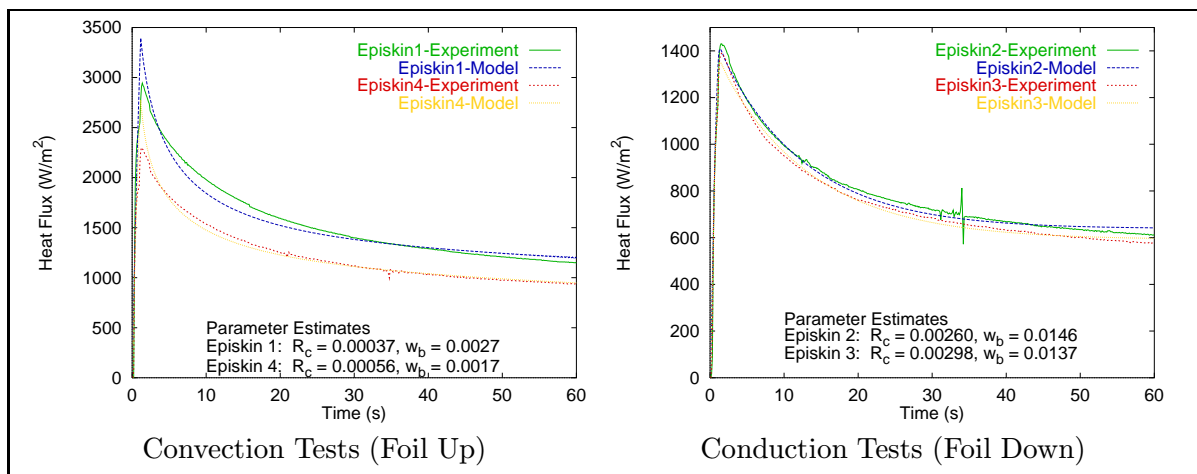


Fig. 6.30 Results of Arm Experiments with Bioprobe B, Episkin Tests

Chapter 7

Sponge Phantom Experimental Results and Evaluation

Due to the failure of the porous aluminum experiments, the media needed to be changed to a substance with much different thermal properties. The cellulose sponge as described in 4.4.2 provided such a change. From Tables 5.4 and 5.13 it is evident that the sponge has effective thermal properties close to those generally used for skin tissue. Also, the softness of the sponge material allows for more intimate contact between sponge and probe, reducing the high contact resistance problems encountered with the aluminum media. This system provides a much better simulation of the arm experiments. The results and subsequent evaluations of the 36 sponge experiments are described here.

7.1 Results

7.1.1 Qualitative Evaluation of Sponge Phantom Thermal Response

First, some representative sponge data were compared to the arm experiments with bioprobe B to check for similarity of shape and magnitude, something lacking in the aluminum media experiments. Figure 7.1 displays heat flux data from sponge tests Sp111, Sp311 (Table 5.14) and arm tests Episkin 2,3 (Table 5.9). The general shape and magnitudes match well, giving confidence that the sponge media provides an acceptable thermal phantom for skin tissue. Next, Figure 7.2 contains representative heat flux curves from each of the four experimental flow rates (0, 1.01, 1.95, 2.92 ml/s). There are distinct differences in slope and magnitude

of these curves in correlation with experimental flow rate. This observation is further supported by the sensitivity coefficients for this system given in Fig. 7.3. As expected, these dimensionless sensitivity coefficients, calculated at nominal values of $R_c = 0.00302 \text{ m}^2\text{K/W}$ and $w_b = 0.03872 \text{ ml/ml/s}$, behave much like the sensitivity coefficients for skin tissue. Notice that at these higher values of perfusion, the imbalance between perfusion and contact resistance sensitivity is not quite as great. Also, the values for perfusion sensitivity are above the 10% range, unlike in some of the other experiments. This system should provide experimental data sensitive to flow rate.

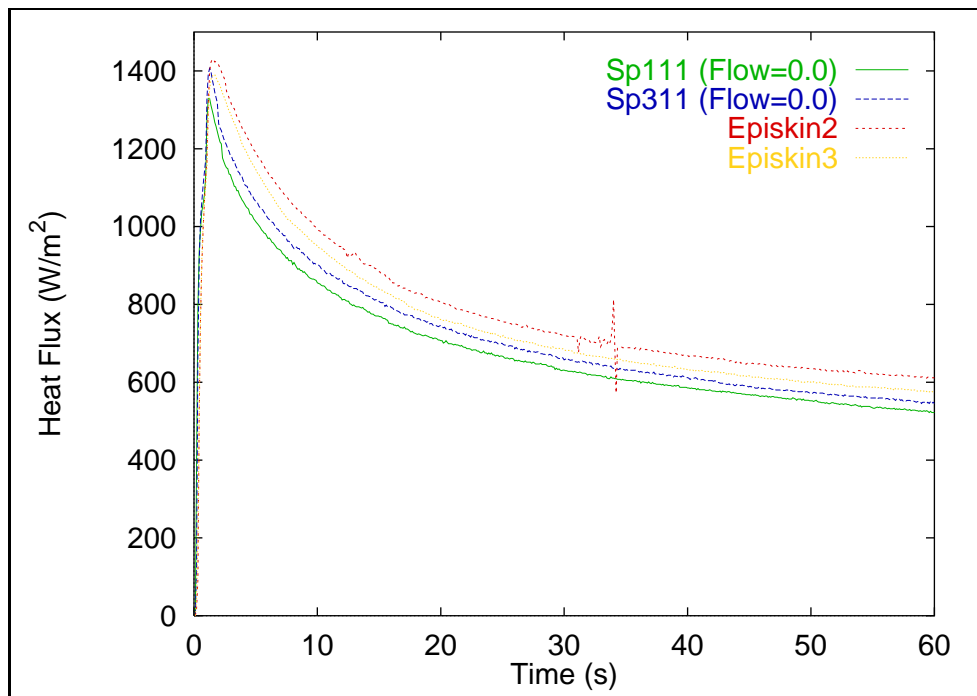


Fig. 7.1 Comparison of Heat Flux from Sponge and Arm Experiments Using Bioprobe B

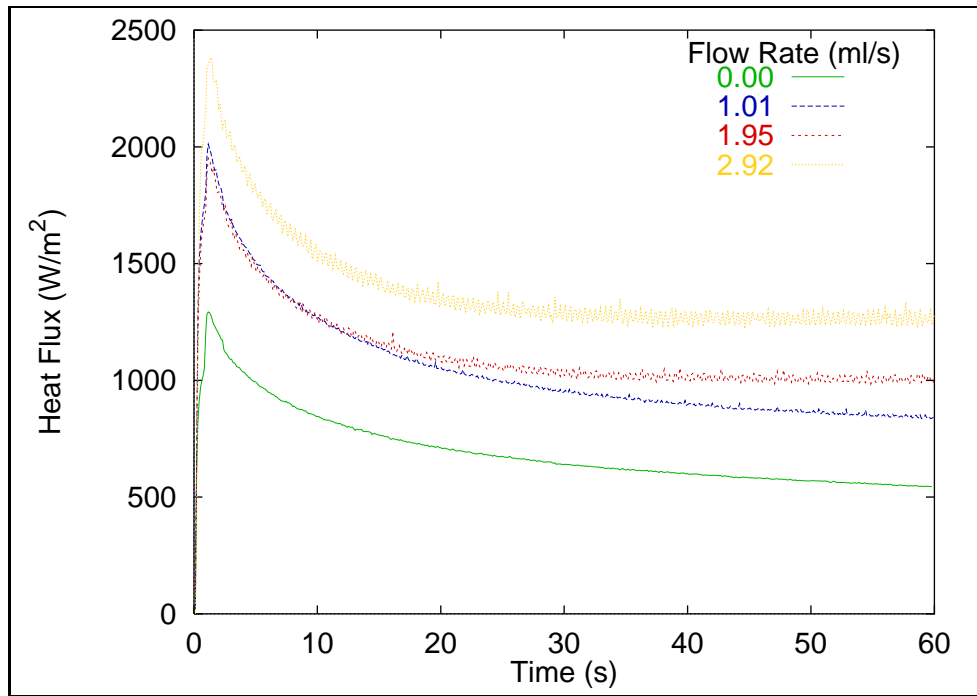


Fig. 7.2 Representative Heat Flux Data from Four Sponge Tests at Different Flow Rates

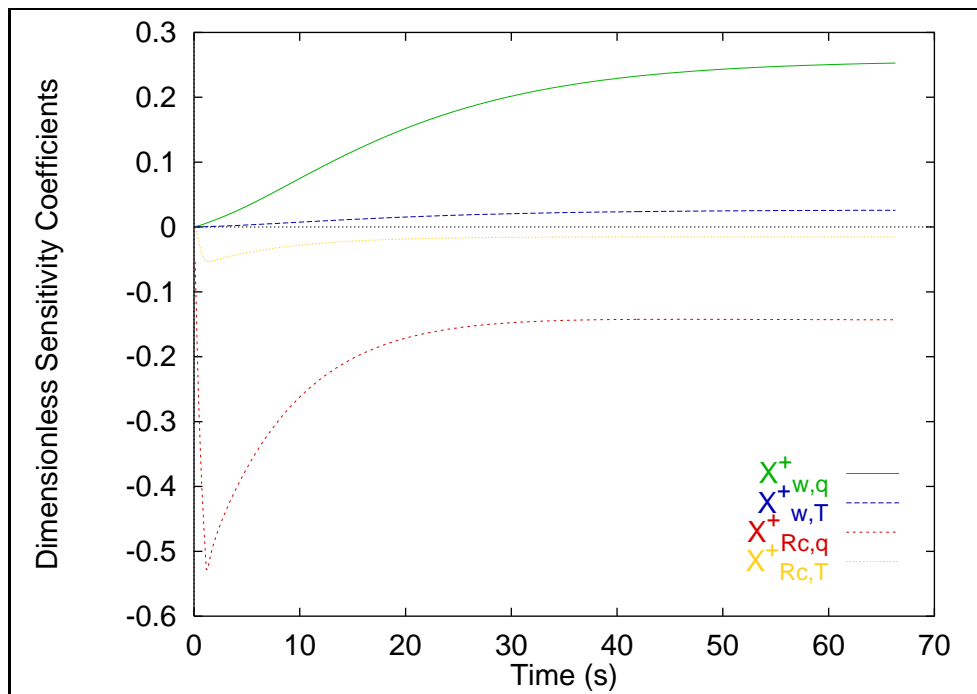


Fig. 7.3 Sensitivity Coefficients of Heat Flux and Temperature to Contact Resistance and Perfusion for Sponge Experiments

7.1.2 Parameter Estimation Results

The experimental data collected in the 36 sponge tests (Section 5.4.2) were used in the estimation scheme. Since the absolute heat flux measurements should coincide well with the model, and not overlap each other as in the aluminum media experiments, the slope estimation method described before was abandoned for the original parameter estimation process. Here, though, the Box-Kanemasu Modification was not used. The unmodified Gauss method was applied to all the heat flux data with no scaling. Upon comparison with the straight Gauss and B-K Modification, the same estimates were obtained. The B-K modification took at least the same if not more permutations through the model to converge and give the same amount of information as the Gauss method alone. Therefore, the extra steps involved with the B-K method were deemed unnecessary.

The results of four estimation attempts with sponge data (one for each experimental flow rate) are given in Table 7.1. The test names, estimates for contact resistance and perfusion, along with their 95 % confidence intervals, and the RMS_q values are tabulated. The resulting model heat flux from these estimates is compared to the experimental heat flux in Fig. 7.4. Note that some bias is still present in the beginning part of the curves. Once again, this could be due to errors in the values set for the thermal properties of the probe or tissue. Overall, the curves match fairly well as signified by the low confidence intervals for the individual estimates. Similar results are apparent for all 36 sponge tests, given in Appendix D.

All the individual contact resistance and perfusion estimates are plotted against the corresponding experimental flow rate in Figs. 7.5, 7.6 respectively. The error bars are for the 95% confidence intervals for each estimate as calculated by the model uncertainty method described in Chapter 4. A description of this process as applied to the sponge data

Table 7.1 Results of Parameter Estimation for Four Sponge Experiments

Test Name	Flow Rate (ml/s)	R_c (m ² K/W)	w_b (ml/ml/s)	RMS_q
Sp211	0.00	$0.00395 \pm 9.6 \times 10^{-7}$	$0.01326 \pm 4.0 \times 10^{-6}$	75.0
Sp511	1.01	$0.00274 \pm 3.1 \times 10^{-6}$	$0.02328 \pm 2.5 \times 10^{-5}$	18.8
Sp811	1.95	$0.00302 \pm 1.1 \times 10^{-5}$	$0.03872 \pm 1.6 \times 10^{-4}$	5.4
Sp1111	2.92	$0.00243 \pm 1.6 \times 10^{-5}$	$0.04867 \pm 3.2 \times 10^{-4}$	3.0

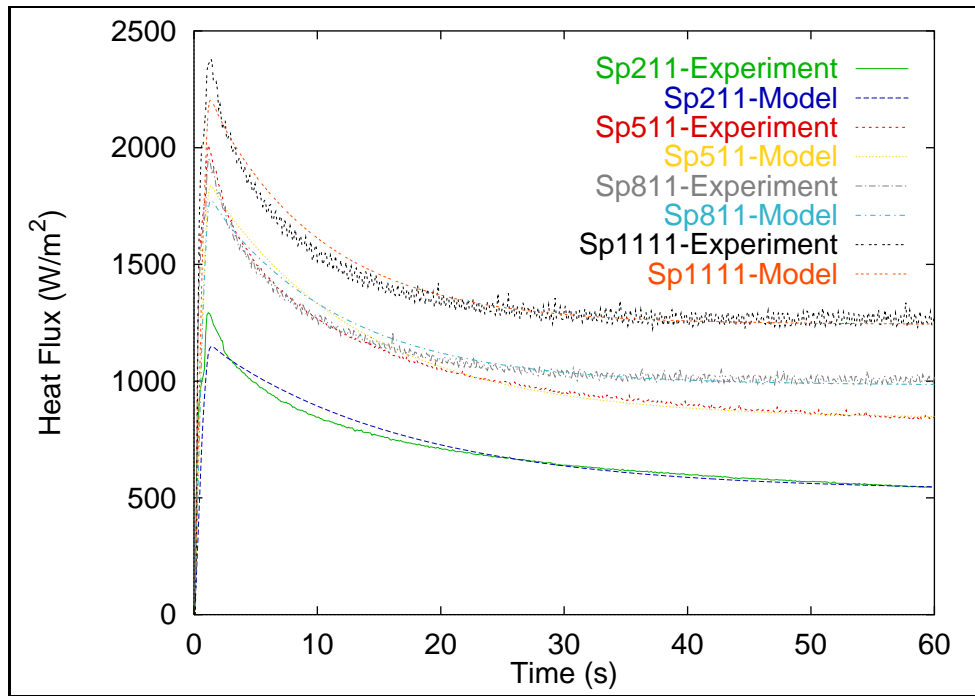


Fig. 7.4 Heat Flux from Experiment and Model Based on Parameter Estimates for Four Sponge Experiments; Representative of all the sponge experimental results.

is given below. Recall that three separate sets of experiments were performed on different days. The lines in the figures are through the estimate averages for each flow rate on each different day.

From the lines in Fig. 7.5 it appears that no strong correlation exists between contact resistance and flow rate. The curves do exhibit some downward slope with respect to flow rate. However, this phenomena is not consistent, as shown by the line through the Test 2 averages. Also, the changes in the R_c estimate averages between each flow rate are small, around 10%.

As mentioned before, it is expected that while the perfusion estimates will not equal the flow rate, some nearly linear, positive correlation will be present. This is true for all three sets of tests as shown in Fig. 7.6. The average lines for the three separate days do not fall atop one another, but do lie within reasonable experimental error of one another. Many experimental factors, such as differing environmental conditions, changes in thermal properties over time, or slightly different flow settings, to name a few, can cause variations in experimental data from day to day. Even with these slight offsets, the fact that the

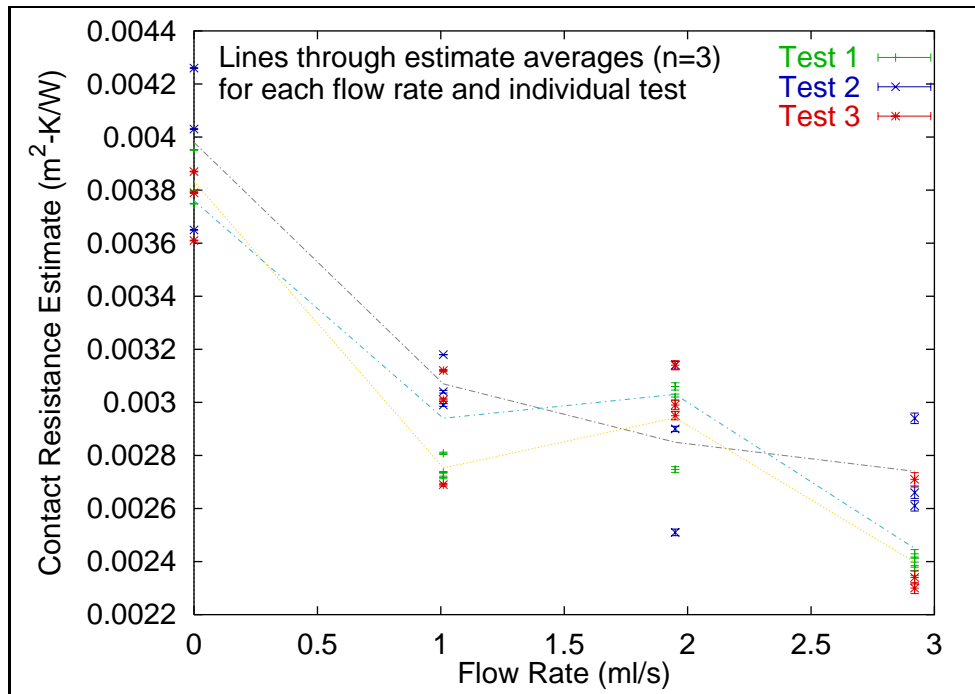


Fig. 7.5 Contact Resistance Estimates vs. Experimental Flow Rate for Sponge Phantom Tests; Three tests run on different days. Error bars coincide with the total 95% confidence intervals for the individual estimates.

estimates are close in magnitude and the average lines are roughly parallel proves that the trends shown in Fig. 7.6 are repeatable. This indicates that the bioprobe can be used to consistently detect changes in flow rate or perfusion through a porous media by surface measurements.

Recall that the reasoning behind comparing the estimated perfusion to the flow rate was that the actual measured volume, in terms of the geometrical section of sponge experiencing perfuse flow, is unknown. If it is assumed that the entire volume of the sponge media contains this perfuse flow, then the flow rate divided by this volume yields an experimental perfusion rate. The volume of the sponge based on the information in Table 5.13 is 88 milliliters. From the four experimental flow rates as in Table 7.1 the possible experimental perfusion rates become 0.00, 0.011, 0.022, and 0.032 ml/ml/s. This merely changes the values of the horizontal axis on the graph in Fig. 7.6 by a factor of 88. The resulting comparison, with a line representing an exact one-to-one relation ($y=x$), is shown in Fig. 7.7. Once again, a perfect match up is not evident. Lines drawn through the estimate averages for each test are all roughly parallel to, but offset from, the one-to-one

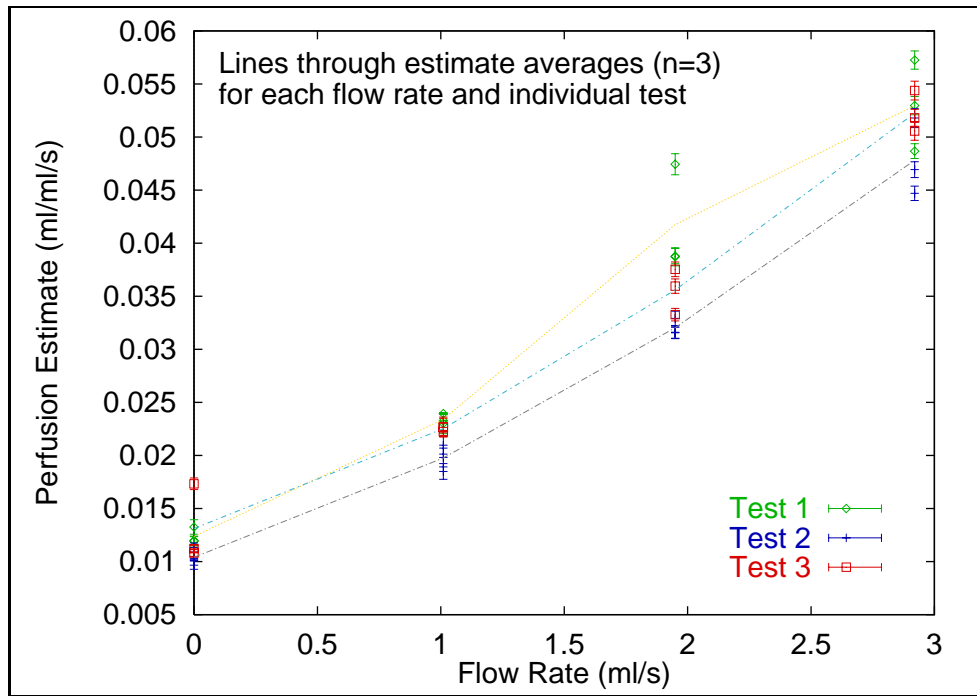


Fig. 7.6 Perfusion Estimates vs. Experimental Flow Rate for Sponge Phantom Tests; Three tests run on different days. Error bars coincide with the total 95% confidence intervals for the individual estimates.

curve. This again proves some linear correlation between the estimated and experimental perfusion with some offset. However, the exact value of the perfuse volume of the sponge is unknown. Changes to this volume could increase or decrease the offset depicted in Fig. 7.7.

It is possible that this offset may simply be inherent in the proposed method. Practical application of this method, then, would need only to compensate for this offset. Indeed, a consistent positive offset does add stability to the estimation procedure. If the actual perfusion rate is low, the possibility exists for the parameter estimates to be negative for some iterations of the Gaussian minimization. While the method is robust enough to handle small jumps to negative parameter values, large jumps could cause a lack of convergence. The biothermal model would yield very erroneous calculations since a negative blood perfusion and negative contact resistances do not physically exist. So, some inherent positive offset in the parameter estimation method may prove desirable as long as it can be consistently quantified.

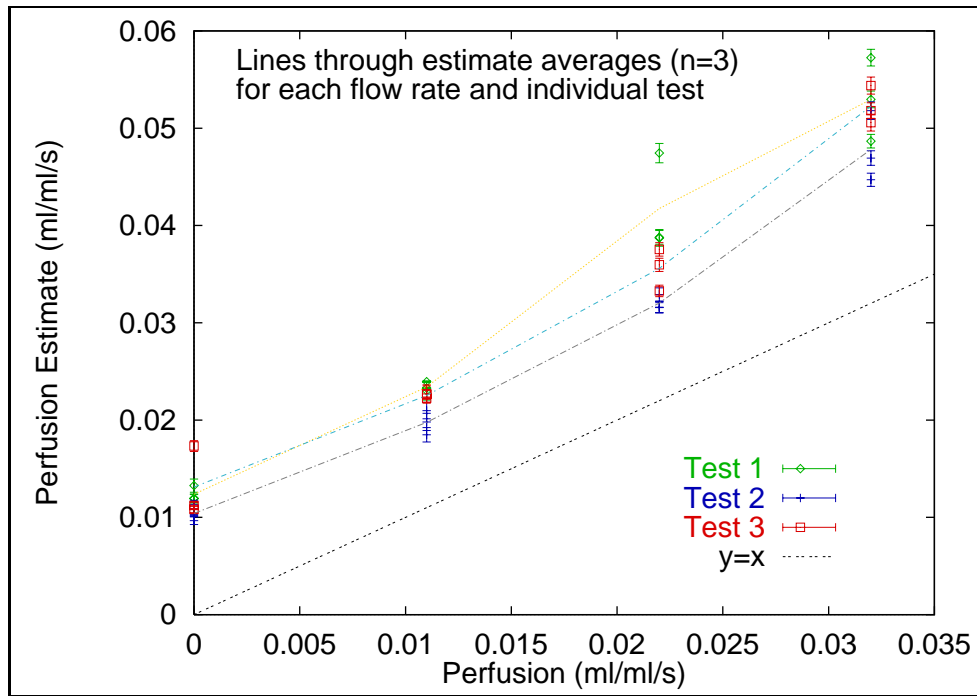


Fig. 7.7 Estimated Perfusion Compared to Experimental ‘Perfusion’ Calculated Using the Entire Sponge Volume

7.2 Further Evaluation of the Parameter Estimation

Procedure

After establishment of a repeatable experimental procedure and resulting data that proved the concept of measuring perfusion with heat flux, the model and parameter estimation scheme was analyzed in further detail. Up to this point, many parameters other than those being estimated have been considered known and held constant for the different materials. These known parameters, such as thermal properties of the porous media, fluid, and bioprobes, were described in Chapters 2 and 4. However, these values are just average values from literature, or in some cases educated guesses based on engineering knowledge of the system. It has been mentioned several times that the bias present between the model and the experiments may be due to some error in these ‘known’ parameters. Therefore, a study was performed to test the effects of such ‘known’ parameters on the estimation procedure.

This test served several purposes. One, it produced some qualitative and quantitative

idea of the effect of assumptions that may have to be made clinically. Some parameters will be impractical to measure and/or control. For example, no two people's skin tissue will have exactly the same thermal conductivity. As with this research, it will be impractical to perform a test of this value on every patient prior to a perfusion measurement. So standard values must be used. A sensitivity analysis for this parameter will yield some concept of how much liberty can be taken in assuming this standard value for all patients. Secondly, the sensitivity analysis can be used to generate the expected error in model output due to uncertainties in the 'known' parameters. This expected error is then used to adjust the confidence intervals, and likewise the expected ranges, of the estimated parameters as discussed in Section 4.2.3 (Eq. (4.18)).

The parameters included in the study are tissue or media thermal conductivity, k_t , tissue or media thermal diffusivity, α_t , fluid (blood or water) specific heat, c_{pb} , and probe thickness, δ . The first three parameters are the most likely to consistently be unmeasurable in clinical applications of the probe. Standard values for these must be utilized from patient to patient. The probe thickness is representative of the probe capacity. While this should be a known upon any real application of the bioprobe, there is some uncertainty as to exactly how the thickness should be included in the model. The bioprobe is a composite structure, so the thickness of any one of the layers (foil, thermopile, substrate) could be used, alone or in addition to the others, in the model. Therefore the thickness is included in this study to determine the importance of resolving its modeling issue for future applications.

The sensitivities of conductive heat flux to each of the four mentioned parameters were calculated as per Eq. (4.9) and Eq. (4.10) using sponge and water properties. The results are graphed in Fig. 7.8. The sensitivity to tissue thermal conductivity is fairly small. As expected, the sensitivities to blood specific heat are similar to the sensitivities for blood perfusion. The specific heat and perfusion are products in the same term of the governing model equation (Eq. (4.2)) and therefore should have the same effect on its output. The sensitivities to tissue thermal diffusivity are similar to those for contact resistance, probably because both effect the transient response of the system. The probe thickness has the largest sensitivity coefficients of any of these parameters. It appears to act differently over two distinct regions of the simulation. This is evidence of some short-term effect and a long term effect. The parameter estimation scheme was applied to a sample set of experimental data, Sp811, four times, each with a 20% change in one of

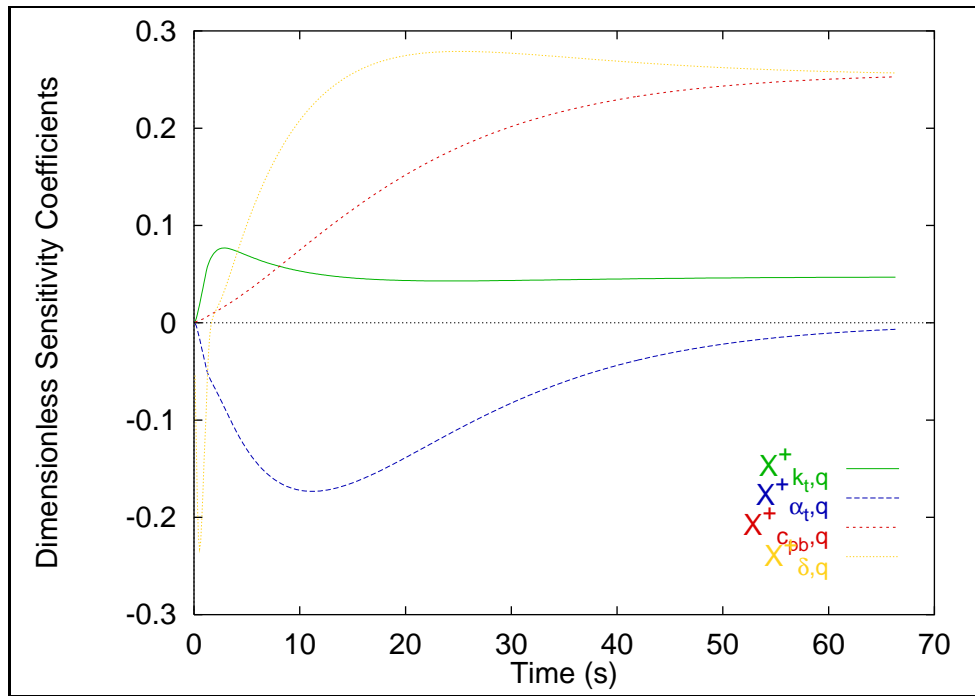


Fig. 7.8 Heat Flux Sensitivities with Respect to ‘Known’ Model Parameters; Tissue thermal conductivity, $X_{kt,q}^+$, Tissue thermal diffusivity, $X_{\alpha_t,q}^+$, Fluid specific heat, $X_{c_{pb},q}^+$, and Probe thickness, $X_{\delta,q}^+$.

the discussed parameters. The estimated parameters of contact resistance and perfusion obtained with these changes in the model are compared to the nominal values in Table 7.2. As expected from the sensitivity coefficients, changing the probe thickness produced the largest sway in the estimates. The resulting calculated heat flux curves with the estimates are shown in Figs. 7.9 and 7.10. Since the blood specific heat and perfusion are in the same term, changing $c_{p,b}$ changes the estimate for w_b but the end heat flux curve is exactly the same (linear parameters). Also following from the sensitivity coefficients, changing the tissue thermal conductivity resulted in a negligible change in the model output. The other parameter changes resulted in small changes to the overall shape of the heat flux curves. Indeed, reducing the thickness of the probe by 20% actually improved the agreement of the model heat flux with experiment during the transient ‘spike’.

This study shows that some liberty can be taken with the tissue thermal properties, but the fluid thermal properties and probe must be modeled correctly to ensure accurate perfusion measurements. The fluid specific heat directly effects the perfusion without any

Table 7.2 Results of Estimation with Changes to ‘Known’ Model Parameters

Model Change	R_c (m ² K/W)	w_b (ml/ml/s)	% Change R_c	% Change w_b
No Change (nominal)	0.00302	0.03872	-	-
$k_t - 20\%$	0.00291	0.03949	-3.8	+2.0
$k_t + 20\%$	0.00311	0.03803	+3.0	-1.8
$\alpha_t - 20\%$	0.00335	0.03909	+10.9	+1.0
$\alpha_t + 20\%$	0.00277	0.03812	-8.3	-1.5
$c_{pb} - 20\%$	0.00302	0.04841	0.0	+25.0
$c_{pb} + 20\%$	0.00302	0.03226	0.0	-16.7
$\delta - 20\%$	0.00283	0.04857	-6.3	+25.4
$\delta + 20\%$	0.00316	0.03186	+4.6	-17.7

effect to the contact resistance estimate. Because they are linear, a change in c_{pb} produces a change of the same order of magnitude in the estimate of w_b . The probe capacitance (represented here by the thickness) also effects the agreement in shape of the heat flux curves between the model and experiment. This can in turn effect convergence. If the probe capacitance is far off, so much bias will be present that no value of contact resistance or perfusion will satisfy the objective function and estimation will be impossible. Probe thickness can be determined using parameter estimation since it is unrelated to other estimated variables, but the blood specific heat can not be determined in this way do to its linearity with blood perfusion. These two quantities must be considered in future applications of the bioprobe.

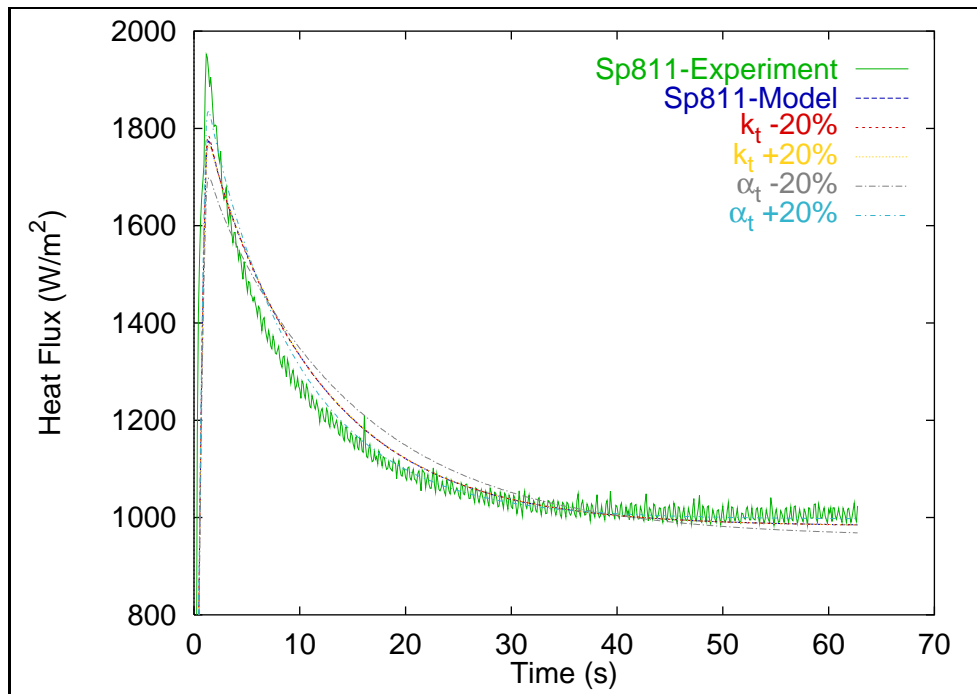


Fig. 7.9 Model Output Based on Changes to Tissue Thermal Conductivity and Diffusivity; No discernible variation in the model heat flux exists for 20% changes in conductivity, k_t . Small variations are observed in the transient shape for 20% changes in diffusivity, α_t .

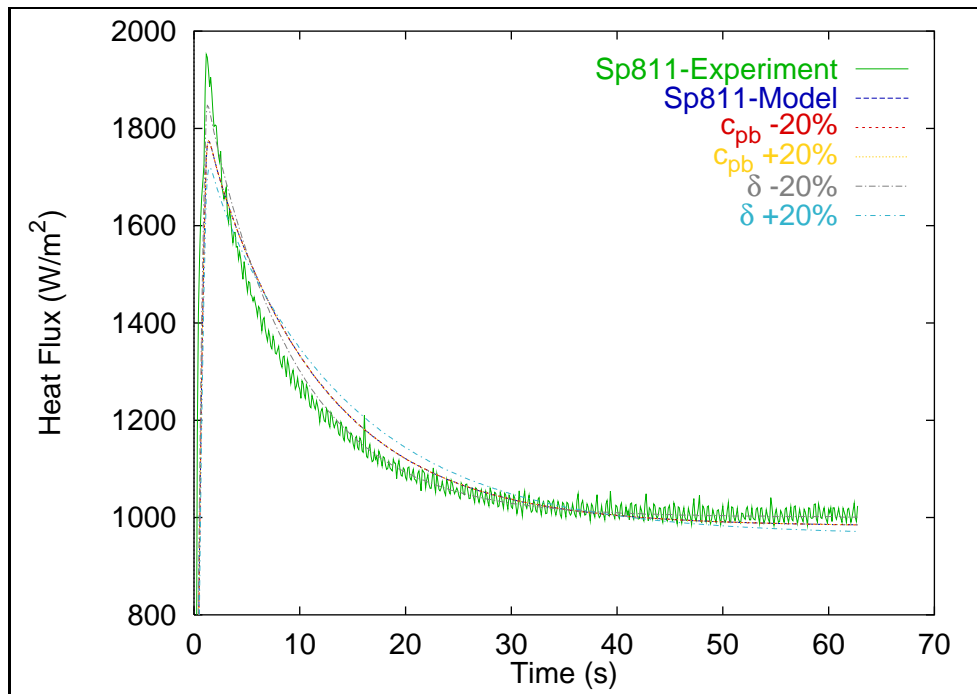


Fig. 7.10 Model Output Based on Changes to Fluid Specific Heat and Probe Thickness; 20% changes in fluid specific heat, c_{pb} , change the estimates, but not the model output. The heat flux curve shape, especially in the transient region, shows distinct differences with changes in probe thickness, δ .

7.3 Statistical Evaluation of Experiments

Three statistical evaluations must be performed to complete the study with the sponge experiments. One, the confidence intervals of the individual estimates must be increased to account for model uncertainty. Second, the overall perfusion estimate averages and bounds for each flow rate must be derived. Third, those averages must be checked for statistical evidence of different perfusion estimates at different flow rates. This will give support to the concept of measuring perfusion with the bioprobe.

The sensitivity analysis provided above is used to find the uncertainty in the model and likewise the parameter estimation process. The sensitivity coefficients in Fig. 7.8 are time averaged as per Eq. (4.20) and used in Eqs. (4.19 - 4.22) to derive the overall uncertainty of the model based on an assumed 10% uncertainty in the ‘known’ parameters of tissue thermal conductivity and diffusivity, fluid specific heat, and probe thickness (capacity). This results in an overall uncertainty of $\sigma_{q,known}^2 = 680 \text{ (W/m}^2\text{)}^2$ that is added to the experimental variance to obtain an overall variance for confidence interval calculations, $\sigma_{q,tot}^2$. The 95% confidence intervals for each individual estimate are recalculated from the Gaussian estimation method by dividing them by the experimental variance and multiplying by $\sigma_{q,tot}^2$. These are the intervals reported by the error bars in Figs. 7.5 and 7.6.

The overall perfusion averages, using the data from all three tests, at each flow rate were calculated by the standard mean and confidence interval equations, as given in Eq. (4.23). The results are tabulated in Table 7.3. The averages and associated confidence intervals are graphed in Fig. 7.11. The overall average confidence intervals for perfusion estimates between flow rates do not overlap. From this, it can be stated with confidence that the mean values for perfusion estimates are different at the different flow rates in this test.

Table 7.3 Overall Perfusion Averages at Each Flow Rate, Sponge Phantom Experiments

Flow Rate (ml/s)	Perfusion \pm 95% CI (ml/ml/s)
0.00	0.01197 \pm 0.00174
1.01	0.02190 \pm 0.00137
1.95	0.03642 \pm 0.00387
2.92	0.05101 \pm 0.00295

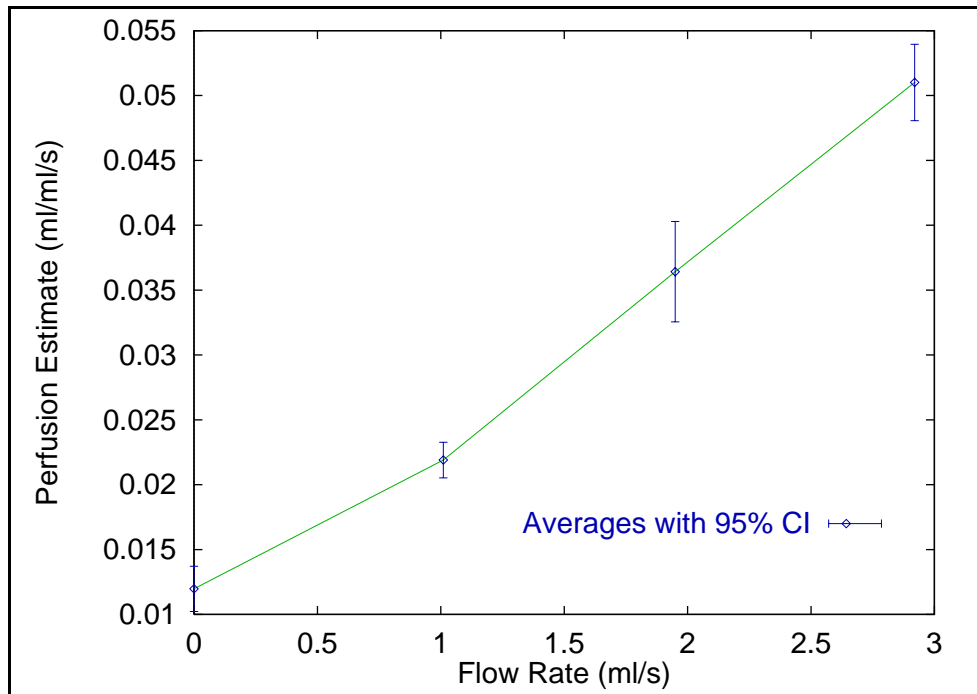


Fig. 7.11 Overall Perfusion Averages at Each Flow Rate, Sponge Phantom Experiments; Error bars correspond to 95% confidence intervals.

7.4 Experimental Noise Evaluation

Of interesting note in the confidence intervals shown in Figs. 7.6, 7.5, 7.11 is that they increase with flow rate. This is because the experimental variance is higher at larger flow rates. This is also evident from the experimental heat flux curves, as in Fig. 7.2. For example, the experimental variance in a zero flow case is 1.1 while this quantity in a flow rate = 2.92 ml/s case is 760. It is this difference in experimental variance, due to noise in the signal, that increases the confidence intervals for the estimates.

A Fast Fourier Transform (FFT) gives a measure of the frequency content of a signal. If a signal contains a large amount of a particular frequency, it will show up as a spike on a FFT frequency spectra magnitude plot. Such a plot for a FFT performed on heat flux signals taken over four different flow rate settings is shown in Fig. 7.12. All the flow cases contain the one low frequency representing the 60 second cycle of the test. As flow rate increases, other spikes appear at ever increasing frequencies. For a flow rate of 1.01 ml/s, the frequency spectra plot is smooth beyond the initial spike. At a flow rate of 1.95 ml/s, a second spike appears at 132 rotations per minute (RPM). For flow rates of 2.92 and 3.77 ml/s spikes are evident at 146 and 154-159 RPM, respectively.

The exact cause of this increase in experimental noise with flow rate is unknown. Two suggestions are some noise effect of the perfusion pump motor on the DAS system or the sensor picking up on the pulsatile flow through the media, even though this should be very small in effect. Several attempts at grounding and further shielding the wires leading from the bioprobe to the DAS-TC board (they are already shielded-twisted pairs) did not alter the noise in the signal. One future consideration might be to use a non-peristaltic pump (impeller or syringe) to see if this effect is still noticeable. Or measurements of the pump motor speed compared to the RPMs given above might show some correlation of noise to pump motor. In any event, this noise is not so overbearing as to cause problems with the data acquisition or the parameter estimation.

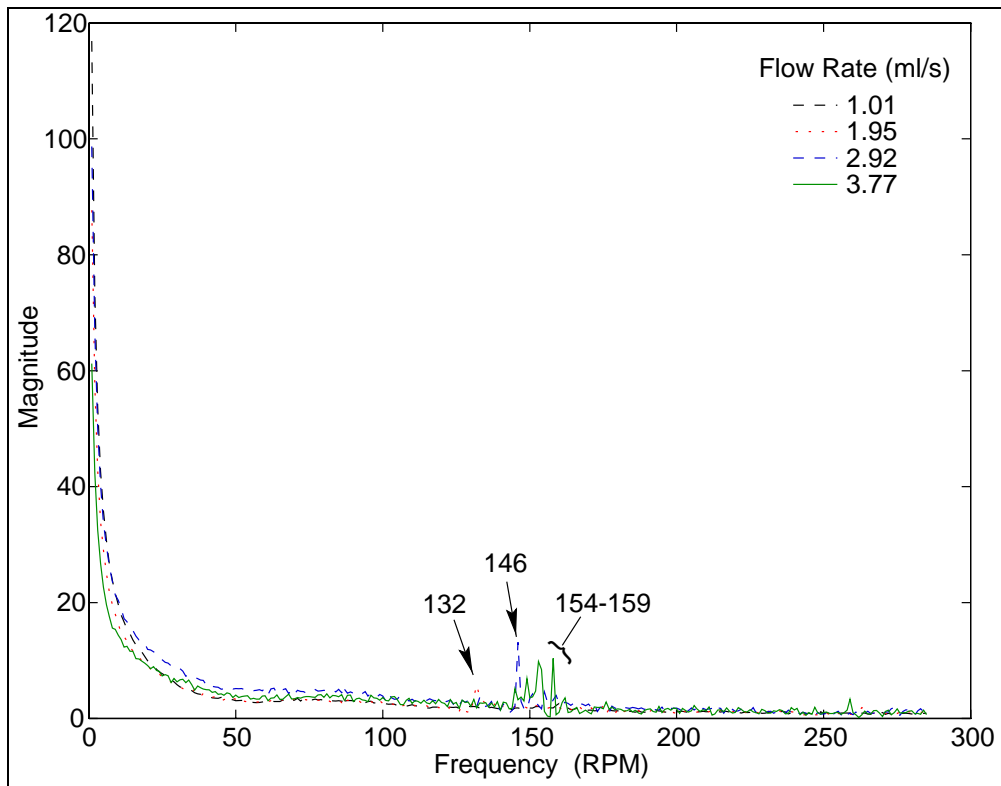


Fig. 7.12 Frequency Spectra Magnitudes for Heat Flux Signals Taken at Four Different Flow Rates

Chapter 8

Summary and Conclusions

8.1 Summary

Blood perfusion is an important factor in the body's maintenance of homeostasis and reaction to abnormal or unwanted situations. Its measurement is a clinically useful tool for predetermination and location of certain physiological disturbances as well as monitoring patient progress for a variety of medical treatments. Several different ways of measuring blood perfusion exist, but none that provide absolute and accurate answers in an inexpensive, noninvasive, and easily portable format. This document detailed the development of a new methodology to provide noninvasive, absolute, inexpensive clinical measurements of blood perfusion. Progress was accomplished by using in combination a biothermal model, parameter estimation techniques, and experimental results.

The biothermal model uses the Pennes equation to theoretically describe a homogeneous bioprobe on some homogeneous section of perfuse tissue. This model was evaluated against several variables to determine dependencies, output trends, and key elements of bioprobe design and implementation. A program for applying the Gauss linearization and minimization with the Box Kanemasu modification of parameter estimation was created that incorporates both the model and experimental measurements. This gradient based method minimizes a sum of squares error function based on either or both heat flux and temperature.

Over the course of this research it was found that parameter estimation was best performed with only the heat flux data, due to a low sensitivity of temperature to the parameters of interest, and large bias between model and experimental temperatures. This was

a departure from previous methods of using only temperature measurements for parameter estimation in heat transfer applications.

To obtain experimental data for use with this estimation procedure, measurements were made on both human forearms and non-biological phantoms. Two phantom materials were tested, porous aluminum and cellulose sponge. An experimental set-up was devised to create multi-directional, capillary perfusion-like flow inside these media. Data was collected with the bioprobe at known nominal flow rates of water. Several iterations of bioprobe design were used in the course of these experiments.

Of the two phantom materials, only the sponge provided acceptable results. Heat flux measurements off the porous aluminum were insensitive to flow rate. This was primarily due to high thermal conductivity and diffusivity of the aluminum media, over ten times higher than those for skin tissue. Also, poor thermal contact was maintained between the aluminum surface and probe because of the roughness and rigidity of the aluminum surface. Estimation of contact resistance and perfusion with the proposed procedure is not effective under those conditions. This problem was corrected by switching to the cellulose sponge media that had thermal properties on the same order of magnitude as skin tissue and allowed more intimate contact with the bioprobe.

Evaluation of the numerical biothermal model revealed that a high convection coefficient leads to larger heat fluxes, making the system more sensitive to blood perfusion. Also, if h is large enough, around $1000 \text{ W/m}^2\text{K}$, the model output is no longer a function of the value of the convection coefficient. The reverse is true for contact resistance. Low R_c values (≈ 0.0001) lead to high heat flux, the desired situation, and less dependence in the model on the absolute value of contact resistance. Although contact resistance can vary with application and probe type, typical experimental values were in the range of $0.002\text{-}0.004 \text{ m}^2\text{K/W}$. The experimental convection coefficients achieved were $400\text{-}700 \text{ W/m}^2\text{K}$.

8.2 Conclusions

The following lists highlight the important and varied conclusions from the research presented in this document. These conclusions cover the areas of experimental protocols, parameter estimation applications, and the bioprobe model and system as outlined in the objectives described in Section 1.1. The experimental protocols section satisfies objective

three of this research, to develop protocols for perfusion testing. The conclusions regarding the best application of parameter estimation relate to objective two, development of parameter estimation techniques for use in perfusion estimation. Conclusions to the first and fourth objectives of this research, developing and evaluating particular variable effects on a biothermal model of the given system, are described in the bioprobe and model system section below.

Experimental Protocols

- 1.) Experimentally, high convection coefficients lead to repeatable heat flux signals that are more sensitive to blood perfusion.
- 2.) Low contact resistance is desired to minimize both its effect on the experimental output and dominance of the parameter estimation procedure.
- 3.) The best experimental protocol for data collection is allowing the system, tissue / phantom and bioprobe, to reach thermal equilibrium, turning on the cooling air, and collecting data for 60 seconds. This protocol yields consistent results that corresponded with expected output based on the theoretical model.
- 4.) The cellulose sponge is an effective experimental phantom for biological tissue, yielding experimental data similar to that seen with experiments on human forearms and good sensitivity to flow rate.
- 5.) Heat flux provides a better measurement than temperature alone. The heat flux signals are more reliable and more robust. Problems encountered with thermocouples alone, such as offset and linearization, do not effect heat flux measurements.

Parameter Estimation Applications

- 1.) In this application, parameter estimation is best performed with only the heat flux data.

2.) Contact resistance dominates the parameter estimation procedures studied here, causing problems with convergence. This can be alleviated by slight alterations to the estimation technique, including

- using only the later portion of the experimental data
- scaling the beginning part of the data by increasing the variance
- a switching method where contact resistance and blood perfusion were estimated separately

The qualitative results of such methods, along with some comments, are tabulated in Table 8.1. The quickest, most robust method leading to acceptable estimates was simultaneous estimation of contact resistance and blood/water perfusion using whole-domain Gauss minimization.

Table 8.1 Summary of Parameter Estimation Methods

Estimation Type	Results	Comments
All Data, Gauss	best convergence	quickest method
End Data, Gauss	same results as All Gauss	more likely not to converge
Scaled Data, Gauss	same results as All Gauss	more likely not to converge
All Data, BK	same results as All Gauss	extra steps not necessary, can lead to convergence problems if sensitivities are small (<0.1)
End Data, BK	slightly different results than All BK, better agreement between experiment and model at later times	did not help convergence
Scaled Data, BK	similar results as End BK	did not help convergence
Switching Method	helped with convergence in early tests (probably due to errors in code)	not necessary in later applications once code was corrected

Bioprobe Model and System

1.) Of all the model parameters other than contact resistance, the probe capacitance, in terms of thickness, density, or specific heat, has the largest effect on model output, measured heat flux, and the estimation procedure. Changing the transient response of the probe via its capacitance can largely alter the shape and magnitude of the heat flux.

- 2.) Improper modeling of probe capacitance causes such a large bias between model output and experimental data that no parameter estimation can be performed; the two curves simply will not match.
- 3.) The value for specific heat of the blood/water also has a large effect on the estimated value for perfusion. This was expected as the fluid specific heat is linear with the perfusion term in the Pennes equation. Because of this linearity, however, the blood perfusion and fluid specific heat can not be estimated simultaneously.
- 4.) Small deviations of the other variables in question, such as probe radius and tissue thermal properties, do not have a large effect on the model output or parameter estimates. Therefore, liberty can be taken in assuming values for these variables without introducing large errors into the estimation of blood perfusion.
- 5.) Even with a ten percent error in the 'known' model variables (probe thickness, tissue and blood thermal properties), the confidence intervals around each individual parameter estimate are still ten percent or less than the estimate values. Therefore, without exact measurements of all the system variables, statistically accurate perfusion estimates are generated.

Overall Conclusion

The final and most important objective of this research, to validate the bioprobe perfusion measurement system, was successfully completed. The experiments with the sponge phantom prove true the concept of using the bioprobe to noninvasively estimate flow or perfusion within tissue. The repeatability and robustness of this observation allow the following overall conclusion. **Changes to system internal perfusion can definitely be monitored by a surface mounted bioprobe.**

Chapter 9

Recommendations

This research represents a large step forward in completing a clinically applicable bioprobe to perform blood perfusion diagnostics. Many more steps must be taken, however, before that end result can be achieved. The overall recommendations for advancement of the bioprobe research, explained in the following paragraphs, are:

- 1.) Run more phantom tests over a large variety of small flow rates
- 2.) Modify the bioprobe housing to gain higher convection cooling.
- 3.) Find a better way of attaching the episor to the bioprobe housing.
- 4.) Perform other experiments to define the capabilities of the bioprobe.
- 5.) Make the biothermal model more complex or try different models
- 7.) Run controlled experiments on biological tissue.
- 8.) Compare the proposed procedure to other perfusion measurement methods.

Within the current experimental setup, more tests should be run over a larger variety of flow rates, especially at lower flow rates. The results presented in this document were positive, but the correlation between experimental flow and perfusion estimate may not be valid for all conditions. The system must be tested over conditions most likely to be found within actual tissue. Also to that end, the difference between experimental flow rate and experimental perfusion needs to be reconciled. Then, experimental and estimated perfusion can be compared directly.

The bioprobe B housing should be modified to create larger cooling convection. The convection coefficient generated with the bioprobe A housing was much larger than the one generated with the bioprobe B housing, even with the same size air hose and pressure.

This could be due to the very small hole size used to create the air jets in the B housing. Decreasing the number of air jet holes, but increasing their size to keep the overall flow area the same, may lead to higher convection coefficients with the B probe.

Also, in the bioprobe B configuration, the heat flux sensor is very loosely attached to the housing. The possibility exists that the cooling air will flow between the sensor and housing instead of exiting out the holes in the Plexiglas spacer. This can cause some inconsistencies in the cooling action that will not be present in the biothermal model. A strong, airtight attachment of the sensor to the housing will provide a known cooling action that will more closely match the current model.

Other experiments that will define the bioprobe's capabilities include introducing 'abnormalities' into the phantom experiments. For example, conducting experiments with a high ($\approx 42^{\circ}\text{C}$) and low ($\approx 28^{\circ}\text{C}$) bath water temperature to simulate hyperthermia and hypothermia, respectively. Other examples include using a perfusion fluid with high and low viscosity, random occlusions in the porous media, or addition of a heat generating element within the porous media. Such experiments will test the sensitivity and robustness of the bioprobe to possible physiologic abnormalities.

Changes to the model may also refine the estimation process. For one, the model could be made more complex to include the different layers of the bioprobe and their thermal interaction. This includes areas of differing thermal capacitance, conductivity, and the thermal resistance between each layer. Also, complexities such as non-homogeneity of the tissue or blood flow within have yet to be considered. This may come into play with estimation attempts on tissue other than the epidermis, such as skeletal muscle or highly vascularized surfaces. Secondly, a different biothermal model may prove insightful. As mentioned in the literature review, many different biothermal models exist. Some, such as the Wulf or Klinger models (Charney, 1992), use a vectored blood velocity term to determine temperature distribution within tissue instead of an overall perfusion term. This could then be tested with the current experiments and with other experiments that have uni- or bi-directional flow through the porous media. The Weinbaum-Jiji equation (Weinbaum and Jiji, 1985) is proposed to fit well with skeletal muscle geometry. Incorporation of these or other biothermal models might provide more accurate estimates in certain situations. It might turn out that different models are best used in different applications of the bioprobe.

Further testing should be performed on a variety of biological tissues in a controlled

setting. Suggestions include starting with highly perfuse tissue easily linked to lab apparatus, kidney, liver or spleen for example. Tests similar to the phantom experiments should be conducted where measurements are taken with the bioprobe during periods of set, known perfusion or flow rate through the tissue. Also, if *in vitro* tests allow this, experimentation with vasodilators, vasoconstrictors, and other blood perfusion altering substances can be conducted. As with the recommendation above, these *in vitro* experiments must try to mimic abnormal conditions. Other experiments could include the introduction of tumors or lesions to the test tissue. This then leads to *in vivo* testing on subjects with known diseases or healthy subjects during periods of altered perfusion, such as sleep, exercise, agitation or metabolic activity (after a big meal). This way, an operating range, that will hopefully include any situation encountered clinically, can be specified for the bioprobe.

Phantom, *in vivo*, and *in vitro* experiments should at some point be directly compared to the other methods of measuring blood perfusion or flow. The ‘gold standard’ of blood flow measurements is radio-isotope clearance. Any new method must be compared to this to gain credibility. Also, comparison to the laser-Doppler flowmetry techniques will prove useful. There are some applications where one may be better than the other and some applications where they may compliment one another.

This research provides the foundation for all the aforementioned recommendations. The described theory and experiments validate the process of combining parameter estimation techniques, biothermal modeling, and heat flux measurements to noninvasively determine blood perfusion. The bioprobe may lead to measuring not only blood perfusion, but also other thermal physiologic reactions to or because of abnormal and undesirable conditions. Studies such as this enhance the understanding of the thermal characteristics of biomaterials and the physiologic aspects of heat transfer. This becomes increasingly important with the advancement and need of thermal therapies such as cryosurgery or hypo-, hyper- thermia treatments. This work contributes to increasing this valuable knowledge.

Bibliography

- Anderson, G. and Burnside, G., 1990, "A Noninvasive Technique to Measure Perfusion Using a Focused Ultrasound Heating Source and a Tissue Surface Temperature Measurement," in: *Advances in Measuring and Computing Temperatures in Biomedicine: Thermal Tomography Techniques*, ed. R. R. et al., ASME, New York, pp. 31–36.
- Beck, J. and Arnold, K., 1977, *Parameter Estimation in Engineering and Science*, John Wiley, New York.
- Bowman, H., 1985, "Estimation of Tissue Blood Flow," in: *Heat Transfer in Medicine and Biology*, eds. A. Shitzer and R. Eberhart, Vol. 1, Chap. 9, Plenum Press, pp. 193–230.
- Bowman, H., Cravalho, E., and Woods, M., 1975, "Theory, Measurement and Application of Thermal Properties of Biomaterials," *Ann. Rev. Biophys. Bioeng.*, Vol. 4, pp. 43–80.
- Brinck, H. and Werner, J., 1994, "Efficiency Function: Improvement of Classical Bioheat Approach," *Journal of Applied Physiology*, Vol. 77, No. 4, pp. 1617–1622.
- Castellana, F., Skalak, R., Cho, J., and Case, R., 1983, "Steady State Analysis and Evaluation of a New Thermal Sensor for Surface Measurements of Tissue Perfusion," in: *Annals of Biomedical Engineering*, Vol. 11, Chap. 8, Who, pp. 101–115.
- Charney, C. K., 1992, "Mathematical Models of Bioheat Transfer," in: *Advances in Heat Transfer*, ed. Y. Cho, Vol. 22, Academic Press, Inc., Boston, pp. 19–155.
- Chato, J., 1985, "Measurments of Thermal Properties of Biological Materials," in: *Heat Transfer in Medicine and Biology*, eds. A. Shitzer and R. Eberhart, Vol. 1, Chap. 8, Plenum Press, N.Y., pp. 93–122.

- Clegg, S., Liauh, C., and Roemer, R., 1988, "Selecting the Optimal Amount of Regularization to Reconstruct Three-Dimensional Temperature Fields from Limited Noisy Temperature Measurements during Hyperthermia," in: *Proceedings of the Winter Annual Meeting of the ASME*, Vol. 9, BED, ASME, Chicago, IL, pp. 281–290.
- Cui, Z. and Barbenel, J., 1991, "The influence of Model Parameter Values on the Prediction of Skin Surface Temperature: II. Contact Problems," *Physics in Medicine and Biology*, Vol. 36, pp. 1607–1620.
- Draghici, M., Savard, P., and Roberge, F., 1990, "A New Regularization Method Applied to Regression Problems in Electrocardiography," in: *Proceedings of the Annual International Conference of the IEEE Engineering in Medicine and Biological Society*, Vol. 12, p. 629.
- Eberhart, R., Shitzer, A., and Hernandez, E., 1980, "Thermal Dilution Methods: Estimation of Tissue Blood Flow and Metabolism," in: *Thermal Characteristics of Tissue: Applications in Detection and Treatment*, Vol. 35, Annals of N.Y. Academy of Sciences, pp. 107–132.
- Emery, A. and Fadale, T., 1996, "Design of Experiments Using Uncertainty Information," *Journal of Heat Transfer*, Vol. 118, pp. 532–538.
- Fouquet, Y., Hager, J., Terrell, J., and Diller, T., 1993, "Blood Perfusion Estimation from Noninvasive Heat Flux Measurements," in: *Advances in Bioheat and Mass Transfer - 1993: Microscale Analysis of Thermal Injury Processes, Instrumentation, Modeling, and Clinical Applications*, ed. R. Roemer, ASME, N.Y., pp. 53–60.
- Ganapathy, R., 1994, "Free Convective Heat and Mass Transfer Flow Induced by an Instantaneous Point Source in an Infinite Porous Medium," *Fluid Dynamics Research*, Vol. 14, pp. 313–329.
- Gonzales, T., 1995, "A Noninvasive Approach to Blood Perfusion Estimates," Undergraduate Research Report for Professor T.E. Diller, Virginia Tech; Unpublished.
- Hoke, J., Burkes, E., White, J., Duffy, M., and Klitzman, B., 1994, "Blood-flow Mapping of Oral Tissues by Laser Doppler Flowmetry," *International Journal of Oral and Maxillofacial Surgery*.

- Holti, G. and Mitchell, K., 1979, "Estimation of the Nutrient Skin Blood Flow Using a Non-Invasive Segmented Thermal Clearance Probe," in: *Non-Invasive Physiological Measurements*, ed. E. Rolfe, Vol. 1, Academic Press, London, pp. 113–123.
- Iavars'kyi, B. and Rafa, T., 1996, "Selection of Regularization Parameters of Inverse Problem by Computer Simulation Model," in: *Proceedings of the VIth International Conference on Mathematical Methods in Electromagnetic Theory*, Ukraine, pp. 478–480.
- Incropera, F. and Dewitt, D., 1990, *Fundamentals of Heat and Mass Transfer*, John Wiley and Sons.
- Johnson, J., Brengelmann, G., Hales, J., Vanhoutte, P., and Wenger, C., 1986, "Regulation of the Cutaneous Circulation," *Fed. Proc.*, Vol. 45, pp. 2841–2850.
- Kress, R. and Roemer, R., 1987, "A Comparative Analysis of Thermal Blood Perfusion Measurement Techniques," *Journal of Biomechanical Engineering*, Vol. 109, pp. 218–225.
- Michener, M., 1991, "Measurements of Thermal Properties and Blood Perfusion Using the Heat Flux Microsensor," Master of science in mechanical engineering, Virginia Polytechnic Institute and State University.
- Michener, M., Hager, J., Terrell, J., Veit, H., and Diller, T., 1991, "Noninvasive Blood Perfusion Measurement with a Heat Flux Microsensor," *Advances in Biological Heat and Mass Transfer*, Vol. 18, pp. 9–14.
- Moffat, R., 1988, "Describing the Uncertainties in Experimental Results," *Experimental Thermal and Fluid Science*, Vol. 1, pp. 3–17.
- Moncman, D., Hanak, J., and Copenhaver, D., 1995, "Optimal Experimental Designs for Estimating Thermal Properties," in: *Proceedings of the ASME-JSME Thermal Engineering Joint Conference*, eds. L. Fletcher and T. Aihara, Vol. 3, ASME, N.Y., pp. 461–468.
- Newman, W., Bowman, H., Orgill, D., and Klar, E., 1995, "A Methodology for In Vivo Measurement of Blood Flow in Small Tissue Volumes," in: *Advances in Heat and Mass Transfer in Biotechnology*, Vol. HTD 322, BED 32, ASME, pp. 99–105.

- Nilsson, G., Tenland, T., and P.Å. Öberg, 1980, "A New Instrument for Continuous Measurement of Tissue Blood Flow by Light Beating Spectroscopy," *IEEE Transactions of Biomedical Engineering*, Vol. 27, pp. 12–19.
- O'Reilly, T., Gonzales, T., and Diller, T., 1996, "Development of a Noninvasive Blood Perfusion Probe," in: *Advances in Biological Heat and Mass Transfer*, eds. L. Hayes and S. Clegg, Vol. HTD 337/BED 34, ASME, pp. 67–73.
- Ott, C. and Vari, R., 1979, "Renal autoregulation of blood flow and filtration rate in the rabbit," *American Journal of Physiology*, Vol. 237, pp. F479–F482.
- Park, L., Park, C., Park, C., and Lee, T., 1997, "Application of Genetic Algorithms to Parameter Estimation of Bioprocesses," *Medical and Biological Engineering and Computing*, Vol. 35, pp. 47–49.
- Patel, P., Valvano, J., Pearce, J., Prah, S., and Denham, C., 1987, "A Self Heated Thermistor Technique to Measure Effective Thermal Properties from the Tissue Surface," *ASME Journal of Biomechanical Engineering*, Vol. 109, pp. 330–335.
- Pennes, H., 1948, "Analysis of Tissue and Arteriole Blood Temperatures in the Resting Forearm," *Journal of Applied Physiology*, Vol. 1, pp. 93–122.
- Qin, Y. and Ciric, I., 1993, "Dielectric Body Reconstruction with Current Modelling and Tikhonov Regularisation," *Electronic Letters*, Vol. 29, No. 16, pp. 1427–1429.
- Riva, C., Ross, B., and Benedek, G., 1972, "Laser Doppler Measurements of Blood Flow in Capillary Tubes and Retinal Arteries," *Investigative Ophthalmology*, Vol. 11, pp. 936–944.
- Saad, Z. and Scott, E., 1996, "Estimation of Temperature Dependent Thermal Properties of Basic Food Solutions During Freezing," *Journal of Food Engineering*, Vol. 28, pp. 1–19.
- Scholz, B. and Schwierz, G., 1994, "Probability-Based Current Dipole Localization from Biomagnetic Fields," *IEEE Transactions on Biomedical Engineering*, Vol. 41, No. 8, pp. 735–742.
- Scott, E. and Beck, J., 1992a, "Estimation of Thermal Properties in Carbon/Epoxy Composite Materials during Curing," *Journal of Composite Materials*, Vol. 26, No. 1, pp. 20–36.

- Scott, E. and Beck, J., 1992b, "Estimation of Thermal Properties in Epoxy Matrix/Carbon Fiber Composite Materials," *Journal of Composite Materials*, Vol. 26, No. 1, pp. 132–149.
- Shepherd, A. and Å. Öberg, P., 1990, *Laser-Doppler Blood Flowmetry*, Kluwer Academic Publishers, Boston, MA.
- Stern, M., 1975, "In Vivo Evaluation of Microcirculation by Coherent Light Scattering," *Nature*, Vol. 254, pp. 56–58.
- Stern, M. and Lappe, D., 1978, "Method and Apparatus for Measurements of Blood Flow Using Coherent Light," in: *Laser-Doppler Blood Flowmetry*, eds. A. Shepherd and P. Å. Öberg, Kluwer Academic Publishers.
- Stern, M., Lappe, D., Bowen, P., Chimosky, J., Holloway, G., Deiser, H., and Bowman, R., 1977, "Continuous Measurement of Tissue Blood Flow by Laser-Doppler Spectroscopy," *American Journal of Physiology*, Vol. 232, pp. H441–H448.
- Valvano, J., Allen, J., and Bowman, H., 1984, "The Simultaneous Measurement of Thermal Conductivity, Thermal Diffusivity, and Perfusion in Small Volumes of Tissue," *Journal of Biomechanical Engineering*, Vol. 106, pp. 192–197.
- Valvano, J., Badeau, A., Prahl, S., Chan, J., and Pearce, J., 1988, "Thermal Camera Imaging to Measure Tissue Surface Perfusion," in: *Association for the Advancement of Medical Instrumentation 23rd Annual Meeting*, Washington, D.C.
- Valvano, J. and Nho, S., 1991, "Tissue Thermal Diffusivity Measured with Sinusoidally Heated Thermistors," *Advances in Biological Heat and Mass Transfer*, Vol. HTD 189/BED 18, pp. 9–14, ASME.
- Vankan, W., Huyghe, J., Janssen, J., and Huson, A., 1996, "Poroelasticity of Saturated Solids with an Application to Blood Perfusion," *International Journal of Engineering Science*, Vol. 34, No. 9, pp. 1019–1031.
- Walker, S. and Kilpatrick, D., 1987, "Studies for the Regularisation Method Applied to the Inverse Calculation of Epicardial Potentials," in: *Proceedings of Computers in Cardiology*, IEEE, Boston, MA, pp. 359–362.

- Walsh, J. and Bowman, H., 1984, "A Noninvasive Technique for Quantifying Tissue Perfusion," in: *Advances in Bioengineering*, ed. R. Spilker, ASME, N.Y., pp. 5–6.
- Wei, D., Saidel, G., and Jones, S., 1995, "Estimation of Cerebral Blood Flow from Thermal Measurement," *Journal of Biomechanical Engineering*, Vol. 117, pp. 74–85.
- Weinbaum, S. and Jiji, L., 1985, "A New Simplified Bioheat Equation for the Effect of Blood Flow on Local Average Tissue Temperature," *Journal of Biomechanical Engineering*, Vol. 107, pp. 131–139.
- Weinbaum, S., Xu, L., Zhu, L., and Ekpene, A., 1997, "A New Fundamental Bioheat Equation for Muscle Tissue: Part 1-Blood Perfusion Term," *Journal of Biomechanical Engineering*, Vol. 119, pp. 1–12.
- Winget, J., Dewhirst, M., Engler, M., and Oleson, J., 1986, "The Use of Limited Temperature Observations to Predict Complete Temperature Fields," in: *Proceedings of the IEEE/Eighth Annual Conference of the Engineering in Medicine and Biology Society*, IEEE, pp. 1507–1511.
- Yang, W.-J., 1989, *Biothermal Fluid Sciences*, Hemisphere Publishing Corp.

Appendix A

Biothermal Heat Transfer Model

A.1 Biothermal Model Subroutine

The following program is a generic form of the biothermal model used throughout this research. This model can be run alone, or used as a subroutine within the parameter estimation method, objective function calculator, sensitivity coefficient generator, or other applications described in subsequent appendices. The *CALL* statement is left blank here. The proper *CALL* statements for each application using this subroutine are given with the code for that application.

```

* File bioprobe.f (subroutine MODEL)
*
* This FORTRAN code is a subroutine used in the bioprobe modelling and
* parameter estimation efforts. It forms the core biothermal model of the
* bioprobe on skin tissue based on the Pennes bioheat equation.
* It uses an ADI, Crank-Nicolson finite difference method to solve for the
* transient heat transfer produced by a noninvasive heat flux probe. The
* model includes the tissue under the probe, convection on the reverse side
* of the probe, and contact resistance between probe and skin.
*
* This subroutine is based on a program written by Michael Michener, 1991 and
* modified by Thomas O'Reilly, 1996
*
* Last modified by Paul Robinson, December 1997
* Department of Mechanical Engineering
* Virginia Polytechnic Institute and State University
* Blacksburg, VA 24061
*****
                EXPLANATION OF VARIABLES
*
*   ALPHT = Tissue thermal diffusivity (m^2/s)
*   RHOB = Blood density (kg/m^3)
*   SHB = Blood specific heat at constant pressure (J/kg-K)
*   WB = Blood perfusion (ml/ml/s)
*   KT = Tissue conductivity (W/m-K)
*   R = Probe radius (m)
*   M = Nondimensionalized perfusion coefficient
*   artetemp = Artery temperature (C)
*   airtemp = Air temperature, T infinity (C)
*   CONV = Convection coefficient between probe and air (W/m^2-K)
*   RC = Contact resistance (K-m^2/W)
*   Thickness = Probe thickness (m)
*   RHOP = Probe density (kg/m^3)
*   SHP = Probe specific heat at constant pressure (J/kg-K)
*   KP = Probe conductivity (W/m-K)
*   ALPHP = Probe thermal diffusivity (m^2/s)
*   FF = Ratio to equate time constant in the probe equations to time
*       constant in the tissue equations (ALPHP/ALPHT)
*   NEDGE = Number of nodes in the probe in the radial direction
*   LEDGE = Number of nodes in the probe in the y direction
*   DH = Nondimensionalized radial delta
*   DZ = Nondimensionalized thickness (y) delta
*   TIME = Time of from beginning of test (s)
*   XTIME = Nondimensionalized time
*   TTIME = Variable to store time since last temperature profile output
*
*   STEP = Time step for temperature profile output (s)
*   DT = Nondimensional time step
*   texceed = variable to check output
*   dtlim = variable to check output
*   NTSTP = Number of time steps (determines length of test)
*   N = Total number of nodes in the radial direction
*   L = Total number of nodes in the thickness (y) direction
*   CRFP = Contact resistance coefficient for probe equations
*   CRFT = Contact resistance coefficient for tissue equations
*   A(I,J) - H(I,J) = Coefficient matrices
*   ETA(I) = Radial position matrix
*   BETA(I,J), GAMMA(I,J) = Matrices for tridiagonal solver
*   THETA(I,J) = Dimensionless temperature matrix at each time step
*   TEMP(I,J) = Temperature matrix at each time step
*   POS = y position from probe top along probe centerline (mm)
*   TTEMP = Temperature corresponding to each value of POS (C)
*   THETAJM1 = Theta value of imaginary node outside of probe top
*   QH = Heat flux due to convection at probe top surface (W/cm^2)
*   TOPTEMP = Temperature of probe top surface (C)
*   QAN = Heat flux across probe-tissue interface (W/m^2)
*   QIN = Heat flux calculated withing probe (W/m^2)
*   QSUM = Summation of heat fluxes across probe radius
*   TTHERM = Temperature of surface thermocouple calculated by
*           lumped capacitance model including thermal glue (C)
*   R2 = Thermal paste (glue) resistance (m^2K/W)
*   BAM = Time constant in lumped capacitance TC model (s)
*   COEF = Coefficient in lumped capacitance model (C)
*   ETMA(I) = Array of model output delivered back to main program
*
*****
                SUBROUTINE MODEL(ITIME, VARIABLES...)
*
* Different applications require different call variables
* These can be adjusted in the above statement and in the subroutine by
* commenting/uncommenting variable definitions according to user demand.
* All the variables and calculations are uncommented here.
*
C   DEFINE RANGE OF ARRAYS FOR VARIABLES
C
  IMPLICIT REAL*8 (A-H,O-Z)
  REAL*8 M,KT,KP,texceed
  PARAMETER(NNODES=25,LNODES=150)
  DIMENSION THETA(NNODES,LNODES),A(NNODES,LNODES),B(NNODES,LNODES)

```

```

$,C(NNODES,LNODES),D(NNODES,LNODES),E(NNODES,LNODES),
$F(NNODES,LNODES),G(NNODES,LNODES),H(NNODES,LNODES),ETA(NNODES),
$BETA(NNODES,LNODES),GAMMA(NNODES,LNODES),TEMP(NNODES,LNODES),
$QAN(NNODES),TGS(NNODES),THETATOP(NNODES),TOPTEMP(NNODES),
$QH(NNODES),THETAJM1(NNODES),TPIM(NNODES),ETMA(3),QIN(NNODES)
C
C   DEFINE TISSUE AND BLOOD PROPERTIES
C
ALPHT=0.15D-06
RHOB= 1000.DO
SHB= 4000.DO
WB= 0.0020D0
KT= 0.5D0
R= .00953D0
M=( (RHOB*SHB*WB)/(KT))*R**2.DO
artetemp=37.0D0
C
C   DEFINE PROBE PROPERTIES
C
airtemp=23.80D0
RC=.0010D0
Thickness=0.00006604D0
RHOP=2022.0D0
SHP=875.0D0
KP=177.0D0
ALPHP=KP/RHOP/SHP
FF=ALPHP/ALPHT
C
C   DEFINE GEOMETRIC PROPERTIES
C
TSTP = 1.D0/9.5D0
NEDGE=10
C LEDGE should be 3 or greater
LEdge=10
DH=1.0D0/Dble(NEDGE)
DZ=Thickness/(Dble(LEdge)*R)
TIME = 0.D0+DBLE(ITIME)*TSTP
XTIME = ALPHT*TIME/(R**2.DO)
DT=ALPHT*TSTP/(2.D0*R**2.DO)
NTSTP=1
N=20
L=150
THETAINF=1.0D0
CRFP=(DZ*R)/(KP*(RC+((DZ*R)/(2.D0*KT))+((DZ*R)/(2.D0*KP))))

CRFT=(DZ*R)/(KT*(RC+((DZ*R)/(2.D0*KT))+((DZ*R)/(2.D0*KP))))
C
C   INITIALIZE PROBE MATRICES
C
DO 1 I=1,NEDGE,1
DO 2 J=1,LEdge,1
THETA(I,J)=0.DO
A(I,J)=0.DO
B(I,J)=0.DO
C(I,J)=0.DO
D(I,J)=0.DO
E(I,J)=0.DO
F(I,J)=0.DO
G(I,J)=0.DO
H(I,J)=0.DO
ETA(I)=0.DO
BETA(I,J)=0.DO
GAMMA(I,J)=0.DO
TEMP(I,J)=0.DO
2 CONTINUE
1 CONTINUE
C
C   INITIALIZE TISSUE THETA MATRIX
C
DO 91 I=1,N,1
DO 92 J=LEdge+1,L,1
THETA(I,J)=0.DO
A(I,J)=0.DO
B(I,J)=0.DO
C(I,J)=0.DO
D(I,J)=0.DO
E(I,J)=0.DO
F(I,J)=0.DO
G(I,J)=0.DO
H(I,J)=0.DO
ETA(I)=0.DO
BETA(I,J)=0.DO
GAMMA(I,J)=0.DO
TEMP(I,J)=0.DO
92 CONTINUE
91 CONTINUE
C
C   COMPUTE ETA(I) VALUES
C
DO 50 I=1,N,1

```



```

      ETA(I)=((2.DO*DBLE(I)-1.DO)/2.DO)*DH
50 CONTINUE
C
      DO 29 NT=1,NTSTP,1
C
      DEFINE CONVECTION COEFFICIENT WITH GRADUAL INCREASE FROM 1.0 TO
      MAXIMUM VALUE OVER THE FIRST 11 TIME STEPS (ASSUMING A TIMESTEP
      OF 1/9.5 SECONDS)
      IF (ITIME.LE.11) THEN
          CONV = (480.DO-1.DO)/11.DO*DBLE(ITIME)+1.DO
      ELSE
          CONV = 480.DO
      ENDIF
C
      DEFINE COEFFICIENTS OF 1ST TIME STEP MATRICES
      A(I,J),B(I,J),C(I,J)
      1ST COLUMN PROBE
C
      I=1
      DO 31 J= 1,LEGE,1
      A(1,J)=0.DO
      B(1,J)=1.DO/(FF*DT)+1.DO/((DH)**2.DO)+1.DO/(2.DO*ETA(I)*DH)
      C(1,J)=-1.DO/(DH**2.DO)-1.DO/(2.DO*ETA(I)*DH)
31 CONTINUE
C
      MIDDLE COLUMNS, PROBE
C
      DO 32 I= 2,NEDGE-1,1
      DO 33 J= 1,LEGE,1
      A(I,J)=-1.DO/(DH)**2.DO+1.DO/(2.DO*ETA(I)*DH)
      B(I,J)=1.DO/(FF*DT)+2.DO/(DH)**2.DO
      C(I,J)=-1.DO/(DH)**2.DO-1.DO/(2.DO*ETA(I)*DH)
33 CONTINUE
32 CONTINUE
C
      FINAL COLUMN, PROBE
C
      I=NEDGE
      DO 34 J=1,LEGE,1
      A(I,J)=1.DO/(2.DO*ETA(I)*DH)-1.DO/(DH)**2.DO
      B(I,J)=1.DO/(FF*DT)+1.DO/(DH)**2.DO-1.DO/(2.DO*ETA(I)*DH)
      C(I,J)=0.DO
34 CONTINUE
C

```

```

C      1ST COLUMN TISSUE
C
      I=1
      DO 3 J=LEGE+1,L,1
      A(1,J)=0.DO
      B(1,J)=1.DO/(ETA(I)*(2.DO*Dh))+1.DO/((DH)**2.DO)+1.DO/DT+M
      C(1,J)=-1.DO/(DH)**2.DO-1.DO/(ETA(I)*(2.DO*Dh))
3 CONTINUE
C
      MIDDLE COLUMNS
C
      DO 4 I=2,N-1,1
      DO 5 J=LEGE+1,L,1
      A(I,J)= 1.DO/(ETA(I)*(2.DO*Dh))-1.DO/(DH)**2.DO
      B(I,J)=1.DO/DT+2.DO/(DH)**2.DO+M
      C(I,J)=-1.DO/(DH)**2.DO-1.DO/(ETA(I)*(2.DO*Dh))
5 CONTINUE
4 CONTINUE
C
      FINAL COLUMN
C
      I=N
      DO 6 J=LEGE+1,L,1
      A(N,J)= 1.DO/(ETA(I)*(2.DO*Dh))-1.DO/(DH)**2.DO
      B(N,J)= 1.DO/DT+1.DO/(DH)**2.DO-1.DO/(ETA(I)*(2.DO*Dh))+M
      C(N,J)=0.DO
6 CONTINUE
C
      DEFINE E(I,J),F(I,J),G(I,J)
      COEFFICIENTS OF 2ND TIME STEP MATRIX
      FIRST ROW,PROBE
C
      J=1
      DO 35 I=1,NEDGE,1
      E(I,1)=0.DO
      F(I,1)=((-CONV/2.DO+KP/(DZ*R))/(KP/(DZ*R)+CONV/2.DO))*(-1.DO/((DZ)
      **2.DO))+2.DO/((DZ)**2.DO)+1.DO/(FF*DT)
      G(I,1)=-1.DO/(DZ)**2.DO
35 CONTINUE
C
      MIDDLE ROWS
C
      DO 36 J=2,LEGE-1,1
      DO 37 I=1,NEDGE,1
      E(I,J)=-1.DO/(DZ)**2.DO

```

```

      F(I,J)=2.DO/((DZ)**2.DO)+1.DO/(FF*DT)
      G(I,J)=-1.DO/(DZ)**2.DO)
37 CONTINUE
36 CONTINUE
C
C   BOTTOM ROW, PROBE
C
      J=LEDGE
      DO 38 I = 1,NEDGE,1
      E(I,J)=-1.DO/((DZ)**2.DO)
      F(I,J)=2.DO/((DZ)**2.DO)+1.DO/(FF*DT)+(-CRFP+1.DO)*(-1.DO/(DZ
      **2.DO))
      G(I,J)=CRFP*(-1.DO/((DZ)**2.DO))
38 CONTINUE
C
C   TOP ROW OF TISSUE UNDER PROBE SURFACE
C
      J=LEDGE+1
      DO 39 I=1,NEDGE,1
      E(I,J)=(CRFT)*(-1.DO/((DZ)**2.DO))
      F(I,J)=(-CRFT+1.DO)*(-1.DO/((DZ)**2.DO))+1.DO/DT
      $+2.DO/((DZ)**2.DO)+M
      G(I,J)=-1.DO/((DZ)**2.DO)
39 CONTINUE
C
C   DEFINE TOP TISSUE ROW, OUTSIDE OF PROBE
C
      J=LEDGE+1
      DO 8 I=NEDGE+1,N,1
      E(I,J)=0.DO
      F(I,J)=1.DO/DT+1.DO/(DZ**2.DO)+M
      G(I,J)=-1.DO/(DZ**2.DO)
8 CONTINUE
C
C   DEFINE MIDDLE ROWS
C
      DO 9 J=LEDGE+2,L-1,1
      DO 10 I=1,N,1
      E(I,J)=-1.DO/(DZ**2.DO)
      F(I,J)=1.DO/DT+2.DO/(DZ**2.DO)+M
      G(I,J)=-1.DO/(DZ**2.DO)
10 CONTINUE
9 CONTINUE
C
C   BOTTOM ROW

```

```

C
      J=L
      DO 11 I=1,N,1
      E(I,L)=-1.DO/(DZ**2.DO)
      F(I,L)=1.DO/DT+1.DO/(DZ**2.DO)+M
      G(I,L)=0.DO
11 CONTINUE
C
C   DO 29 NT=1,NTSTP,1
C
C   FIRST TIME STEP CALCULATIONS
C   DEFINE RHS COLUMN D(I,J)
C   PROBE ELEMENTS
C
C   TOP ROW PROBE
C
      J=1
      DO 40 I=1,NEDGE,1
      D(I,1)=((CONV*THETAINF)/(KP/(DZ*R)+CONV/2.DO))*(1.DO/((DZ)**2.DO))
      $+THETA(I,1)*(-2.DO/((DZ)**2.DO)+1.DO/(FF*DT))+((-CONV/2.DO+KP/(DZ
      $*R))/(KP/(DZ*R)+CONV/2.DO))*(1.DO/((DZ)**2.DO))+THETA(I,2)*(1.DO
      $/((DZ)**2.DO))
40 CONTINUE
C
C   MIDDLE ROWS, PROBE
C
      DO 41 J=2,LEDGE-1,1
      DO 42 I=1,NEDGE,1
      D(I,J)=THETA(I,J-1)*(1.DO/((DZ)**2.DO))+THETA(I,J)*(-2.DO/
      $((DZ)**2.DO)+1.DO/(FF*DT))+THETA(I,J+1)*(1.DO/((DZ)**2.DO))
42 CONTINUE
41 CONTINUE
C
C   BOTTOM ROW, PROBE
C
      J=LEDGE
      DO 43 I=1,NEDGE,1
      D(I,J)=THETA(I,J-1)*(1.DO/((DZ)**2.DO))+THETA(I,J)*((-2.DO/
      $((DZ)**2.DO)+1.DO/(FF*DT))+(-CRFP+1.DO)*(1.DO/((DZ)**2.DO)))
      $+THETA(I,J+1)*((CRFP)*(1.DO/((DZ)**2.DO)))
43 CONTINUE
C
C   TISSUE ELEMENTS
C   TOP ROW UNDER PROBE

```

```

C
  J=LEDGE+1
  DO 12 I=1,NEDGE,1
    D(I,LEDGE+1)=THETA(I,LEDGE)*((CRFT)*(1.DO/((DZ
$$$2.DO))) + THETA(I,LEDGE+1)*((-CRFT+1.DO)*(1.DO/((DZ
$$$2.DO))) + 1.DO/DT - 2.DO/(DZ**2.DO)) + THETA(I,LEDGE+2)*(1.DO/(DZ**2.DO
$$$))
12 CONTINUE

  DO 13 I=NEDGE+1,N,1
    D(I,LEDGE+1)=THETA(I,LEDGE+1)*(1.DO/DT - 1.DO/(DZ**2.DO)) +
    $THETA(I,LEDGE+2)*(1.DO/(DZ**2.DO))
13 CONTINUE

  DO 14 J=LEDGE+2,L-1,1
  DO 15 I=1,N,1
    D(I,J)=THETA(I,J-1)*(1.DO/(DZ**2.DO)) + THETA(I,J)*(1.DO/DT -
    $2.DO/(DZ**2.DO)) + THETA(I,J+1)*(1.DO/(DZ**2.DO))
15 CONTINUE
14 CONTINUE

  DO 16 I=1,N,1
  J=L
  D(I,L)=THETA(I,L-1)*(1.DO/(DZ**2.DO)) + THETA(I,L)*(1.DO/DT - 1.DO/
    $(DZ**2.DO))
16 CONTINUE

C
C   USE TRIDIAGONAL MATRIX SOLVER TO GET
C   THETA VALUES AT THE FIRST TIME STEP
C
  IF=1
  DO 17 J=1,LEDGE,1
    BETA(IF,J)=B(1,J)
    GAMMA(IF,J)=D(1,J)/BETA(IF,J)
    IFP1=IF+1

  DO 18 I=IFP1,NEDGE
    BETA(I,J)=B(I,J)-A(I,J)*C(I-1,J)/BETA(I-1,J)
    GAMMA(I,J)=(D(I,J)-A(I,J)*GAMMA(I-1,J))/BETA(I,J)
18 CONTINUE

  THETA(NEDGE,J)=GAMMA(NEDGE,J)
  LAST=NEDGE-IF
  DO 19 K=1,LAST
  I=NEDGE-K

    THETA(I,J)=GAMMA(I,J)-C(I,J)*THETA(I+1,J)/BETA(I,J)
19 CONTINUE
17 CONTINUE

C
C   MATRIX SOLVER FOR TISSUE ELEMENTS
C
  IF=1
  DO 117 J=LEDGE+1,L,1
    BETA(IF,J)=B(1,J)
    GAMMA(IF,J)=D(1,J)/BETA(IF,J)
    IFP1=IF+1

  DO 118 I=IFP1,N,1
    BETA(I,J)=B(I,J)-A(I,J)*C(I-1,J)/BETA(I-1,J)
    GAMMA(I,J)=(D(I,J)-A(I,J)*GAMMA(I-1,J))/BETA(I,J)
118 CONTINUE

  THETA(N,J)=GAMMA(N,J)
  LAST=N-IF
  DO 119 K=1,LAST
  I=N-K
  THETA(I,J)=GAMMA(I,J)-C(I,J)*THETA(I+1,J)/BETA(I,J)
119 CONTINUE
117 CONTINUE

  XTIME=XTIME+DT

C
C   SECOND TIME STEP CALCULATIONS
C   DEFINE H(I,J) VALUES
C   1ST ROW PROBE
C
  H(1,1)=((-CONV*THETAINF)/(KP/(DZ*R)+CONV/2.DO))*(-1.DO/((DZ)**2.
    $0)) + THETA(1,1)*(1.DO/(FF*DT) - 1.DO/((DH)**2.DO) - 1.DO/(2.DO*ETA(I
    $)*DH)) + THETA(2,1)*(1.DO/((DH)**2.DO)) + 1.DO/(2.DO*ETA(I)*DH))

  J=1
  DO 44 I=2,NEDGE-1,1
    H(I,1)=((-CONV*THETAINF)/(KP/(DZ*R)+CONV/2.DO))*(-1.DO/((DZ**
    $2.DO)) + THETA(I-1,1)*(1.DO/((DH)**2.DO) - 1.DO/(2.DO*ETA(I)*
    $DH)) + THETA(I,1)*(1.DO/(FF*DT) - 2.DO/((DH)**2.DO)) + THETA(I+1,1)*
    $(1.DO/((DH)**2.DO)) + 1.DO/(2.DO*ETA(I)*DH))
44 CONTINUE

  H(NEDGE,1)=((-CONV*THETAINF)/(KP/(DZ*R)+CONV/2.DO))*(-1.DO/((DZ**
    $2.DO)) + THETA(NEDGE-1,1)*(1.DO/((DH)**2.DO) - 1.DO/(2.DO*

```

```

$ETA(I)*DH))+THETA(NEDGE,1)*(1.DO/(FF*DT)-1.DO/((DH**2.DO))+1.DO/
$(2.DO*ETA(I)*DH))
C
C LEFT PROBE COLUMN
C
I=1
DO 45 J=2,LEDGE,1
H(1,J)=THETA(1,J)*(1.DO/(FF*DT)-1.DO/((DH**2.DO))-1.DO/(2.DO*
$ETA(I)*DH))+THETA(2,J)*(1.DO/((DH**2.DO))+1.DO/(2.DO*
$ETA(I)*DH))
45 CONTINUE
C
C RIGHT PROBE COLUMN
C
I=NEDGE
DO 46 J=2,LEDGE,1
H(NEDGE,J)=THETA(NEDGE-1,J)*(1.DO/((DH**2.DO))-1.DO/(2.DO*
$ETA(I)*DH))+THETA(NEDGE,J)*(1.DO/(FF*DT)-1.DO/((DH**2.DO))+1.DO/
$(2.DO*ETA(I)*DH))
46 CONTINUE
C
C MIDDLE AND BOTTOM MIDDLE ROW PROBE ELEMENTS
C
DO 47 I=2,NEDGE-1,1
DO 48 J=2,LEDGE,1
H(I,J)=THETA(I-1,J)*(1.DO/((DH**2.DO))-1.DO/(2.DO*ETA(I)
*$DH))+THETA(I,J)*(1.DO/(FF*DT)-2.DO/((DH**2.DO))+THETA(I+1,J)*
$(1.DO/((DH**2.DO))+1.DO/(2.DO*ETA(I)*DH))
48 CONTINUE
47 CONTINUE
C
C DEFINE TISSUE ELEMENTS
C TOP LEFT CORNER NODE
C
I=1
J=LEDGE+1
H(I,J)=THETA(1,LEDGE+1)*(1.DO/DT-1.DO/(DH**2.DO))-1.DO/
$(ETA(I)*(2.DO*DH))+THETA(2,LEDGE+1)*(1.DO/(DH**2.DO)+1.DO/(ETA(I)
$(2.DO*DH)))
DO 20 J=LEDGE+2,L,1
H(1,J)=THETA(1,J)*(1.DO/DT-1.DO/(DH**2.DO))-1.DO/(ETA(I)*(2.DO*DH
$)))+THETA(2,J)*(1.DO/(DH**2.DO)+1.DO/(ETA(I)*(2.DO*DH)))
20 CONTINUE
C

```

```

C REST OF TOP ROW UNDER PROBE
C
J=LEDGE+1
DO 21 I=2,NEDGE,1
H(I,LEDGE+1)=THETA(I-1,LEDGE+1)*(1.DO/(DH**2.DO))-1.DO/(
$ETA(I)*(2.DO*DH))+THETA(I,LEDGE+1)*(1.DO/DT-2.DO/(DH**2.DO))+
$THETA(I+1,LEDGE+1)*(1.DO/(DH**2.DO)+1.DO/(ETA(I)*(2.DO*DH)))
21 CONTINUE
DO 22 I=NEDGE+1,N-1,1
H(I,LEDGE+1)=THETA(I-1,LEDGE+1)*(1.DO/(DH**2.DO))-1.DO/(
$ETA(I)*(2.DO*DH))+THETA(I,LEDGE+1)*(1.DO/DT-2.DO/(DH**2.DO))
$+THETA(I+1,LEDGE+1)*(1.DO/(DH**2.DO)+1.DO/(ETA(I)*(2.DO*DH)))
22 CONTINUE
DO 23 J=LEDGE+2,L,1
DO 24 I=2,N-1,1
H(I,J)=THETA(I-1,J)*(1.DO/(DH**2.DO))-1.DO/(ETA(I)*(2.DO*DH))
$+THETA(I,J)*(1.DO/DT-2.DO/(DH**2.DO))+THETA(I+1,J)*(1.DO/(DH**
$2.DO)+1.DO/(ETA(I)*(2.DO*DH)))
24 CONTINUE
23 CONTINUE
DO 25 J=LEDGE+1,L,1
I=N
H(N,J)=THETA(N-1,J)*(1.DO/(DH**2.DO))-1.DO/(ETA(I)*(2.DO*DH))
$+THETA(N,J)*(1.DO/DT-1.DO/(DH**2.DO)+1.DO/(ETA(I)*(2.DO*DH)))
25 CONTINUE
C
C USE TRIDIAGONAL MATRIX SOLVER TO GET
C THETA VALUES AT SECOND TIME STEP
C
IF=1
DO 26 I=1,NEDGE,1
BETA(I,IF)=F(I,1)
GAMMA(I,IF)=H(I,1)/BETA(I,IF)
IFP1=IF+1
DO 27 J=IFP1,L,1
BETA(I,J)=F(I,J)-E(I,J)*G(I,J-1)/BETA(I,J-1)
GAMMA(I,J)=(H(I,J)-E(I,J)*GAMMA(I,J-1))/BETA(I,J)
27 CONTINUE
THETA(I,L)=GAMMA(I,L)
LAST=L-IF

```

```

DO 28 K=1, LAST, 1
  J=L-K
  THETA(I, J)=GAMMA(I, J)-G(I, J)*THETA(I, J+1)/BETA(I, J)
28 CONTINUE
26 CONTINUE
C
C   MATRIX SOLVER FOR ADDITIONAL ELEMENTS
C
  IF=LEDGE+1
  DO 126 I=NEDGE+1, N, 1
    BETA(I, IF)=F(I, IF)
    GAMMA(I, IF)=H(I, IF)/BETA(I, IF)
    IFP1=IF+1

    DO 127 J=IFP1, L, 1
      BETA(I, J)=F(I, J)-E(I, J)*G(I, J-1)/BETA(I, J-1)
      GAMMA(I, J)=(H(I, J)-E(I, J)*GAMMA(I, J-1))/BETA(I, J)
127 CONTINUE

    THETA(I, L)=GAMMA(I, L)
    LAST=L-IF
    DO 128 K=1, LAST, 1
      J=L-K
      THETA(I, J)=GAMMA(I, J)-G(I, J)*THETA(I, J+1)/BETA(I, J)

128 CONTINUE
126 CONTINUE

  XTIME = XTIME +DT
  TIME=XTIME*R**2.DO/ALPHT
C
  DO 200 I=1, N, 1
    DO 199 J=1, L, 1
      TEMP(I, J)=THETA(I, J)*(airtemp-artetemp)+artetemp
199 CONTINUE
200 CONTINUE
C
C   LUMPED CAPACITANCE MODEL FOR SURFACE THERMOCOUPLE
C   ATTEMPT AT ADDING EFFECT OF GLUE TO TC TEMPERATURE
  R2 = 0.0013DO
  R1 = RC - R2
  COEF = (R2*TEMP(1, LEDGE+1)+R1*TEMP(1, LEDGE))/RC

  BAM = (R1+R2)/(508.0DO*R1*R2)
  TTHERM = (TEMP(1, LEDGE+1)-COEF)*EXP(-BAM*TIME)+COEF

  DO 300 I=1, NEDGE, 1

C   COMPUTE HEAT FLUX AT PROBE TOP
  THETAJM1(I) = (((KP/(DZ*R))-(CONV/2.DO))*THETA(I, 1)+(CONV*
$THETAINF))/((KP/(DZ*R))+CONV/2.DO)
  THETATOP(I) = (THETA(I, 1)+THETAJM1(I))/2.DO
  QH(I)=CONV*((THETATOP(I)-THETAINF)*(airtemp-artetemp))
  TOPTEMP(I) = THETATOP(I)*(airtemp-artetemp)+artetemp

C   COMPUTE HEAT FLUX AT INTERFACE OF TISSUE AND PROBE
  QAN(I)=((airtemp-artetemp)*((THETA(I, LEDGE+1)-THETA(I, LEDGE))
$/ (RC+((DZ*R)/(2.DO*KT))+((DZ*R)/(2.DO*KP))))))

C   COMPUTE HEAT FLUX USING NODES WITHIN PROBE
  QIN(I)=KP*(TEMP(I, 10)-TEMP(I, 1))/(2.DO*DZ*R)

C   COMPUTE GAGE SURFACE TEMPERATURE
  TPIM(I)=CRFP*(TEMP(I, LEDGE+1)-TEMP(I, LEDGE))+TEMP(I, LEDGE)
  TGS(I)=(TEMP(I, LEDGE)+TPIM(I))/2.DO

300 CONTINUE

  QSUM = 0.DO
  QSUM2 = 0.DO
  DO 305 I=1, NEDGE, 1
    QSUM2 = QSUM2 + QAN(I)
    QSUM = QSUM + QH(I)
305 CONTINUE

  ETMA(1) = QSUM/DBLE(NEDGE)
  ETMA(2) = QSUM2/DBLE(NEDGE)
  ETMA(3) = TGS(1)

29 CONTINUE

  RETURN
  END
*****

```

A.2 Main Program for Calling Biothermal Model Alone

```

* File *mod.f
* Written and modified by Paul Robinson, November 1997 and counting....
* This is a main program that uses the bioprobe model for testing the
* properties of the probe and tissue by user input.
* Virginia Polytechnic Institute & State University
*
  INTEGER I,J,COUNT
  REAL *8 ETA,BP,CRES,THETA,TIME,TINIT,airtemp
  DIMENSION ETA(3), THETA(25,150)
  CHARACTER*20 OUTFILE

  WRITE(*,*)'ENTER THE NAME OF THE OUTPUT FILE'
  READ(*,'(A20)')OUTFILE
  OPEN(10,FILE=OUTFILE)

C   INPUT STATEMENTS FOR MODEL PARAMETERS
C   THESE CAN BE CHANGED TO ANY DESIRED PARAMETER UNDER TESTING,
C   OR COMMENTED OUT TO ALLOW JUST SPECIFICATION OF RC,WB FOR
C   TRIAL AND ERROR ESTIMATION

  WRITE(*,*)'THETA INITIAL?'
  READ(*,*)TINIT
  WRITE(*,*)'AIR TEMP?'
  READ(*,*)airtemp
  WRITE(*,*)'CONTACT RESISTANCE?'
  READ(*,*)CRES
  WRITE(*,*)'BLOOD PERFUSION?'
  READ(*,*)BP

C   THE FOLLOWING WRITE STATEMENTS CAN BE ADJUSTED TO PROVIDE STRAIGHT
C   MODEL OUTPUT OR A FORMATTED DATA FILE FOR INPUT TO THE PARAMETER
C   ESTIMATION PROGRAM (For simulated testing)

  WRITE(10,5)CRES,BP
5  FORMAT('#',5F15.6)

  WRITE(10,*)'# TIME,QH,QINT,TGS'
C   VAR = 1.0D0
C   BP = 0.00200D0
C   CRES = 0.005D0
  COUNT = 0

  DO 12 I = 1,25,1
    DO 10 J = 1,150,1
      THETA(I,J)=TINIT
10   CONTINUE
12  CONTINUE

C   CALCULATION LOOP. UNCOMMENT THE COUNT STATEMENTS IN ORDER TO
C   WRITE DATA TO THE FILE EVERY X TIME STEPS INSTEAD OF AT EVERY
C   TIME STEP.

  DO 30 I = 1,600,1
C   COUNT = COUNT + 1
    TIME = DBLE(I)/9.5D0
    CALL MODEL(I,BP,CRES,ETA,THETA,airtemp)
C   IF(COUNT.EQ.40) THEN
      WRITE(10,25)TIME,ETA(1),ETA(2),ETA(3)
C   COUNT = 0
C   END IF
25  FORMAT(4F15.4)
30  CONTINUE

  CLOSE(10)
  END

*****
SUBROUTINE MODEL(ITIME,WB,RC,ETMA,THETA,airtemp)
*   SEE APPENDIX A1

```

Appendix B

Model Related Application Programs

B.1 Objective Function Calculation

This main program calculates the sum of squares error between model and experiment for a range of parameters. The user can specify the parameters, the bounds, and the increment size. The output is a multicolumn file containing the objective function values for each combination of parameters.

```
* File objtve.f
* Written and modified by Paul Robinson, November 1997
* Virginia Polytechnic Institute & State University
*
* This main program uses the bioprobe model to perform a
* parametric study for a range of contact resistance and perfusion.
* The objective function is the sum of squared error for heat flux
* and temperature. The file 'real.dat' is some typical experimental
* data against which the model output is compared.
*
*****
      INTEGER I,J,L,M
      REAL *8 ETA,BP,CRES,THETA,TINIT,SSY,RESID
      DIMENSION ETA(3),THETA(25,150),Q(1000),T(1000),RESID(2)

      OPEN(10,FILE='real.dat')
      DO 5 J = 1,591,1
        READ(10,*)I,Q(I),T(I)
5     CONTINUE
      WRITE(*,*)Q(2),T(2)
      OPEN(12,FILE='s2.dat')

      BP = 0.0D0
      CRES = 0.0D0
      TINIT = 0.4040D0
      SSY = 0.D0

      DO 12 I = 1,20,1
```

```

        DO 10 J = 1,150,1
            THETA(I,J) = TINIT
10     CONTINUE
12     CONTINUE

        DO 70 J = 1,10,1
            BP = 0.0000DO+DBLE(J)/10000.DO
            DO 60 K = 1,10,1
                CRES = 0.00DO+DBLE(K)/1000.DO
                DO 30 I = 1,607,1
                    CALL MODEL(I,BP,CRES,ETA,THETA)
                    RESID(1) = Q(I)-ETA(2)
                    RESID(2) = T(I)-ETA(3)
                    SSY = SSY + RESID(1)**2.DO + RESID(2)**2.DO
30             CONTINUE
                WRITE(12,35)BP,CRES,SSY
35             FORMAT(2F10.4,1X,F20.4)
                DO 50 L = 1,20,1
                    DO 40 M = 1,150,1
                        THETA(L,M) = TINIT
40             CONTINUE
50             CONTINUE
                SSY = 0.DO
60             CONTINUE
70             CONTINUE

            CLOSE(10)
            CLOSE(12)
            END
*****
        SUBROUTINE MODEL(ITIME,WB,RC,ETMA,THETA)
*
*     SEE APPENDIX A.1

```

B.2 Main Program for Calculating Sensitivity Coefficients

This main program calculates the sensitivity coefficients of heat flux and temperature to specified parameters and/or model variables. This program can be adjusted to provide either dimensional or non-dimensional coefficients with respect to time. The output is columnar to provide easy graphing capability with a spreadsheet or other graphical program.

```

* File sensbio.f
* Written and modified by Paul Robinson, November 1997 and counting....
*
* This program uses the bioprobe model program as a subroutine to
* calculate dimensionless sensitivity coefficients for specified model
* parameters. The output is the non-dimensionalized sensitivity
* coefficients of heat flux and temperature as a function of time.
* This current code is set up to calculate the sensitivity
* coefficients to blood perfusion and contact resistance.
*****
*     VARIABLE DEFINITIONS
*     STIME = BEGINING TIME OF CALCULATIONS (s)
*     ETIME = END TIME OF CALCULATIONS (s)
*     TMSTEP = TIME STEP
*     NTSTP = NUMBER OF TIME STEPS
*     WBLow = NOMINAL BLOOD PERFUSION VALUE
*     WBHI = PERMUTATION OF BLOOD PERFUSION

```



```

* CRES = NOMINAL VALUE OF CONTACT RESISTANCE
* TIME = CURRENT TIME
* QMAX = MAXIMUM HEAT FLUX VALUE OVER TIME
* TMAX = MAXIMUM TEMPERATURE VALUE OVER TIME
* CRESHI = PERMUTATION OF CONTACT RESISTANCE
* GSTLOW = GAGE SURFACE TEMPERATURE AT NOMINAL VALUES
* QLOW = HEAT FLUX AT NOMINAL VALUES
* GSTWHI = SURFACE TEMPERATURE AT HIGH PERFUSION
* QWHI = HEAT FLUX AT HIGH PERFUSION
* GSTRHI = SURFACE TEMPERATURE AT HIGH CONTACT RESISTANCE
* QRHI = HEAT FLUX AT HIGH CONTACT RESISTANCE
* GSTW = SURFACE TEMPERATURE SENSITIVITY COEFFICIENT TO PERFUSION
* QINTW = HEAT FLUX SENSITIVITY COEFFICIENT TO PERFUSION
* GSTR = SURFACE TEMPERATURE SENSITIVITY COEFFICIENT TO CONT. RES.
* QINTR = HEAT FLUX AT SENSITIVITY COEFFICIENT TO CONT. RES.
*****

```

```

INTEGER STIME, ETIME, I, NTSTP
REAL *8 TMSTEP, QWHI, QLOW, QINTW, GSTWHI, GSTLOW, GSTW, CRES, TIME
$, WBHI, WBLow, QMAX, TMAX, CRESHI, QINTR, GSTR, QRHI, GSTRHI
DIMENSION QWHI(6000), QLOW(6000), GSTWHI(6000), GSTLOW(6000),
$QRHI(6000), GSTRHI(6000)

```

```

OPEN(10, FILE='sens.dat')

```

```

STIME = 0
ETIME = 70
TMSTEP = 1.DO/9.5D0
NTSTP = (ETIME-STIME)*INT(1.DO/TMSTEP)
WBLow = 0.03872D0
WBHI = 1.01D0*WBLow
CRES = 0.00302D0
TIME = DBLE(STIME)
QMAX = 0.DO
TMAX = 0.DO
CRESHI = 1.01D0*CRES

```

```

CALL MODEL(STIME, ETIME, TMSTEP, WBHI, CRES, QWHI, GSTWHI)
CALL MODEL(STIME, ETIME, TMSTEP, WBLow, CRES, QLOW, GSTLOW)
CALL MODEL(STIME, ETIME, TMSTEP, WBLow, CRESHI, QRHI, GSTRHI)

```

```

DO 300 I=1, NTSTP, 1
  IF(QLOW(I).GT.QMAX) THEN
    QMAX = QLOW(I)
  ENDIF
  IF(GSTLOW(I).GT.TMAX) THEN
    TMAX = GSTLOW(I)
  ENDIF
300 CONTINUE

```

```

DO 410 I = 1, NTSTP, 1
  TIME = TIME + TMSTEP
  QINTW = (QWHI(I)-QLOW(I))/(WBHI-WBLow)*(WBLow/QMAX)
  GSTW = (GSTWHI(I)-GSTLOW(I))/(WBHI-WBLow)*(WBLow/TMAX)
  QINTR = (QRHI(I)-QLOW(I))/(CRESHI-CRES)*(CRES/QMAX)
  GSTR = (GSTRHI(I)-GSTLOW(I))/(CRESHI-CRES)*(CRES/TMAX)
  WRITE(10, 400) TIME, QINTW, GSTW, QINTR, GSTR
400 FORMAT(5F12.4)
410 CONTINUE
C   WRITE(10, *) WBHI, WBLow
  CLOSE(10)
END

```

```

*****
SUBROUTINE MODEL(ITIME, LTIME, TSTP, WB, RC, QAV, TGSM)

```

```

* SEE APPENDIX A.1

```

B.3 Main Program for Estimating Inherent Error

The main program detailed below uses set uncertainties in certain biothermal model variables to find the inherent uncertainty in the heat flux and temperature calculations due to error in the “known” model variables. This is accomplished by calculating a time-averaged sensitivity coefficient for each variable and multiplying by the variable uncertainty (in this case, about 10%) to gain an uncertainty in heat flux and temperature for each individual variable. The overall heat flux and temperature uncertainties are found by the sum of squares average of all the uncertainty contributions from each individual variable. The end result is a number representing the standard deviation of the heat flux and temperature calculations as output from the biothermal model. This error estimate can then be included within the parameter estimation procedure.

```
* File knownstdcalc.f
*
* Written and modified by Paul Robinson, December 1997
* Virginia Polytechnic Institute and State University
*
* The following is a main program that uses the biothermal model to
* calculate the standard deviation, or error estimate, of the model output
* based on uncertainty in set model variables. For example, the code as
* given here calculates the uncertainty in model heat flux output based on
* a ten percent uncertainty in tissue thermal conductivity and diffusivity.
* Any model variable can be specified as long as the call statement and model
* subroutine are changed accordingly.
*****
*
*           EXPLANATION OF VARIABLES
*
* STIME = TEST BEGINNING TIME
* ETIME = TEST END TIME
* TMSTEP = TIME STEP
* NTSTP = NUMBER OF TIME STEPS
* VAR1 = MODEL VARIABLE 1
* VAR1HI = PERMUTATION OF MODEL VARIABLE 1
* VAR2 = MODEL VARIABLE 2
* VAR2HI = PERMUTATION OF MODEL VARIABLE 2
* TIME = CURRENT TIME
* STD# = ERROR IN VARIABLE #
* QLOW = BASE HEAT FLUX VALUE
* GSTLOW = BASE TEMPERATURE VALUE
* Q#HI = HEAT FLUX AT HIGH VALUE OF VARIABLE #
* GST#HI = TEMPERATURE AT HIGH VALUE OF VARIABLE #
* QINT# = SUMMATION OF HEAT FLUX SENSITIVITY TO VARIABLE #
* GST# = SUMMATION OF TEMPERATURE SENSITIVITY TO VARIABLE #
* QSIG# = HEAT FLUX ERROR ESTIMATE FOR VARIABLE #
* TSIG# = TEMPERATURE ERROR ESTIMATE FOR VARIABLE #
*****
      INTEGER STIME, ETIME, I, NTSTP
      REAL *8 TMSTEP, Q1HI, QLOW, QINT1, GST1HI, GSTLOW, GST1, VAR1, TIME, QSIG1
      $, VAR1HI, VAR2, VAR2HI, QINT2, GST2, Q2HI, GST2HI, STD1, STD2, QSIG2, TSIG1
      $, TSIG2
      DIMENSION Q1HI(6000), QLOW(6000), GST1HI(6000), GSTLOW(6000),
      $Q2HI(6000), GST2HI(6000)
```

```

OPEN(10,FILE='knownstd.dat')

STIME = 0
ETIME = 70
TMSTEP = 1.DO/9.5D0
NTSTP = (ETIME-STIME)*INT(1.DO/TMSTEP)
VAR1 = 0.5804D0
VAR1HI = 1.01D0*WBLOW
VAR2 = 0.146D-6
VAR2HI = 1.01D0*CRES
TIME = DBLE(STIME)
STD1 = 0.1D0*VAR1
STD2 = 0.1D0*VAR2
QINT1 = 0.DO
GST1 = 0.DO
QINT2 = 0.DO
GST2 = 0.DO

CALL MODEL(STIME,ETIME,TMSTEP,VAR1HI,VAR2,Q1HI,GST1HI)
CALL MODEL(STIME,ETIME,TMSTEP,VAR1,VAR2,QLOW,GSTLOW)
CALL MODEL(STIME,ETIME,TMSTEP,VAR1,VAR2HI,Q2HI,GST2HI)

DO 410 I = 1,NTSTP,1
    TIME = TIME + TMSTEP
    QINT1 = QINT1+(Q1HI(I)-QLOW(I))/(VAR1HI-VAR1)
    GST1 = GST1+(GST1HI(I)-GSTLOW(I))/(VAR1HI-VAR1)
    QINT2 = QINT2+(Q2HI(I)-QLOW(I))/(VAR2HI-VAR2)
    GST2 = GST2+(GST2HI(I)-GSTLOW(I))/(VAR2HI-VAR2)
410 CONTINUE

    QSIG1 = QINT1*TMSTEP/DBLE(ETIME-STIME)*STD1
    TSIG1 = GST1*TMSTEP/DBLE(ETIME-STIME)*STD1
    QSIG2 = QINT2*TMSTEP/DBLE(ETIME-STIME)*STD2
    TSIG2 = GST2*TMSTEP/DBLE(ETIME-STIME)*STD2
    WRITE(10,420)QSIG1,TSIG1,QSIG2,TSIG2
420 FORMAT('#',4F12.4)
CLOSE(10)
END

*****
SUBROUTINE MODEL(ITIME,LTIME,TSTP,KT,ALPHT,QAV,TGSM)

* SEE APPENDIX A.1

```

B.4 Main Program for Calculating Heat Flux and Temperature Slopes

This main program uses the biothermal model subroutine to calculate the slopes over time of the heat flux and temperature curves for set values of contact resistance and blood perfusion. The endpoints for the slope calculation were determined by observation, but can be adjusted by changing the PARAMETER statement below. The program provides output of the time, conductive heat flux, convective heat flux and surface temperature in formatted columns followed by the various slope and y-intercept calculations. The file is formatted for direct use in Gnuplot or a spreadsheet application.

```

* File slopemod.f
* Written and modified by Paul Robinson, November 1997
* Virginia Polytechnic Institute and State University
*
* Main program to calculate beginning and end slopes with respect to time of
* the model heat flux and temperature output. This is performed for various
* values of contact resistance and blood perfusion. The program reads in the
* file 'params' that contains the values of RC and WB to be used. By using
* this file, the program can be run in batch mode. The end result is a
* comparison of how certain model parameters effect the slope of the heat
* flux and temperature curves at different regions in time.
*
*****
*                               EXPLANATION OF VARIABLES
*
* I, J = INTEGER COUNTERS
* RH1, RH2, RK1, RK2, RT1, RT2 = TIME STEP ENDPOINTS FOR THE CALCLUATION OF
*                               SLOPE OF THE CURVES IN THE CONTACT
*                               RESISTANCE DOMINATED REGIONS OF THE
*                               CONVECTIVE, CONDUCTIVE HEAT FLUX AND
*                               TEMPERATURE, RESPECTIVELY
* W1, W2 = TIME STEP ENDPOINTS FOR ALL THE SLOPE CALCULATION IN THE BLOOD
*          PERFUSION DOMINATED PORTION OF THE VARIOUS CURVES
* CONV() = CONVECTIVE HEAT FLUX
* COND() = CONDUCTIVE HEAT FLUX
* ST() = SURFACE TEMPERATURE
* BP = BLOOD PERFUSION
* CRES = CONTACT RESISTANCE
* THETA() = NONDIMENSIONAL TEMPERATURE MATRIX
* TIME() = TIME ARRAY
* TINIT = INITIAL SYSTEM TEMPERATURE
* airtemp = COOLING AIR TEMPERATURE
* ETA() = MODEL VALUES FOR HEAT FLUX AND TEMPERATURE
* SLRH = SLOPE OF CONVECTIVE HEAT FLUX AT EARLY TIMES
* SLRK = SLOPE OF CONDUCTIVE HEAT FLUX AT EARLY TIMES
* SLRT = SLOPE OF TEMPERATURE AT EARLY TIMES
* SLWH = SLOPE OF CONVECTIVE HEAT FLUX AT END TIMES
* SLWK = SLOPE OF CONDUCTIVE HEAT FLUX AT END TIMES
* SLWT = SLOPE OF TEMPERATURE AT END TIMES
*****

      INTEGER I, J, RH1, RH2, RK1, RK2, RT1, RT2, W1, W2
      REAL *8 CONV, COND, ST, BP, CRES, THETA, TIME, TINIT, airtemp, ETA,
+SLRH, SLRK, SLRT, SLWH, SLWK, SLWT
      PARAMETER(RH1=14, RH2=19, RK1=1, RK2=14, RT1=9, RT2=19, W1=144, W2=600)
      DIMENSION CONV(600), COND(600), ST(600), THETA(25, 150), TIME(600),
+ETA(3)

      OPEN(8, FILE='params')
      OPEN(10, FILE='output')

      READ(8, *) CRES, BP
      WRITE(10, 5) CRES, BP
5  FORMAT('#', 2F10.4)

      TINIT = 0.06000D0

      DO 12 I = 1, 25, 1
        DO 10 J = 1, 150, 1
          THETA(I, J) = TINIT
10  CONTINUE
12  CONTINUE

      DO 30 I = 1, 600, 1
        TIME(I) = DBLE(I)/9.5D0
        CALL MODEL(I, BP, CRES, ETA, THETA, airtemp)
        CONV(I) = ETA(1)
        COND(I) = ETA(2)
30  CONTINUE

```

```

      ST(I) = ETA(3)
      WRITE(10,25) I, CONV(I), COND(I), ST(I), TIME(I)
25   FORMAT(I4,4F15.4)
30   CONTINUE

      SLRH = (CONV(RH2)-CONV(RH1))/(TIME(RH2)-TIME(RH1))
      SLRK = (COND(RK2)-COND(RK1))/(TIME(RK2)-TIME(RK1))
      SLRT = (ST(RT2)-ST(RT1))/(TIME(RT2)-TIME(RT1))
      SLWH = (CONV(W2)-CONV(W1))/(TIME(W2)-TIME(W1))
      SLWK = (COND(W2)-COND(W1))/(TIME(W2)-TIME(W1))
      SLWT = (ST(W2)-ST(W1))/(TIME(W2)-TIME(W1))

      WRITE(10,35) SLRH, CONV(RH1), SLRK, COND(RK1), SLRT, ST(RT1)
      WRITE(10,35) SLWH, CONV(W1), SLWK, COND(W1), SLWT, ST(W1)
35   FORMAT(' #',6F12.4)

      CLOSE(8)
      CLOSE(10)
      END

*****
      SUBROUTINE MODEL(ITIME, WB, RC, ETMA, THETA)

*   SEE APPENDIX A.1

```

Appendix C

Parameter Estimation Code

C.1 Main Program

The following code is the final implementation of the Gaussian Minimization with Box-Kanemasu modification as used in this research. This code allows for up to two dependent variables and any number of parameters. If needed, the number of dependent variables allowed can be increased by the inclusion of a matrix inversion program to handle more than a two by two matrix. Flags in the code allow for the skipping of the B-K modification. Also, commented sections are included that, if uncommented, allow the user to perform estimation with scaled data over defined time ranges and/or estimation with just certain portions of the experimental data. The program produces output of the parameter estimates, confidence intervals, and objective function (sum of squares error) at each overall iteration followed by columnar output of the time, calculated and experimental values, and sum of squares error as calculated with the final estimate values. This output can be used directly in Gnuplot or imported to a spreadsheet application.

```

* File pest.f PARAMETER ESTIMATION ROUTINE
*
* Written and modified by:
* Paul Robinson
* Department of Mechanical Engineering
* Virginia Polytechnic Institute and State University
* Blackburg, VA 24061
*
* Last Modified December, 1997
*****
* BOXKAN(TAG,TINIT,EST,B,Y,VAR,N,NP,NDEP,SSYP,CI,airtemp)
*****
* General Program to apply the modified Box-Kanemasu method to a
* user defined model. The program will consist of three parts: 1)
* the main program that iterates through to estimate the desired
* parameters, 2) a subroutine to estimate the sensitivity coeffic-
* -ients, and 3) a user attached subroutine containing the math-
* -ematical model. The user will be required to provide the model
* and a properly formatted input file containing experimental data
* and other information about the system under examination. This
* program skips the sequential method using just whole-domain Gauss
* and the B-K method with up to two dependent variables and
* parameters.
*****
* EXPLANATION OF VARIABLES
*
* N = NUMBER OF DATA POINTS
* NP = NUMBER OF PARAMETERS TO BE ESTIMATED
* NI = NUMBER OF INDEPENDENT VARIABLES
* MAXIT = MAXIMUM NUMBER OF ITERATIONS TO BE PERFORMED
* NDEP = NUMBER OF DEPENDENT VARIABLES
* B() = PARAMETER ESTIMATES
* Y*() = EXPERIMENTAL DATA VALUES, MEASUREMENT *
* VAR*() = EXPERIMENTAL VARIANCE
* T() = INDEPENDENT VARIABLES (Time, etc...)
* BS() = ARRAY TO STORE THE PARAMETER VALUES AT THE CURRENT ITER.
* BSV() = ARRAY TO STORE THE ORIGINAL PARAMETER ESTIMATES
* C() = P INVERSE COEFFICIENTS
* D() = GAUSS LINEARIZATION TERM
* DELTAB() = CHANGE IN PARAMETERS BASED ON GAUSS METHOD
* SUMG = SUMMATION TERM NEEDED TO FIND "G" IN BOX-KANEMASU
* P() = THE "P" MATRIX USED IN GAUSS METHOD
* PS() = A SQUARE OF THE P MATRIX DIAGONALS
* MAX = COUNTER OF NUMBER OF ITERATIONS
* SSY = SUM OF SQUARED ERRORS IN GAUSS METHOD

```

```

* ETA = MODEL DATA
* SC() = SENSITIVITY COEFFICIENTS FOR CURRENT TIME
* RESID() = ERROR BETWEEN EXPERIMENTAL AND MODEL DATA
* BSS() = UPDATED ESTIMATES IN B-K BASED ON STEP SIZE GUESS(ALPHA)
* ALPHA = THE ALPHA USED IN THE BOX-KANEMASU EQUATIONS
* AA = THE "A" COEFFICIENT (1.1) IN THE B-K EQUATIONS
* G = THE "G" USED IN THE B-K EQUATIONS (THE SLOPE)
* SSYP = SUM OF SQUARE ERRORS USING B-K ESTIMATES
* SUMCH = SUMMATION TERM NEEDED IN INEQUALITY TO DETERMINE THE
* PROPER EQUATION FOR "h"
* H = THE "h" USED AS A STEP SIZE IN THE B-K EQUATIONS
* R() = THE CORRELATION MATRIX
* CRITER = THE CONVERGENCE CRITERION
* CHANGE = A COUNTER TO DETERMINE WHEN ALL THE PARAMETERS HAVE
* CONVERGED
* RATIO = THE RATIO OF THE CHANGE IN THE PARAMETER ESTIMATE TO
* THE OLD ESTIMATE AT EACH ITERATION
* MARK = FLAG TO PRINT DATA AND MODEL OUTPUT AFTER CONVERGENCE
* MK2 = FLAG TO SKIP THE B-K MODIFICATION
* I*,J*,K*,L* = COUNTERS AND INTEGER INCREMENTS(FOR DO LOOPS)
*
*****
* Define Variables and Constants used in program
IMPLICIT DOUBLE PRECISION (A-H,O-Z)
INTEGER N,NI,NP,I,J,K,L,NDEP,M,CHANGE,MAXIT,K1,L1,MARK,MK2
PARAMETER (NNODES=25,LNODES=150)
DIMENSION B(3), Y(2,2048), VAR(2,2048), CI(3),
$BS(3), P(3,3), RESID(3), R(3,3), DELTAB(3), C(3,3),
$SC(4), ETA(3), PINV(3,3), BSS(3), D(3), T(2048),
$THETAM(NNODES,LNODES), THETAW(NNODES,LNODES),
$THETAB(NNODES,LNODES), THETAZ(NNODES,LNODES)
CHARACTER*40 INFILE,OUTFILE

* Prompt user for desired input and output filenames
C WRITE(*,*)'ENTER THE NAME OF THE INPUT DATA FILE'
C READ(*,'(A40)')INFILE
OPEN(8,FILE='input')
C WRITE(*,*)'ENTER THE NAME OF THE OUTPUT FILE'
C READ(*,'(A40)')OUTFILE
OPEN(7,FILE='output')

C*****
C Read Inputs From 'INFILE'
C*****
C Read in model and data general information

```

```

      READ(8,*)N,NP,NI,NDEP
C      WRITE(7,'(5I10)')N,NP,NI,NDEP

C      Read in initial parameter estimates
      READ(8,*)(B(I),I=1,NP)
C      Read in initial conditions
      READ(8,*)TINIT,airtemp
C      Read in experimental data
      DO 10 I = 1,N
        READ(8,*)J,(Y(L,I),L=1,NDEP),(VAR(LT,I),LT=1,NDEP),
        +T(I)

C      Uncomment the following section to scale the variance or to set
C      the variance to 1.0 for OLS estimation

C      IF (I.LT.100) THEN
C        DO 9 K = 1,NDEP
C          VAR(K,J) = 10.0DO*VAR(K,J)
C 9      CONTINUE
C      END IF

10 CONTINUE

C      END OF INPUT
*****
C      INITIALIZE THE MATRICES AND ARRAYS

      MAXIT = 30
      DO 20 I = 1,NP
        BS(I)=B(I)
        DELTAB(I) = 0.DO
        D(I) = 0.DO
        BSS(I) = 0.DO
        DO 15 K = 1,NP
          P(I,K)=0.DO
          PINV(I,K) = 0.DO
          C(I,K) = 0.DO
15      CONTINUE
20      CONTINUE

      DO 24 I = 1,NNODES
        DO 22 J = 1,LNODES
          THETAM(I,J)=TINIT

          THETA(I,J)=TINIT
          THETAZ(I,J)=TINIT
          THETAB(I,J)=TINIT
22      CONTINUE
24      CONTINUE

C      Write statement to check that the input file is being read properly
      WRITE(*,*)TINIT,airtemp,Y(1,1),VAR(1,1)

      I = 0
      MAX = 0
      MARK = 0
      MK2 = 1

C      MAIN LOOP OF GAUSS METHOD, RETURN POINT FOR ALL ITERATIONS

35      MAX = MAX+1
      SSY = 0.DO

C      Uncomment this section to use only end data in the estimation
C      procedure (adjust range of K and then adjust range of N in the
C      next section accordingly)

C      DO 38 K = 1,99,1
C        CALL MODEL(K,B(1),B(2),ETA,THETAM,airtemp)
C        CALL SENS(K,B(1),B(2),SC,ETA,THETAZ,airtemp)
C        WRITE(*,*)I,K,SC,B(1)
C 38      CONTINUE

      DO 120 I = 1,N,1

        CALL MODEL(I,B(1),B(2),ETA,THETAM,airtemp)
        CALL SENS(I,B(1),B(2),SC,ETA,THETAZ,airtemp)
        DO 39 J = 1,NDEP
          RESID(J) = Y(J,I)-ETA(J)
          SSY = SSY + RESID(J)*RESID(J)/VAR(J,I)
39      CONTINUE
C        WRITE(*,*)I,RESID(1),SC,SSY

C      Calculate C matrix at the current time
      DO 47 K = 1,NP
        DO 46 K1 = 1,NP
          DO 45 J = 1,NDEP
            L = 2*J-2+K
            L1 = 2*J-2+K1

```



```

          C(K,K1) = C(K,K1)+SC(L)*SC(L1)/VAR(J,I)
45      CONTINUE
46      CONTINUE
47      CONTINUE
C      Calculate "D"
      DO 60 K = 1,NP
          DO 55 J = 1,NDEP
              L = 2*J-2+K
              D(K) = D(K)+SC(L)*RESID(J)/VAR(J,I)
55      CONTINUE
60      CONTINUE

C If this is the last time through with the converged estimates,
C then write out all the time step information

      IF (MARK.GT.0) THEN
          WRITE(7,115)T(I),(Y(L,I),ETA(L),L=1,NDEP),SSY
115      FORMAT(6E12.4)
          ENDIF

120 CONTINUE

      IF (MARK.GT.0) GOTO 1000

C      CALCULATE P MATRIX FROM C COEFFICIENTS

      DO 122 K = 1,NP
          DO 121 J = 1,NP
              PINV(K,J) = C(K,J)
121      CONTINUE
122 CONTINUE

      IF(NP.EQ.1) THEN
C          WRITE(*,*)'inverse one'
          P(1,1) = 1.DO/PINV(1,1)
      ELSE
C          Invert P matrix by formula
          DET = (PINV(1,1)*PINV(2,2)-PINV(1,2)*PINV(2,1))
          P(1,1) = PINV(2,2)/DET
          P(2,2) = PINV(1,1)/DET
          P(1,2) = -1.DO*PINV(1,2)/DET
          P(2,1) = -1.DO*PINV(2,1)/DET
      ENDIF

          C      WRITE(*,*)PINV(1,1),PINV(2,2),P(1,1),P(2,2)

          DO 124 K = 1,NP
              DO 123 J = 1,NP
                  DELTAB(K) = DELTAB(K) + P(K,J)*D(J)
123      CONTINUE
124 CONTINUE

C          WRITE(*,*)DELTAB

          DO 125 K = 1,NP
              B(K) = BS(K) + DELTAB(K)
125 CONTINUE

          DO 126 K = 1,NP
              CI(K) = SQRT(ABS(P(K,K)))*1.96DO
126 CONTINUE

C          END OF SEQUENTIAL GAUSS ESTIMATION PROCEDURE, CONTINUE WITH
C          BOX-KANEMASU PROCEDURE USING ALL THE TIME STEP INFORMATION
C          OR SKIP TO CRITERIA CHECK IF ONLY GAUSS ESTIMATION IS DESIRED
*****

C      Check flag for skipping B-K modification
      IF (MK2.EQ.1) THEN
          WRITE(7,127)MAX,(B(K),CI(K),K=1,NP),SSY
127      FORMAT('#',I4,5E12.4)
          GOTO 169
      END IF

C          SET UP CONSTANTS
          ALPHA = 3.DO/2.DO
          AA = 1.1DO
130 ALPHA = ALPHA*2.DO/3.DO

C          Calculate the parameters using the modified step size
          DO 135 K = 1,NP
              BSS(K) = BS(K)+ALPHA*DELTAB(K)
135 CONTINUE

C          Calculate the slope, "G"
          G = 0.DO
          DO 140 K = 1,NP
              DO 139 J = 1,NP

```

```

      G = G + DELTAB(J)*PINV(J,K)*DELTAB(K)
139  CONTINUE
140  CONTINUE
      WRITE(*,*)G

C      Check to see if G is positive
      IF (G.LT.0.DO) THEN
          WRITE(7,*)'G IS NEGATIVE, TERMINATE CALCULATIONS'
          MARK = 1
          GOTO 35
      ENDIF

C      Calculate the sum of squares based on the modified
C      parameters
      SSYP = 0.DO
      DO 145 I = 1,N
          CALL MODEL(I,BSS(1),BSS(2),ETA,THETAB,airtemp)
          DO 143 J = 1,NDEP
              RESID(J) = Y(J,I)-ETA(J)
C      Uncomment the IF statement if only end data is being used
C      in the estimation process.

C      IF (I.GE.100) THEN
          SSYP = SSYP+RESID(J)*RESID(J)/VAR(J,I)
C      END IF

143  CONTINUE
145  CONTINUE
C      WRITE(*,*)SSYP
C      Check to see if the sum of squares decreased. If not,
C      re-evaluate with a smaller ALPHA
      IF(SSYP.GT.SSY) THEN
          IF (ALPHA.LE.0.01DO) THEN
              WRITE(7,150)ALPHA,SSYP,SSY
150      FORMAT(3X,'ALPHA IS TOO SMALL, ALPHA =',F12.6,2X,'SSYP =',
+          E15.6,2X,'SSY =',E15.6)
              GOTO 1000
          ELSE
              DO 152 J=1,NNODES
                  DO 151 K=1,LNODES
                      THETAB(J,K)=TINIT
151      CONTINUE
152      CONTINUE
              GOTO 130
          ENDIF

      G = G + DELTAB(J)*PINV(J,K)*DELTAB(K)
      ENDIF

C      Calculate the step size "h" for Box-Kanemasu after checking the
C      governing inequality (condition placed on "h")
      SUMCH = SSY-ALPHA*G*(2.DO-(1.DO/AA))
      IF (SSYP.GT.SUMCH) THEN
          H = (ALPHA*ALPHA*G)/(SSYP-SSY+(2.DO*ALPHA*G))
      ELSE
          H = ALPHA*AA
      ENDIF
      WRITE(*,*)H

C      Calculate the final parameter estimates using h
      DO 155 K = 1,NP
          B(K) = BS(K)+H*DELTAB(K)
C      WRITE(*,*)B(K),BS(K),BSS(K)
155  CONTINUE

C      Calculate the correlation matrix
      DO 165 I = 1,NP
          DO 160 J = 1,I
              AR = ABS(P(I,I)*P(J,J))
              R(I,J) = P(I,J)/SQRT(AR)
160  CONTINUE
165  CONTINUE

C      DONE WITH CALCULATIONS, PRINT OUT DESIRED VALUES TO THE OUTPUT
C      FILE(P MATRIX, CORRELATION MATRIX, PARAMETER ESTIMATES...)
      WRITE(7,168)MAX,(B(J),CI(J),J=1,NP),SSYP,SSY
C      WRITE(7,*) (BS(J),BSS(J),J=1,NP)
168  FORMAT('#',I3,6E12.4)
*****

C      Check each parameter estimate against the criteria for a
C      converged solution. Increment "CHANGE" accordingly.
169  CRITER = 0.0001DO
      CHANGE = 0
      DO 170 J = 1,NP
          RATIO = (B(J)-BS(J))/(BS(J))
          RATIO = ABS(RATIO)
          IF (RATIO.LE.CRITER) THEN
              CHANGE = CHANGE+1
          ENDIF
170  CONTINUE

```

```

C      Reset all the variable matrices to zero or original values
DO 180 K = 1,NP
  BS(K) = B(K)
  D(K) = 0.DO
  DELTAB(K) = 0.DO
  DO 175 J = 1,NP
    C(J,K) = 0.DO
175  CONTINUE
180  CONTINUE

      DO 190 J = 1,NNODES
        DO 185 K = 1,LNODES
          THETAM(J,K)=TINIT
          THETAW(J,K)=TINIT
          THETAB(J,K)=TINIT
          THETAZ(J,K)=TINIT
185  CONTINUE
190  CONTINUE

C      Check to see if all parameters have converged, and if not, if
C      the maximum number of iterations have been used.  If no
C      convergence and the program is not at the maximum number of
C      iterations, then the process begins again with the sequential
C      Gauss loop using the latest parameter estimates as the initial
C      guesses.

      IF (NP.GT.CHANGE) THEN
        M = MAXIT
        IF (MAX.LE.M) GOTO 35
      ENDIF

      IF (CHANGE.EQ.NP) THEN
        MARK = 1
        GOTO 35

```

```

      ENDIF
1000 CONTINUE

      STOP
      END
*****
      SUBROUTINE SENS(I,BETA1,BETA2,CO,ETA,THETAW,THETAZ,airtemp)
      DOUBLE PRECISION BETA1,CO,HI1,BETA1P,THETAZ,BETA2,HI2,
+ETA,THETAW,airtemp,BETA2P
      PARAMETER (NNODES=25,LNODES=150)
      DIMENSION CO(4),HI1(3),ETA(3),
+THETAW(NNODES,LNODES),THETAZ(NNODES,LNODES),HI2(3)
      INTEGER I

      BETA1P = BETA1*1.01DO
      BETA2P = BETA2*1.01DO

      CALL MODEL(I,BETA1P,BETA2,HI1,THETAW,airtemp)
      CALL MODEL(I,BETA1,BETA2P,HI2,THETAZ,airtemp)

      CO(1) = (HI1(1)-ETA(1))/(BETA1P-BETA1)
      CO(3) = (HI1(2)-ETA(2))/(BETA1P-BETA1)
      CO(2) = (HI2(1)-ETA(1))/(BETA2P-BETA2)
      CO(4) = (HI2(2)-ETA(2))/(BETA2P-BETA2)

      RETURN
      END
*****
      SUBROUTINE MODEL(ITIME,RC,WB,ETMA,THETA,airtemp)
*      SEE APPENDIX A.1

```

C.2 Sample Input File

The following outlines the file format required for input to the parameter estimation program given in Appendix C.1. Here, explanations of the fields are given in parentheses above the sample input lines. These parenthetical statements should not be present in an actual input file.

(Number of data points, number of estimated parameters,
number of independent variables, number of dependent variables)

610 2 1 2

(Initial guesses for parameter values)

0.001 0.001

(Initial value of THETA matrix, Cooling air temperature)

0.2496 26.39

(Data: counter, heat flux, temperature, heat flux variance, temperature
variance, time)

1	3620.87	35.10	383.2	0.0006	0.1053
2	3601.06	34.95	383.2	0.0006	0.2105
3	3564.07	34.75	383.2	0.0006	0.3158
4	3536.33	34.61	383.2	0.0006	0.4211
5	3490.09	34.51	383.2	0.0006	0.5263
6	3387.05	34.36	383.2	0.0006	0.6316
7	3332.89	34.21	383.2	0.0006	0.7368
8	3306.47	34.11	383.2	0.0006	0.8421
9	3269.48	34.06	383.2	0.0006	0.9474
10	3187.58	33.97	383.2	0.0006	1.0526
.
.
.
605	1956.41	30.38	383.2	0.0006	63.6842
606	1981.51	30.38	383.2	0.0006	63.7895
607	1960.37	30.38	383.2	0.0006	63.8947
608	1874.50	30.33	383.2	0.0006	64.0000
609	1961.69	30.33	383.2	0.0006	64.1053
610	1981.51	30.33	383.2	0.0006	64.2105

Appendix D

Sponge Experiments Parameter Estimation Results

Table D.1 Results of Parameter Estimation for All the Sponge Experiments with 95% Confidence Intervals Around Each Estimate; calculated to include both experimental and model uncertainty as per section 4.2.3

Test Name	Flow Rate (ml/s)	R_c (m ² K/W)	w_b (ml/ml/s)
Sp111	0.00	0.00380±1.1 × 10 ⁻⁴	0.01198±4.3 × 10 ⁻⁴
Sp211	0.00	0.00395±1.7 × 10 ⁻⁴	0.01326±6.8 × 10 ⁻⁴
Sp311	0.00	0.00375±1.4 × 10 ⁻⁴	0.01191±4.4 × 10 ⁻⁴
Sp411	1.01	0.00281±1.2 × 10 ⁻⁴	0.02301±9.6 × 10 ⁻⁴
Sp511	1.01	0.00274±1.6 × 10 ⁻⁴	0.02328±1.3 × 10 ⁻⁴
Sp611	1.01	0.00217±9.4 × 10 ⁻⁵	0.02394±7.8 × 10 ⁻⁵
Sp711	1.95	0.00275±4.8 × 10 ⁻⁵	0.03878±7.1 × 10 ⁻⁴
Sp811	1.95	0.00302±6.1 × 10 ⁻⁵	0.03872±8.5 × 10 ⁻⁴
Sp911	1.95	0.00306±5.4 × 10 ⁻⁵	0.04744±9.9 × 10 ⁻⁴
Sp1011	2.92	0.00243±3.6 × 10 ⁻⁵	0.04867±7.0 × 10 ⁻⁴
Sp1111	2.92	0.00237±3.6 × 10 ⁻⁵	0.05725±8.6 × 10 ⁻⁴
Sp1211	2.92	0.00240±3.6 × 10 ⁻⁵	0.05296±8.6 × 10 ⁻⁴
Sp119	0.00	0.00365±1.2 × 10 ⁻⁴	0.01133±4.3 × 10 ⁻⁴
Sp219	0.00	0.00403±3.4 × 10 ⁻⁴	0.01021±1.1 × 10 ⁻⁴
Sp319	0.00	0.00426±1.2 × 10 ⁻⁴	0.00966±3.9 × 10 ⁻⁴
Sp419	1.01	0.00318±1.1 × 10 ⁻⁴	0.01849±7.4 × 10 ⁻⁴
Sp519	1.01	0.00304±1.3 × 10 ⁻⁴	0.01981±8.8 × 10 ⁻⁴
Sp619	1.01	0.00299±1.1 × 10 ⁻⁴	0.02097±8.4 × 10 ⁻⁴
Sp719	1.95	0.00290±5.2 × 10 ⁻⁵	0.03161±6.0 × 10 ⁻⁴
Sp819	1.95	0.00251±4.4 × 10 ⁻⁵	0.03156±5.2 × 10 ⁻⁴
Sp919	1.95	0.00314±6.0 × 10 ⁻⁵	0.03291±6.9 × 10 ⁻⁴
Sp1019	2.92	0.00294±4.3 × 10 ⁻⁵	0.05180±9.0 × 10 ⁻⁴
Sp1119	2.92	0.00266±3.9 × 10 ⁻⁵	0.04693±7.4 × 10 ⁻⁴
Sp1219	2.92	0.00261±3.9 × 10 ⁻⁵	0.04470±6.7 × 10 ⁻⁴
Sp121	0.00	0.00361±9.4 × 10 ⁻⁵	0.01733±5.5 × 10 ⁻⁴
Sp221	0.00	0.00387±9.2 × 10 ⁻⁵	0.01122±3.3 × 10 ⁻⁴
Sp321	0.00	0.00379±9.2 × 10 ⁻⁵	0.01081±3.2 × 10 ⁻⁴
Sp421	1.01	0.00269±1.2 × 10 ⁻⁴	0.02268±9.4 × 10 ⁻⁴
Sp521	1.01	0.00312±1.5 × 10 ⁻⁴	0.02225±1.1 × 10 ⁻⁴
Sp621	1.01	0.00301±1.1 × 10 ⁻⁴	0.02266±8.4 × 10 ⁻⁴
Sp721	1.95	0.00295±5.1 × 10 ⁻⁵	0.03327±5.9 × 10 ⁻⁴
Sp821	1.95	0.00299±5.0 × 10 ⁻⁵	0.03754±6.9 × 10 ⁻⁴
Sp921	1.95	0.00314±5.3 × 10 ⁻⁵	0.03596±6.8 × 10 ⁻⁴
Sp1021	2.92	0.00271±4.3 × 10 ⁻⁵	0.05057±8.7 × 10 ⁻⁴
Sp1121	2.92	0.00234±4.0 × 10 ⁻⁵	0.05438±8.8 × 10 ⁻⁴
Sp1221	2.92	0.00230±3.9 × 10 ⁻⁵	0.05181±7.8 × 10 ⁻⁴

Vita

The author, Paul Robinson, was born and raised in a town near Boston, Massachusetts. In 1989, he escaped from the North and came to Virginia Tech to study Mechanical Engineering. While working on his undergraduate degree, Paul CO-OPed for the U.S. Army Research, Development, and Engineering Center in Natick, MA. He then went on to work full time as an engineer for the Joint Warfare Analysis Center in Dahlgren, VA. After two years, he decided to go back to Virginia Tech to pursue a Master's Degree under the direction of Dr. Tom Diller and Dr. Elaine Scott. This document signifies the completion of that degree in February, 1998. Paul plans to begin new employment as a laboratory manager for the orthopaedic research laboratory at the University of Pennsylvania Hospital and Bioengineering Department in Philadelphia.

Permanent Address: 602 Washington St.

Apt 10

Blacksburg, Virginia 24060

This thesis was typeset with $\text{\LaTeX} 2_{\epsilon}$ ¹ by the author.

¹ $\text{\LaTeX} 2_{\epsilon}$ is an extension of \LaTeX . \LaTeX is a collection of macros for \TeX . \TeX is a trademark of the American Mathematical Society. The macros used in formatting this thesis were written by Greg Walker, Department of Mechanical Engineering, Virginia Tech.